Observational signatures of a Black Hole. Determination Black Hole masses

Lev Titarchuk
(University of Ferrara/GSFC/NRL/ICRANET)

Nikolai Shaposhnikov
(UMD/GSFC)

TALK@GR conference in NZ, December 18 2009

Goal of this presentation

To demonstrate that in X-ray observations

- ✓ there is objective (model independent) information regarding the nature of compact objects.
- ✓To illuminate status of our results obtained thus far from Galactic black hole (BH) candidates and neutron star (NS) sources and their impact
- ✓Expectations in the case of AGNs
- ✓ Model independent observational signatures of BH and NS sources

X-ray Binary (artistic conception)

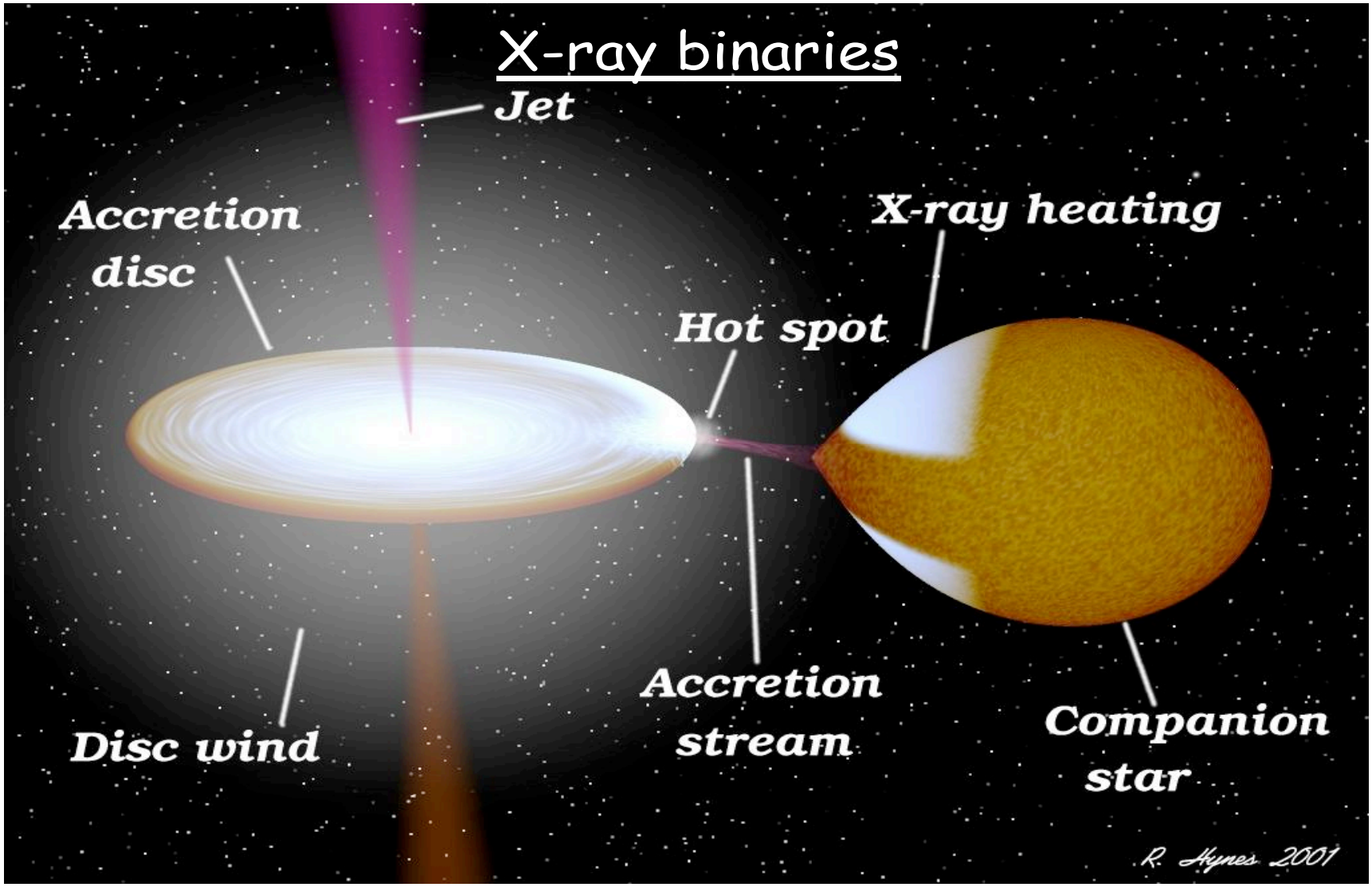

Model of Accretion Process Surrounding a Compact Object (NS or BH)

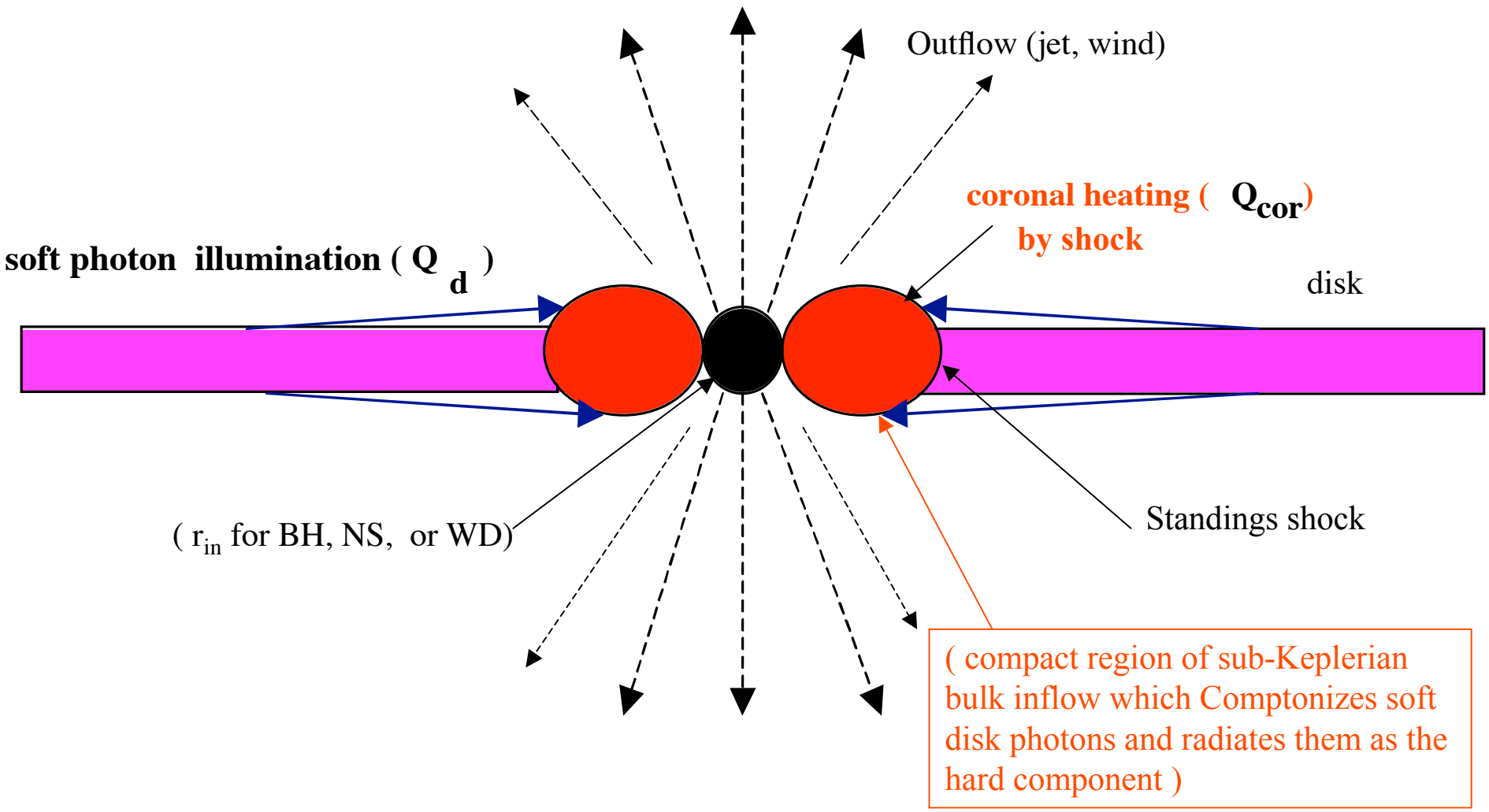

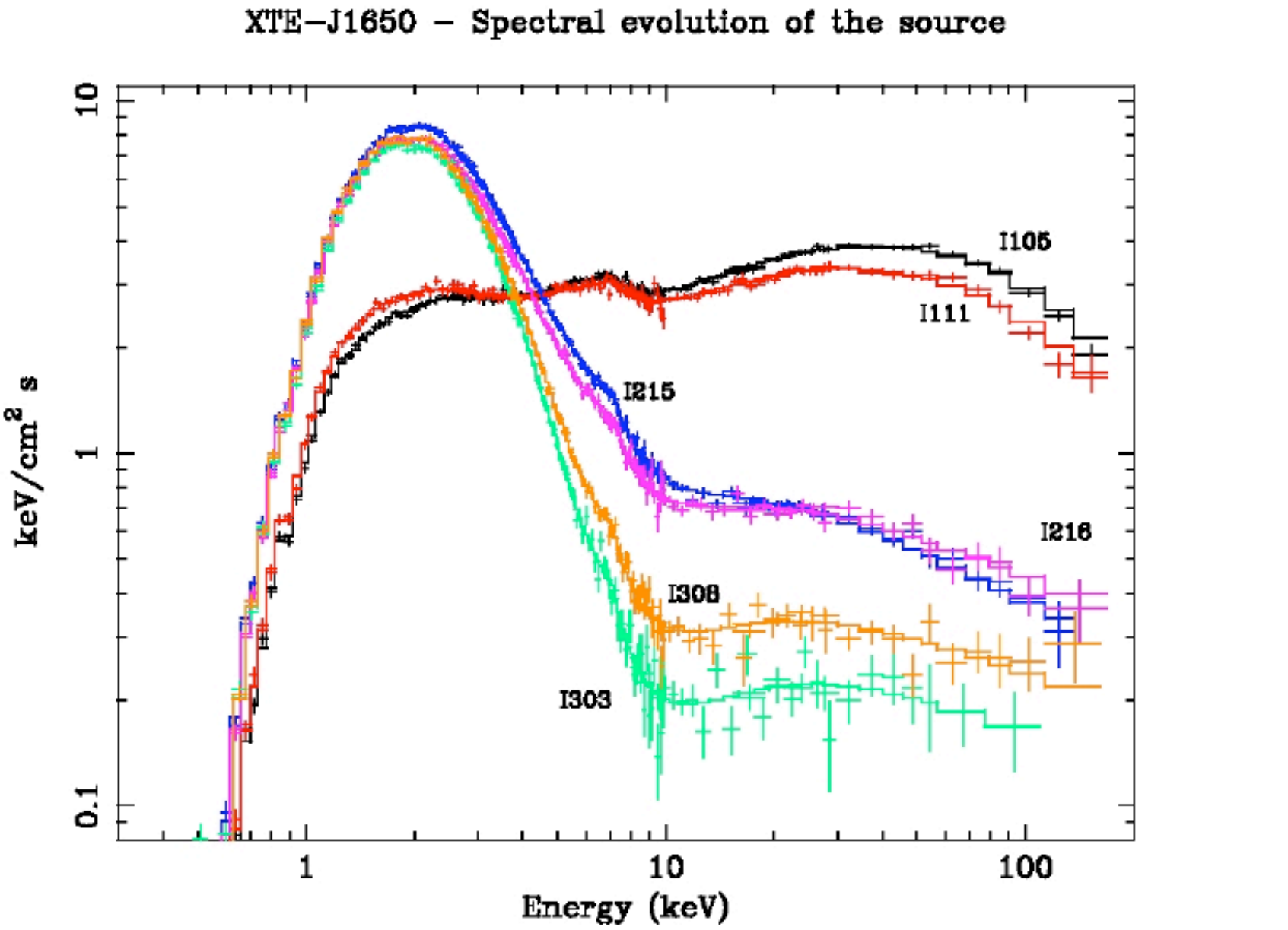

Montanari, T & Frontera 2006

XTE-J1650 (BH)

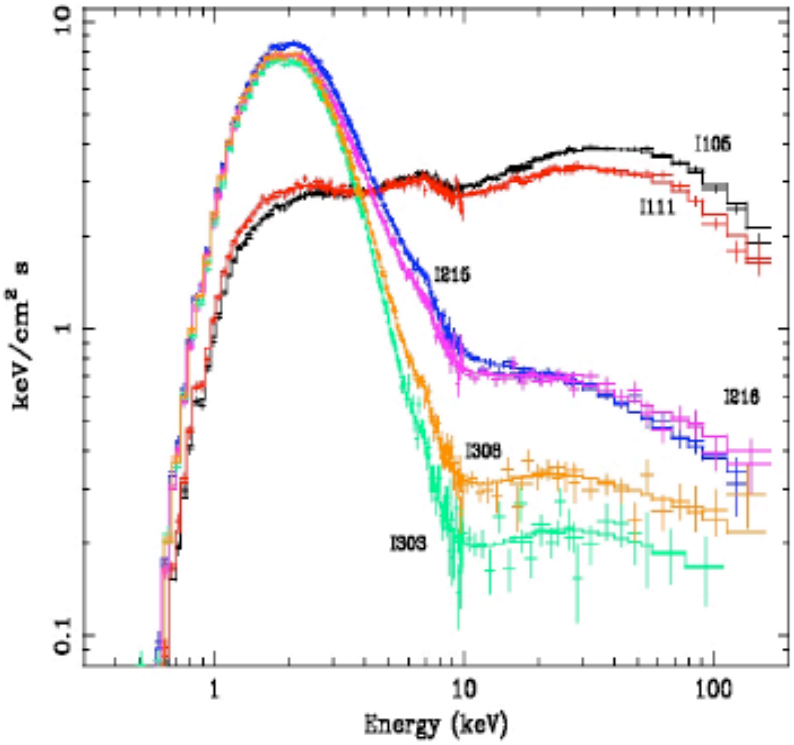

4U 1728-34 (NS)

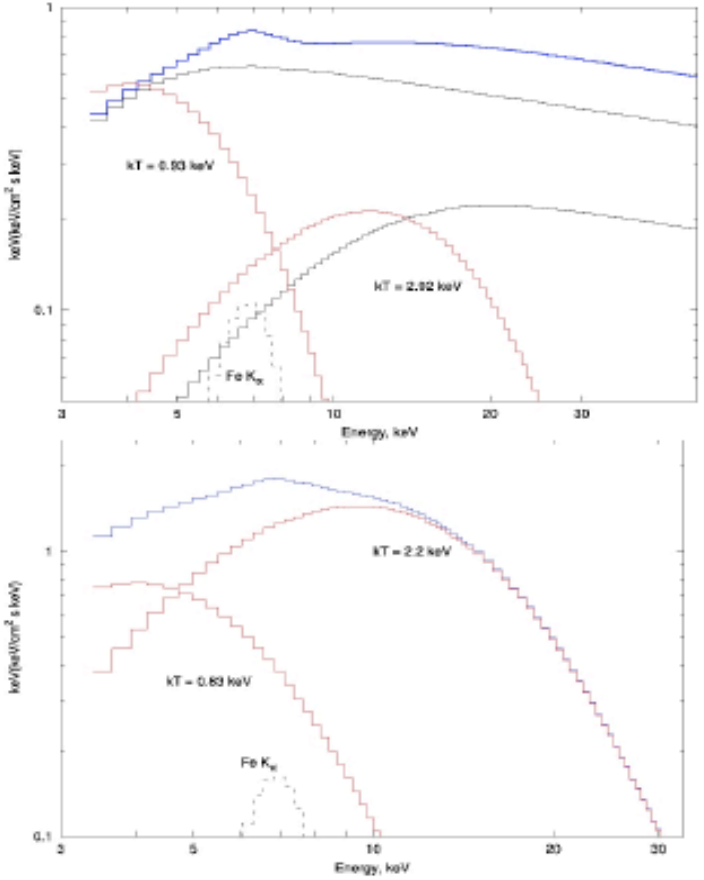

Titarchuk & Shaposhnikov (2005) ApJ 626, 298

Exponential and power-law probability distributions of wealth and income in the United Kingdom and the United States

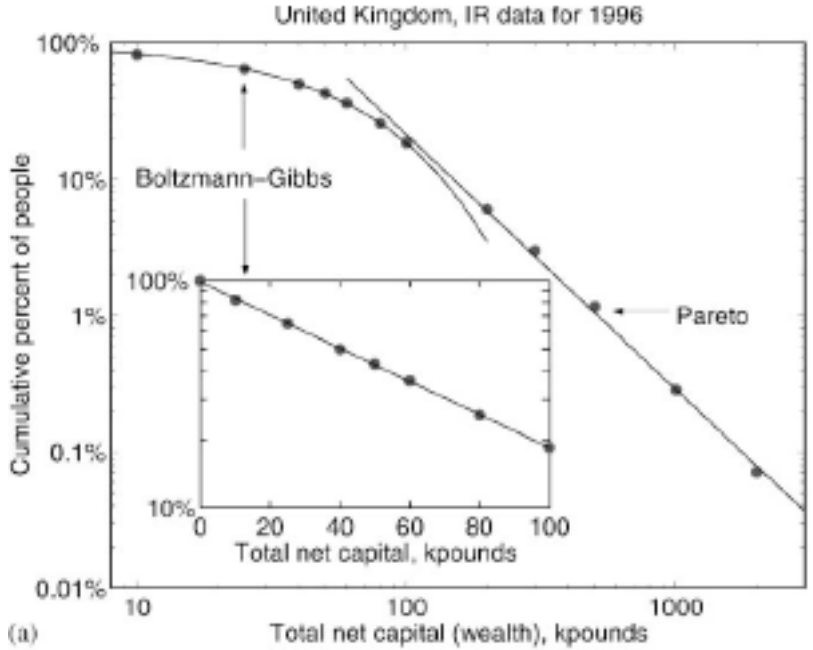

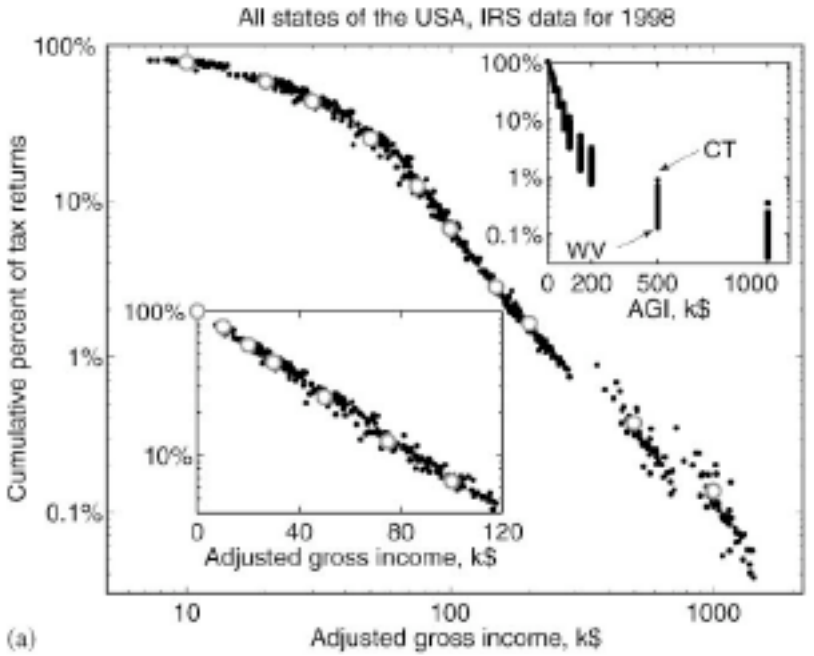

Dragulescu, & Yakovenko Physica A **299**, 213 (2001))

Composite spectrum of Cyg X-2

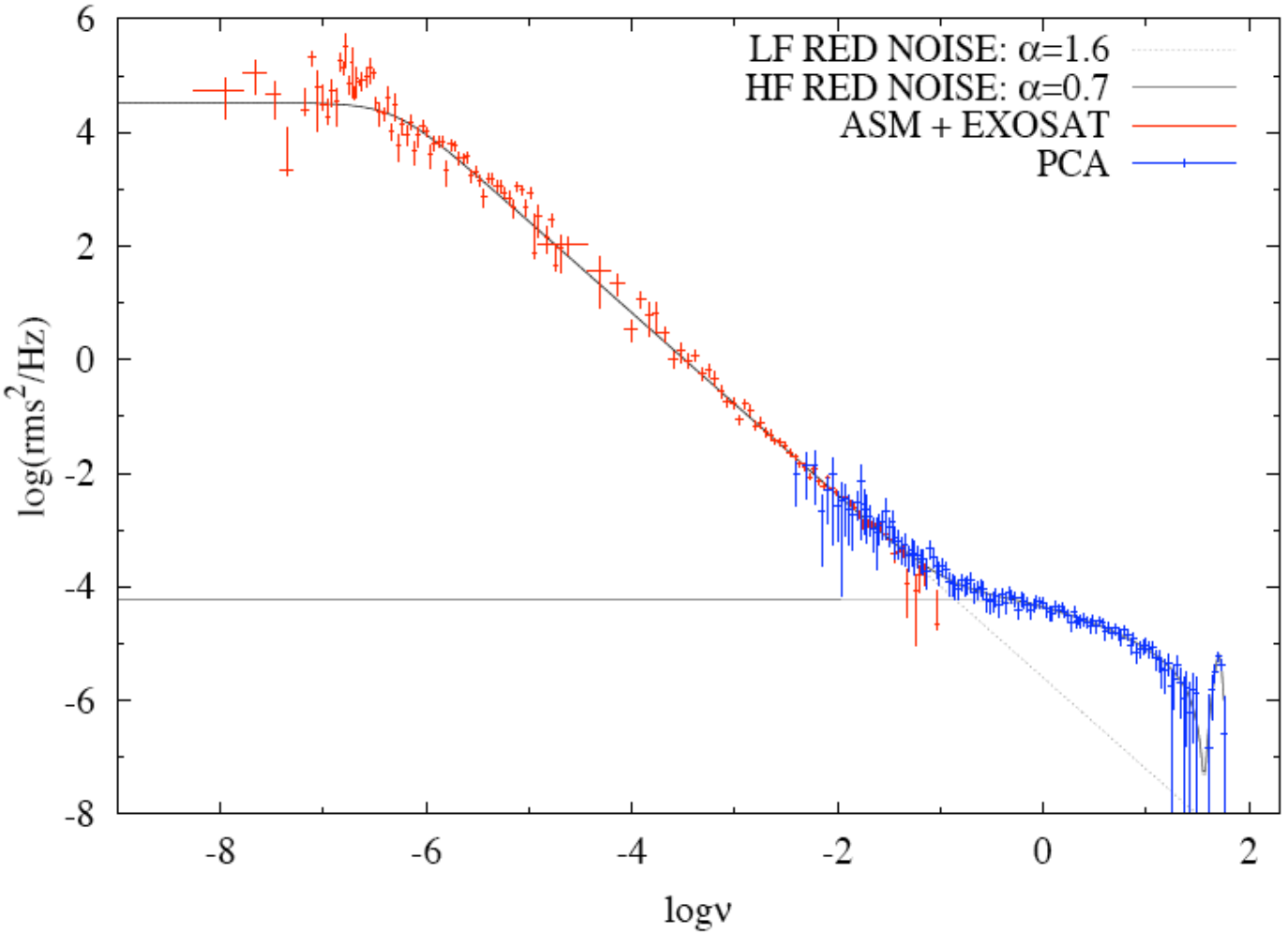

EXOSAT-ASM-PCA (RXTE) power spectrum of Cyg X-2 in frequency range that covers 10 orders of magnitude. One can clearly see low and high frequency (LF and HF) white-red noise components in PDS, related to the extended Keplerian disk and relatively compact, innner disk-like configuration (sub-Keplerian Compton corona) respectively. Each of these two components is perfectly fitted by our white-red noise model (dotted and solid lines are for LF and HF best-fit models respectively.

Soft state power spectrum of Cyg X-1

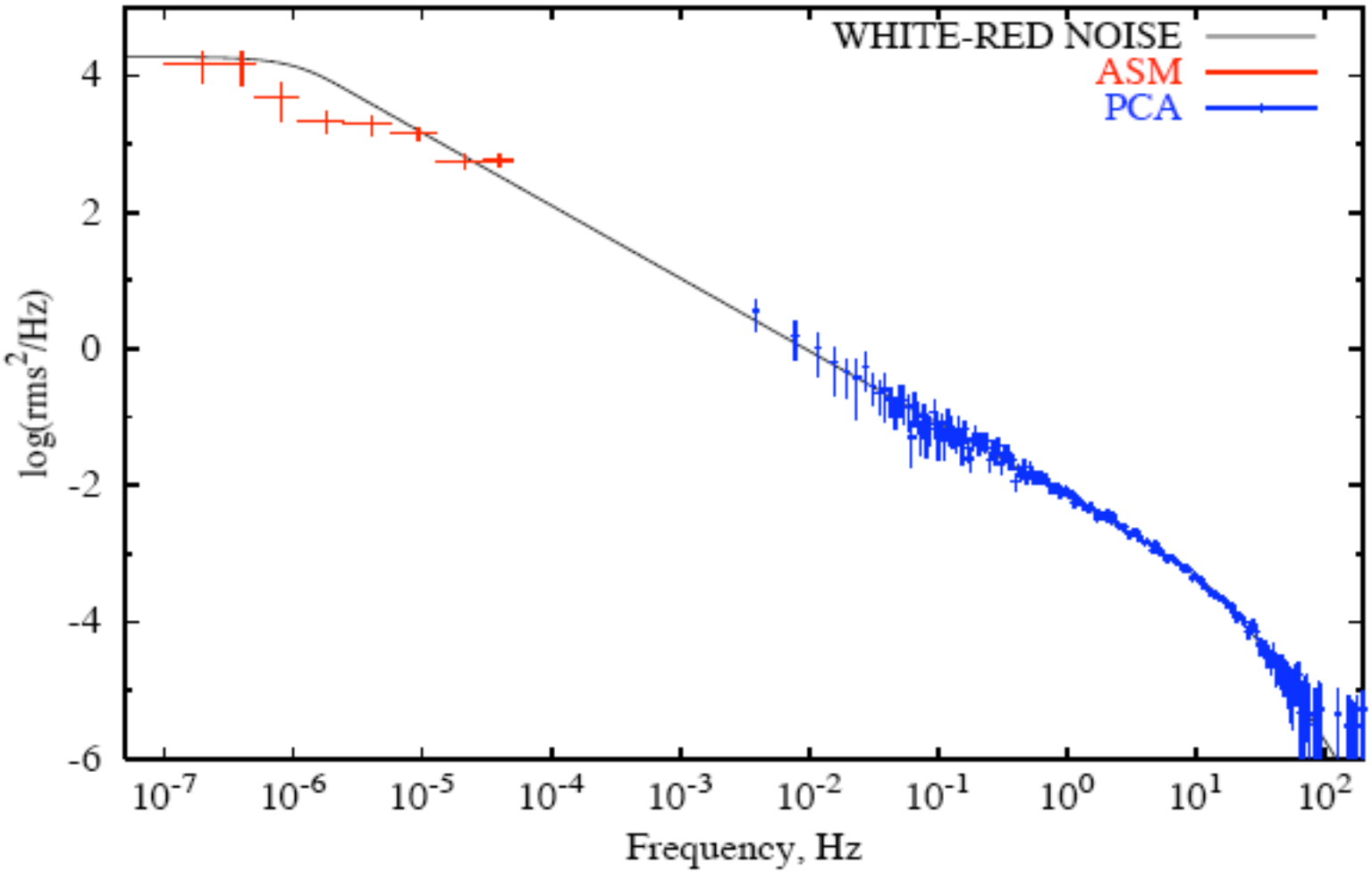

The composite soft state PDS is made by PCA (blue) and ASM (red) PDSs.
The PCA PDS is for ObsID 50110-01-52-00. Data are fitted by LF-HF diffusion model:
χ_2/N_{dof} = 184/228 = 0.81, the best -fit parameters $t_{0,D} = (6 \pm 1.7) \times 10^5$ s, $\psi_D = 2.93 \pm 0.01$.

LF QPOs in Black Holes

Cygnus X-1

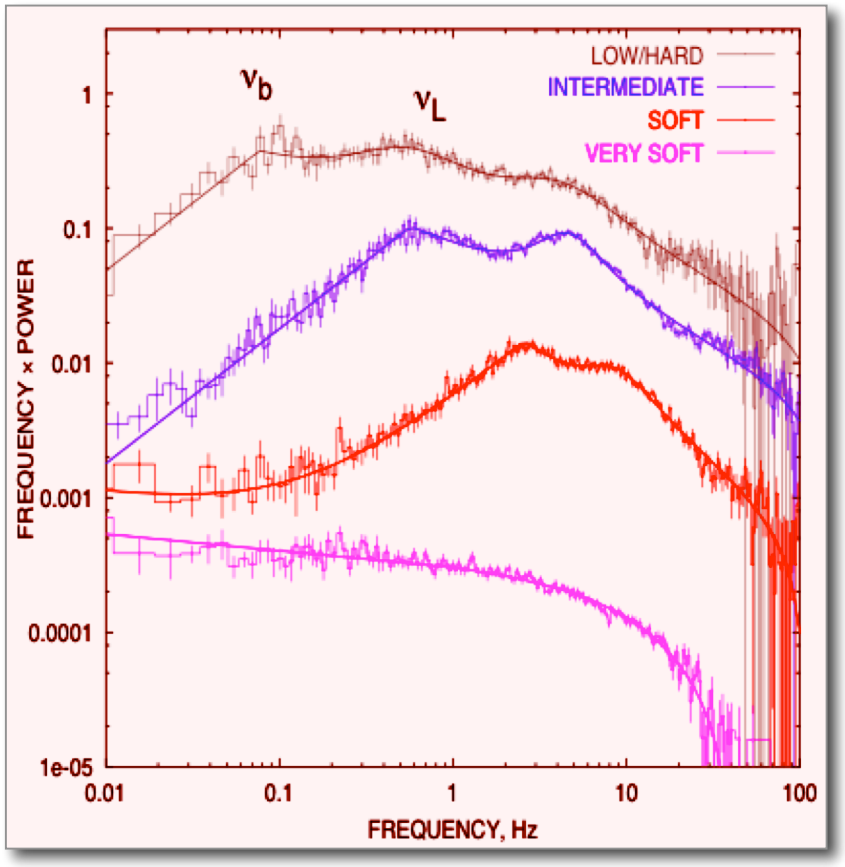

Shaposhnikov & T 2006, ApJ, 643,1098

GRO J1655-40

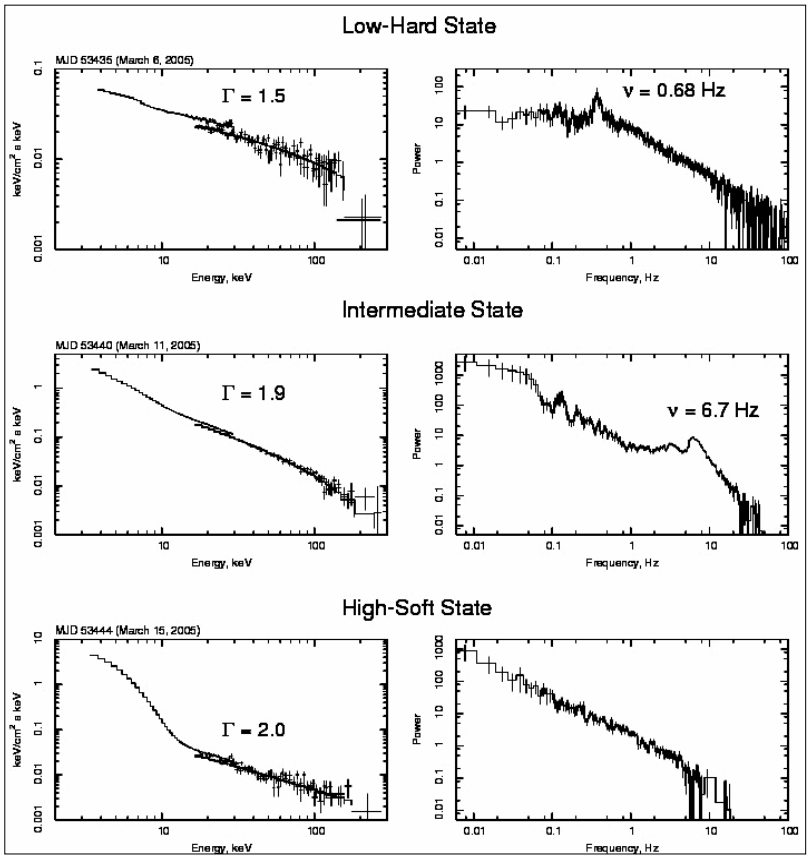

(**Shaposhnikov**, Swank, Rupen, Shrader, Beckmann, Markwardt & Smith 2007, ApJ, 655,434)

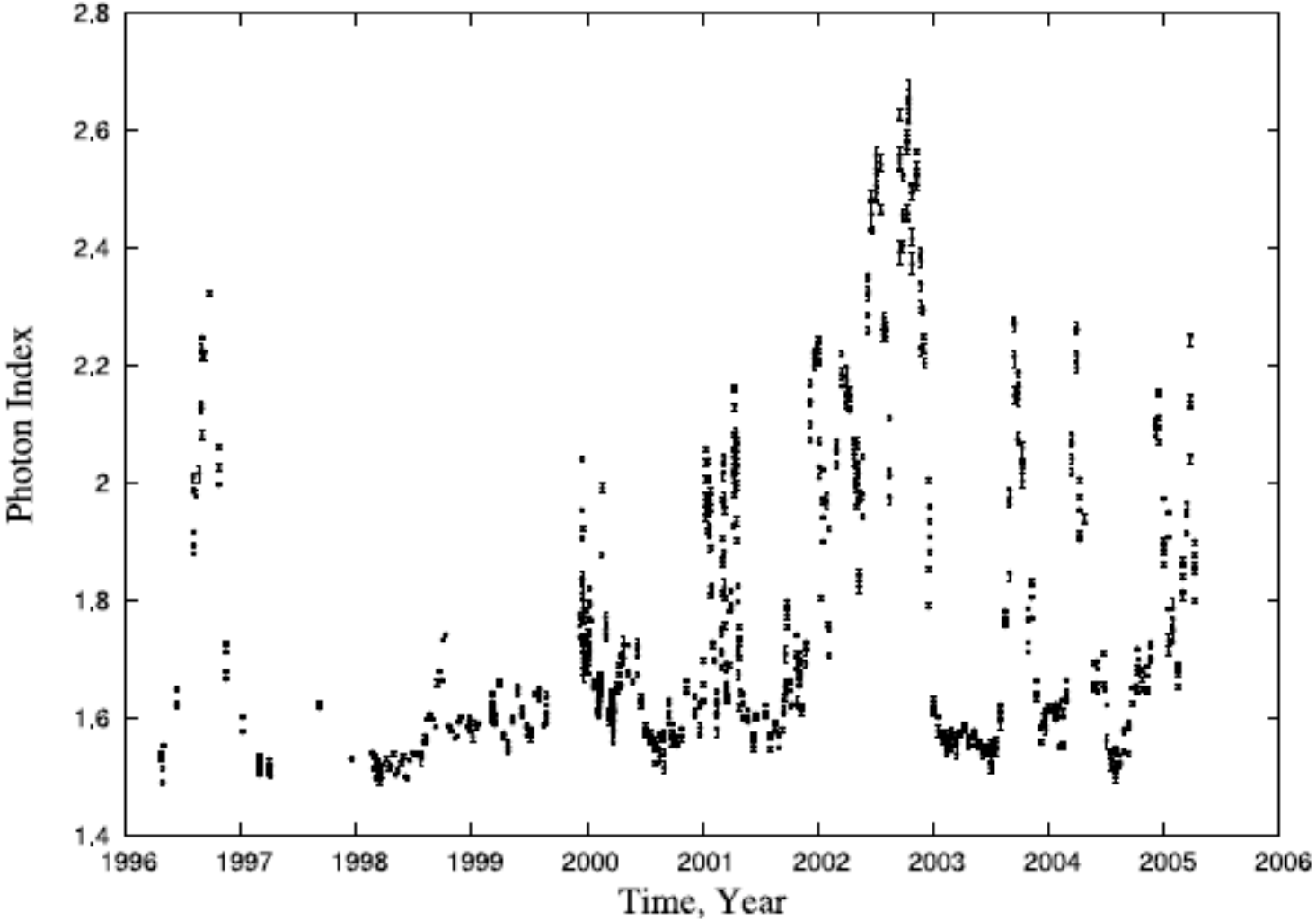

FIG. 15.—The variation of the photon index in Cyg X-1 throughout the entire *RXTE* mission.

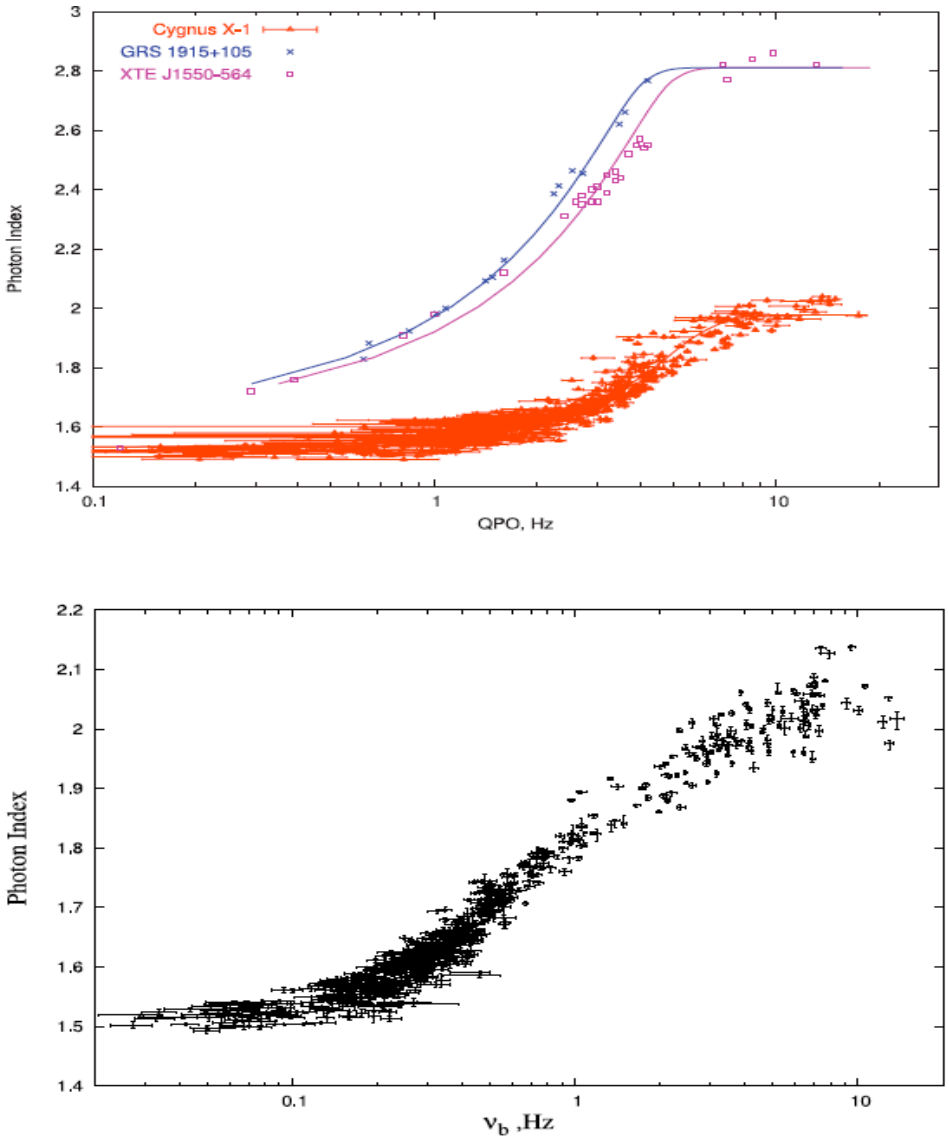

FIG. 8.—*Top*: Observed correlations between photon index Γ and low frequency ν_L (*red points*) compared with those in two other BHC sources, XTE J1550−564 and GRS 1915+105. The saturation value of the index varies from source to source, but it does not exceed the theoretically predicted value of 2.8 for the converging flow of nonrelativistic temperature (see TZ98). Presumably, the saturation value of the index depends on the plasma temperature of the converging flow (LT99). *Bottom*: Observed correlation between photon index Γ and break frequency ν_B for Cyg X-1.

Index- low QPO frequency correlation in BH candidates

Shaposhnikov & T (2006)

The inferred scenario of the spectral transition in Cyg X-1. Strength of disk and outflow (wind) increase towards the soft states

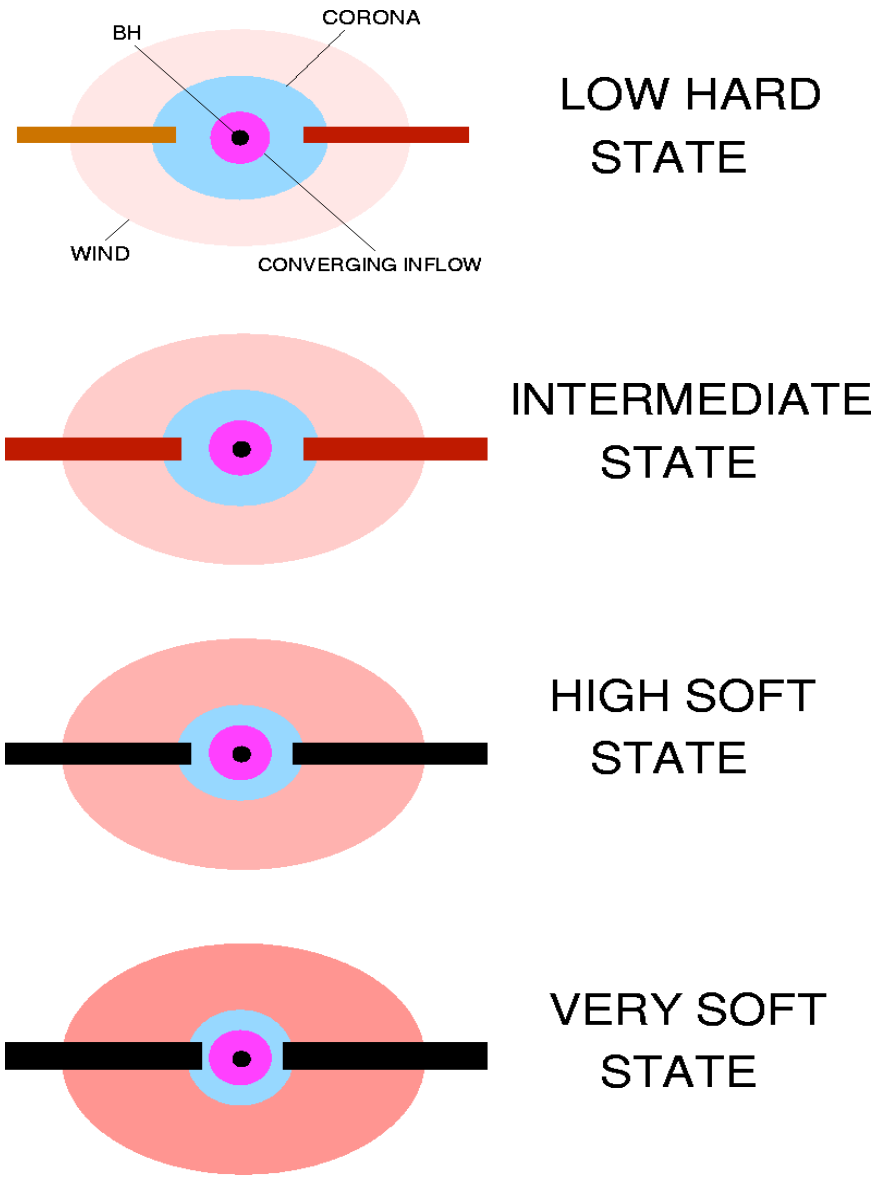

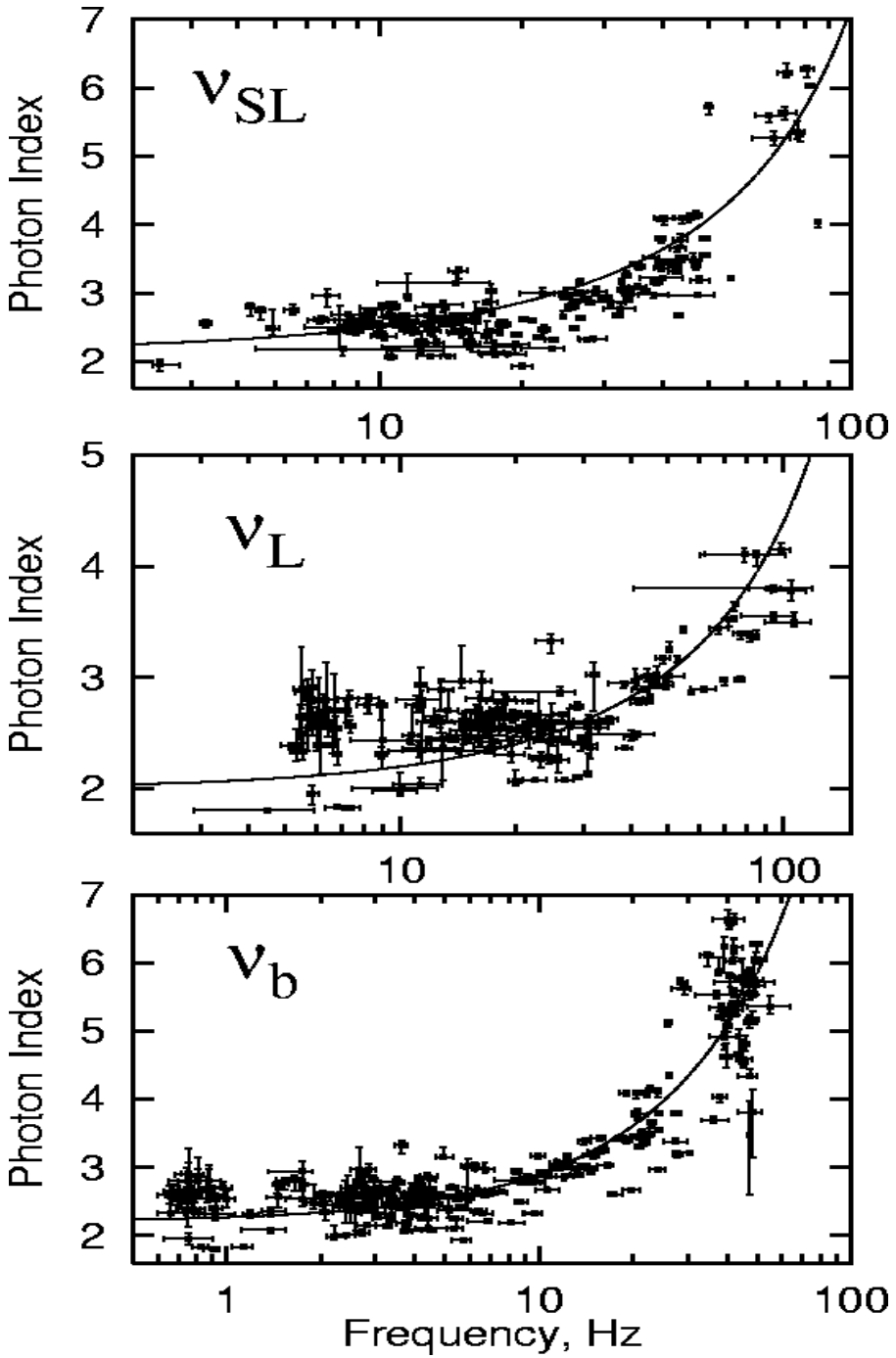

Index-QPO frequency correlation for NS source 4U 1728-34

T & Shaposhnikov (2005)

NS power spectrum

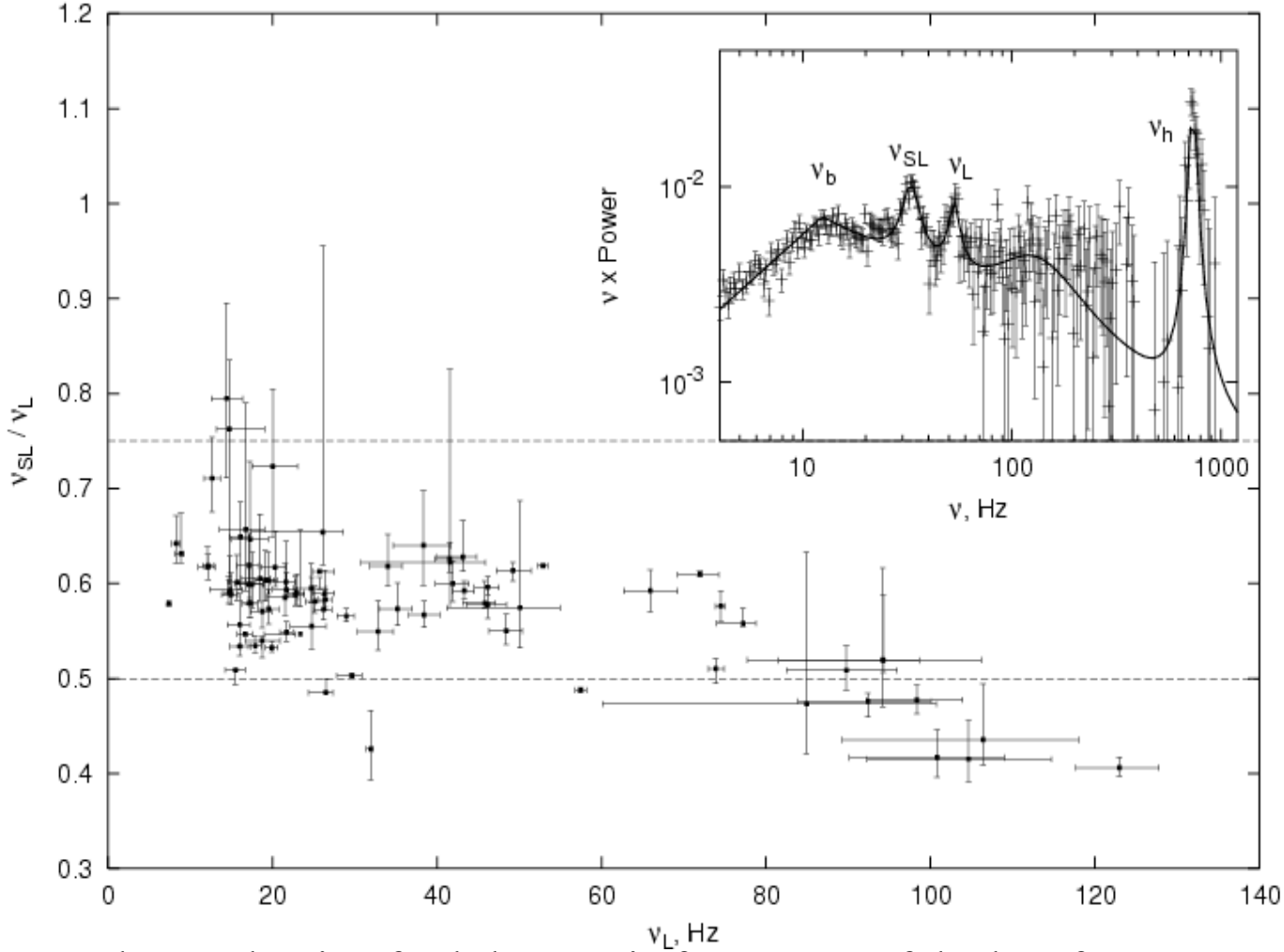

Observed ratio of sub-harmonic frequency of the low frequency ν_{SL} to low frequency ν_L as a function of ν_L . Two horizontal lines indicate the corridor where the most of ratio points are situated.

Spectral index of the converging inflow spectrum

- Main idea of the power law formation:

$$I_\nu \propto p^K,$$

where p is a probability of single scattering .

$$\nu / \nu_0 = 1 + \eta,$$

after k scatterings

$$\nu_k / \nu_0 = (1+\eta)^k.$$

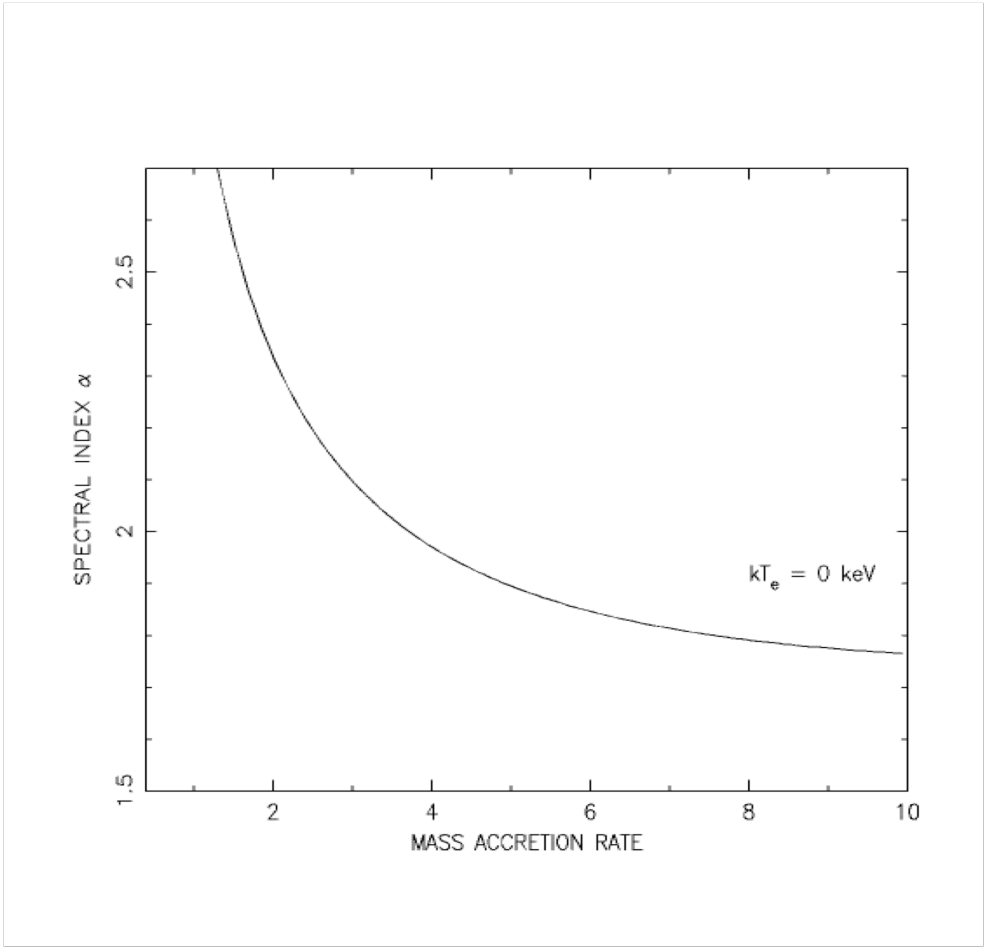

Thus $I = (\nu / \nu_o)^{-\alpha}$ where $\alpha = \ln(1/p)/\ln(1+\eta)$

Black Hole Mass Determination.

The Main Idea

QPO frequency ν_L by definition is a ratio:

$$\nu_L \propto V/L$$

where **V** is a characteristic (acoustic) velocity in a given configuration and **L** is a size of the configuration.

But velocity **V** and dimensionless size $L_{DS} = L/R_S$ are funcition of the spectral Hardness (photon index Γ) (*T, Lapidus & Muslimov 1998)*

Thus for a given index (spectral state) and for two black hole sources of masses $M_1 = M_1/M_\odot$, $M_2 = M_2/M_\odot$

$$\text{Log}\ \nu_1 - \text{Log}\ \nu_2 = \text{LOG}\ (M_2/M_1)$$

The index saturation is a BH signature

Spectral index $\alpha=\Gamma$-1

$$\alpha \approx (\eta N_{sc})^{-1} = Y^{-1}.$$

Number of scatterings

$$N_{sc} \propto L/l = \tau$$

average fractional energy change per scattering

$$\eta \propto 1/\tau \text{ when } \tau \gg 1$$

spectral index saturates when CF optical depth increase!

Verification of the Scaling Method

GRS 1915+105 & GRO J1655-40

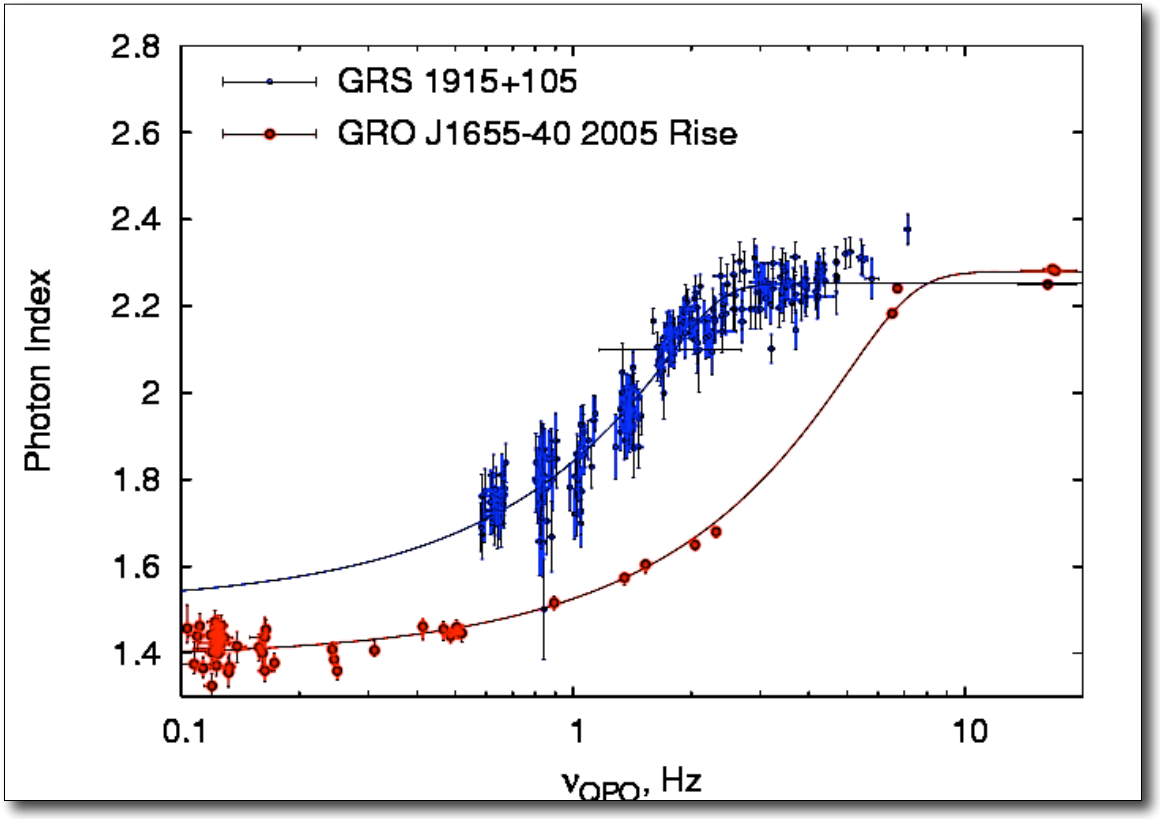

- Scaling Coefficient

$M_{1655}/M_{1915}=0.41\pm0.01$

- Given that

$M_{GRO\ J1655+40}=(6.3\pm0.5)$ solar masses

we obtain that

- $M_{GRS\ 1915+105}=$

(15.6±1.5) solar masses

Optical: 10.0-18.0 M_Sun

(Griener et al. 2001)

Shaposhnikov & T (2007)

BH Mass Determination in Cygnus X-1

Cygnus X-1 & GRO J1655-40

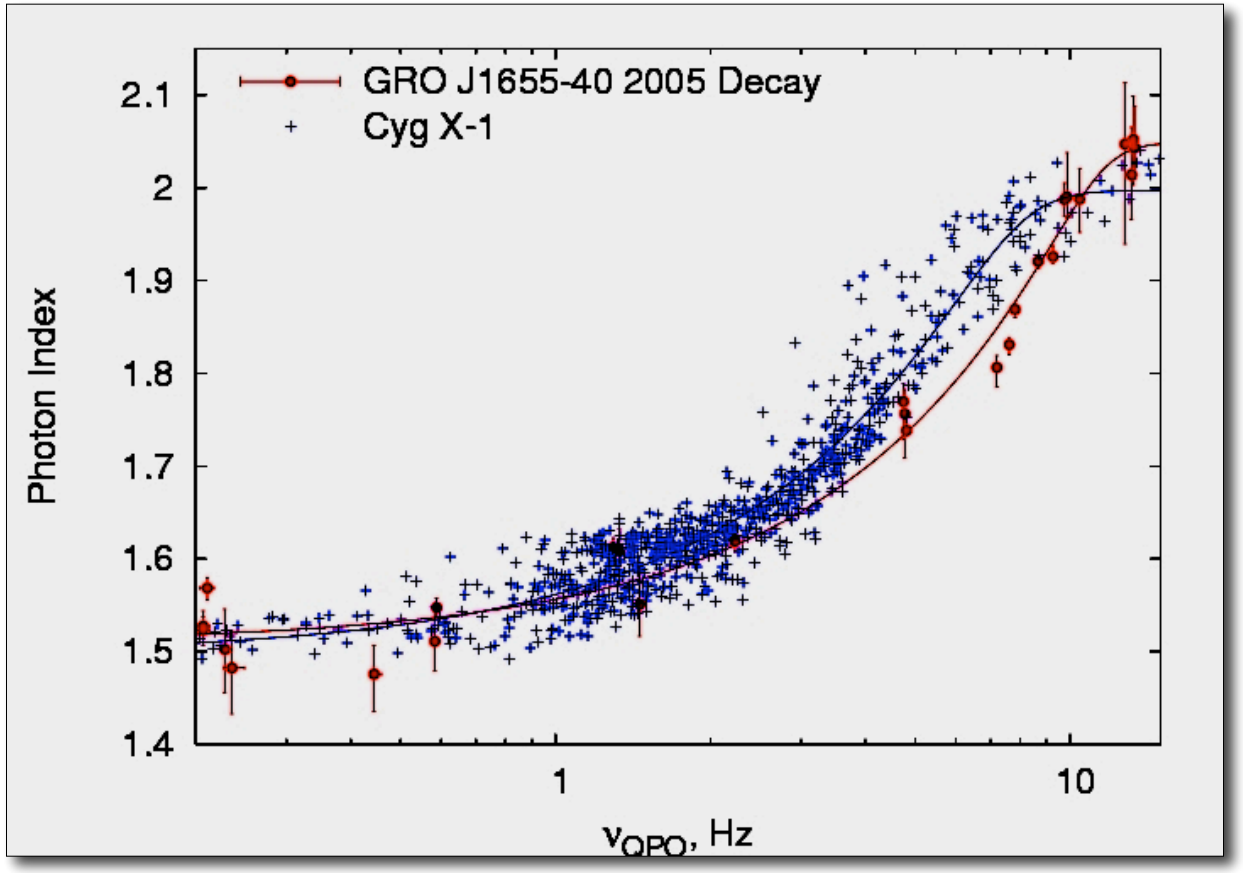

- $M_{\text{Cyg X-1}}$ =

8.7 ± 0.8 solar masses

Optical: 6.85-13.25 M_{sun}

Shaposhnikov & T (2007)

Observable Index-QPO and Index-Mdot correlations. GX 339-4

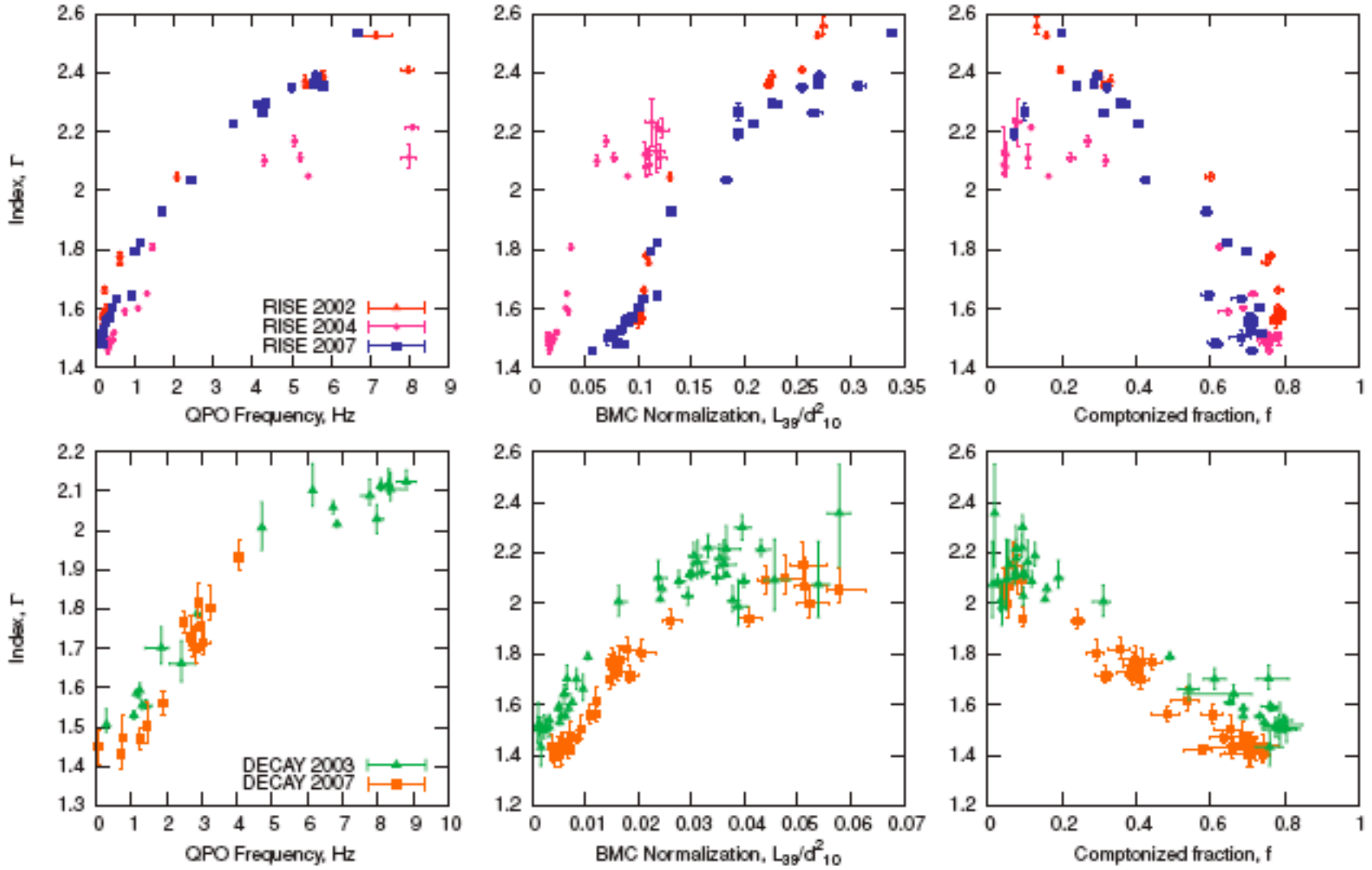

Figure 3. PCA Standard1 count rate (top row) and hardness (second row) for three outbursts from GX 339−4 on 2002 (left), 2004 (middle), and 2007 (right). Third and bottom rows: photon index plotted versus QPO frequency (left), BMC normalization (middle), and Comptonized fraction (right) for transitions in GX 339−4 (each transition is indicated by a different color).

Index-Mdot saturation. GRS 1915+105

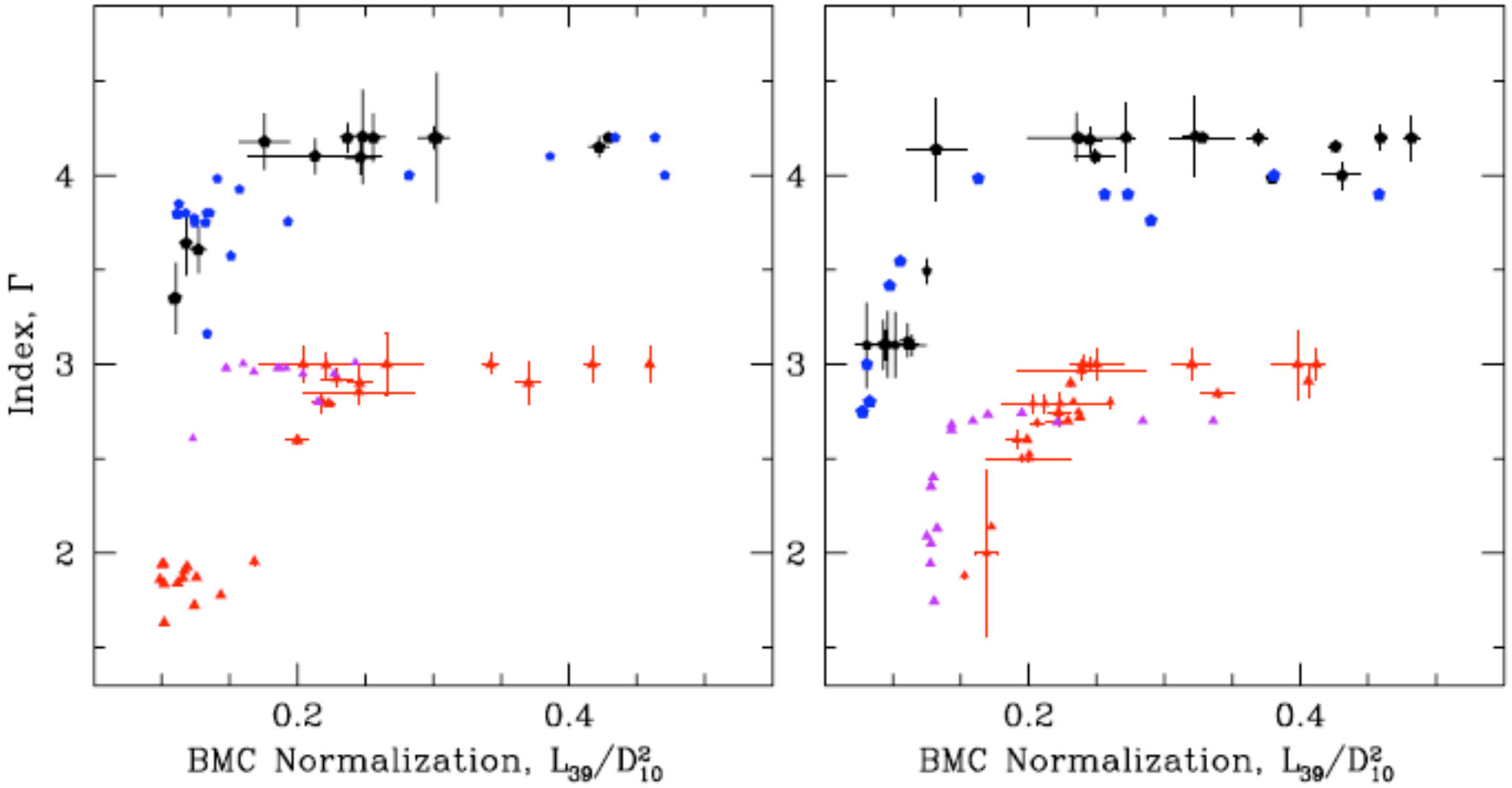

Seifina & T (2009)

Index-Mdot saturation. H1743-322

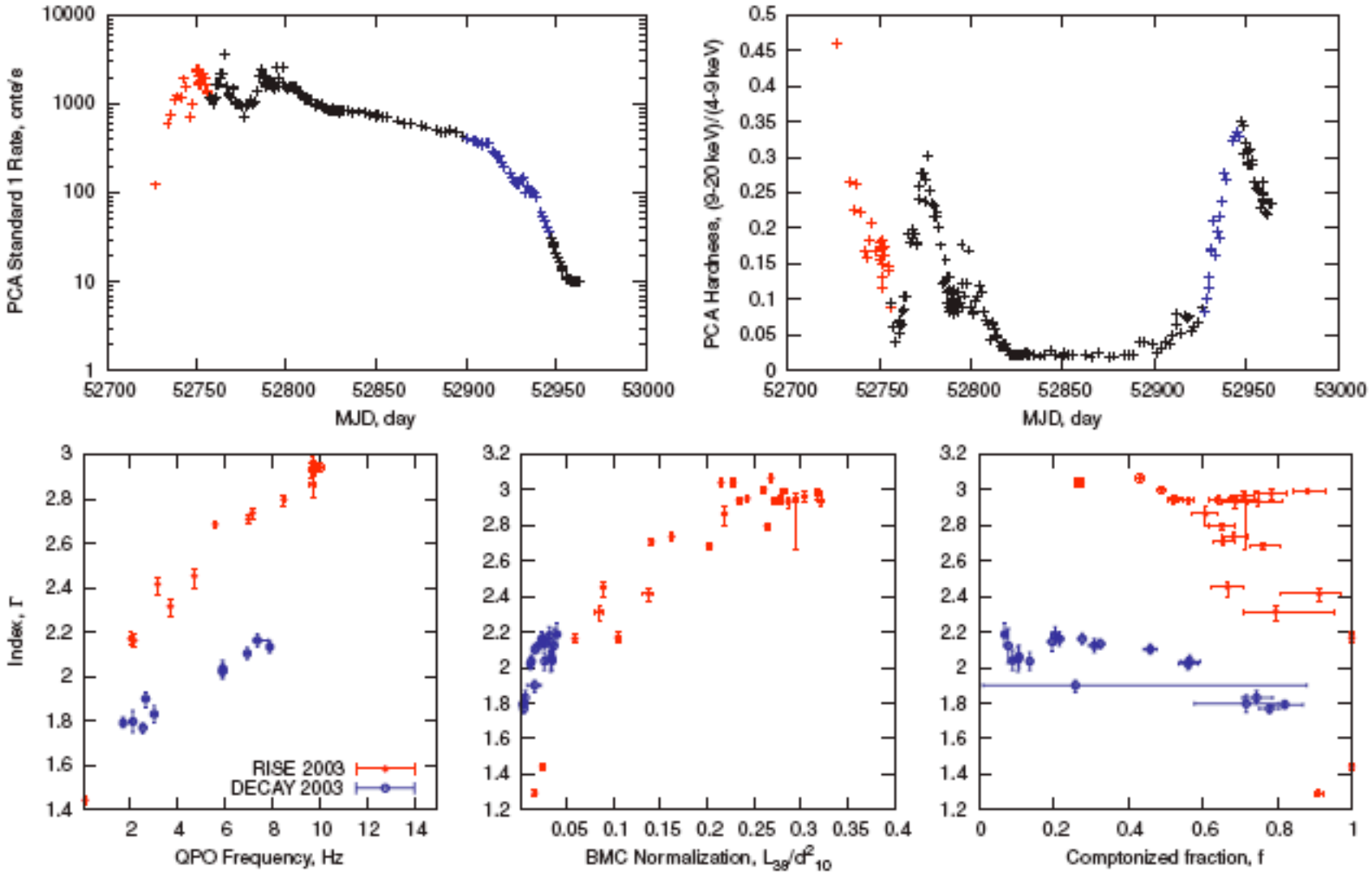

Index-Mdot saturation. 4U 1543-47

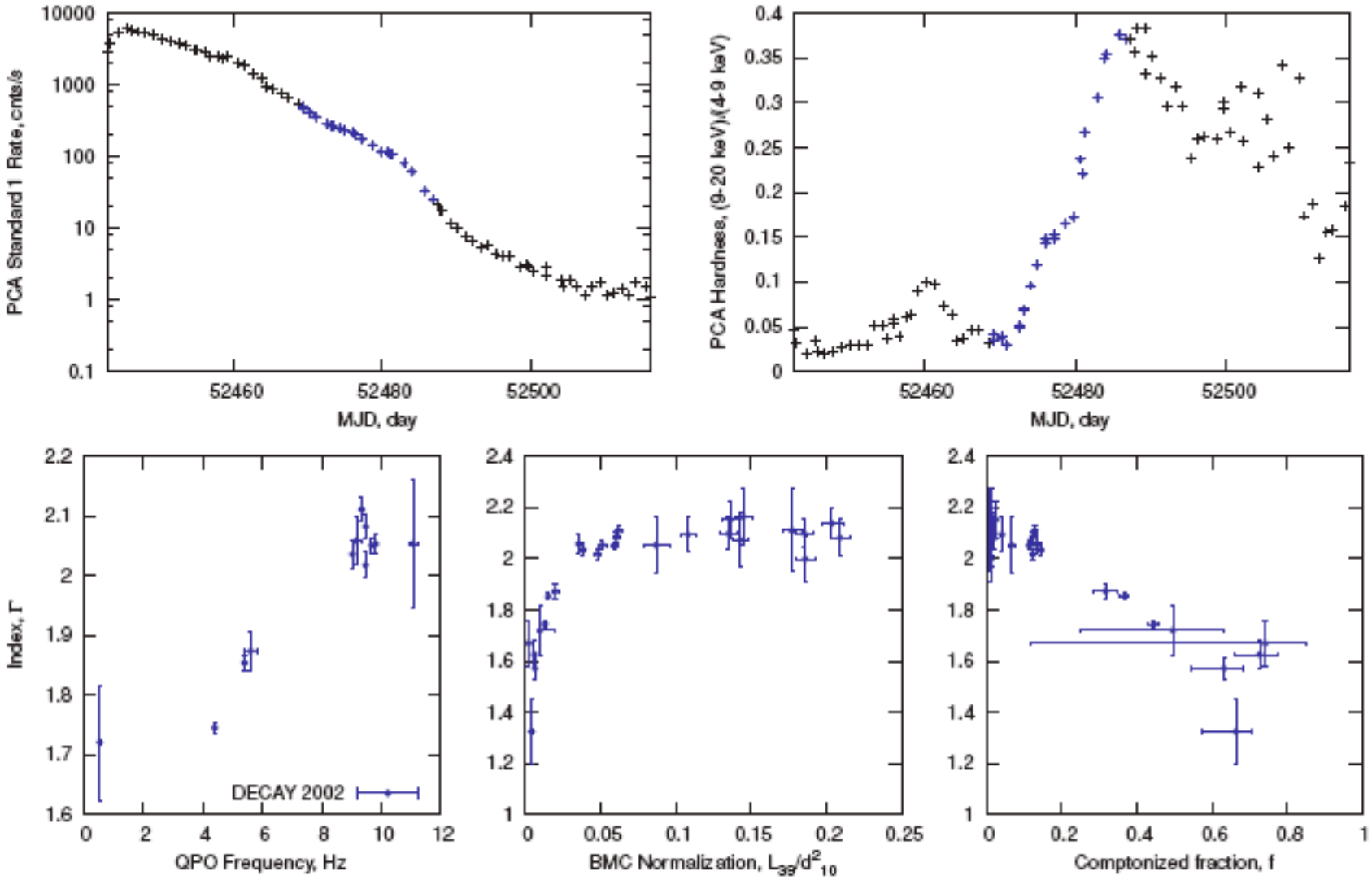

Index-Mdot saturation. Cyg X-1

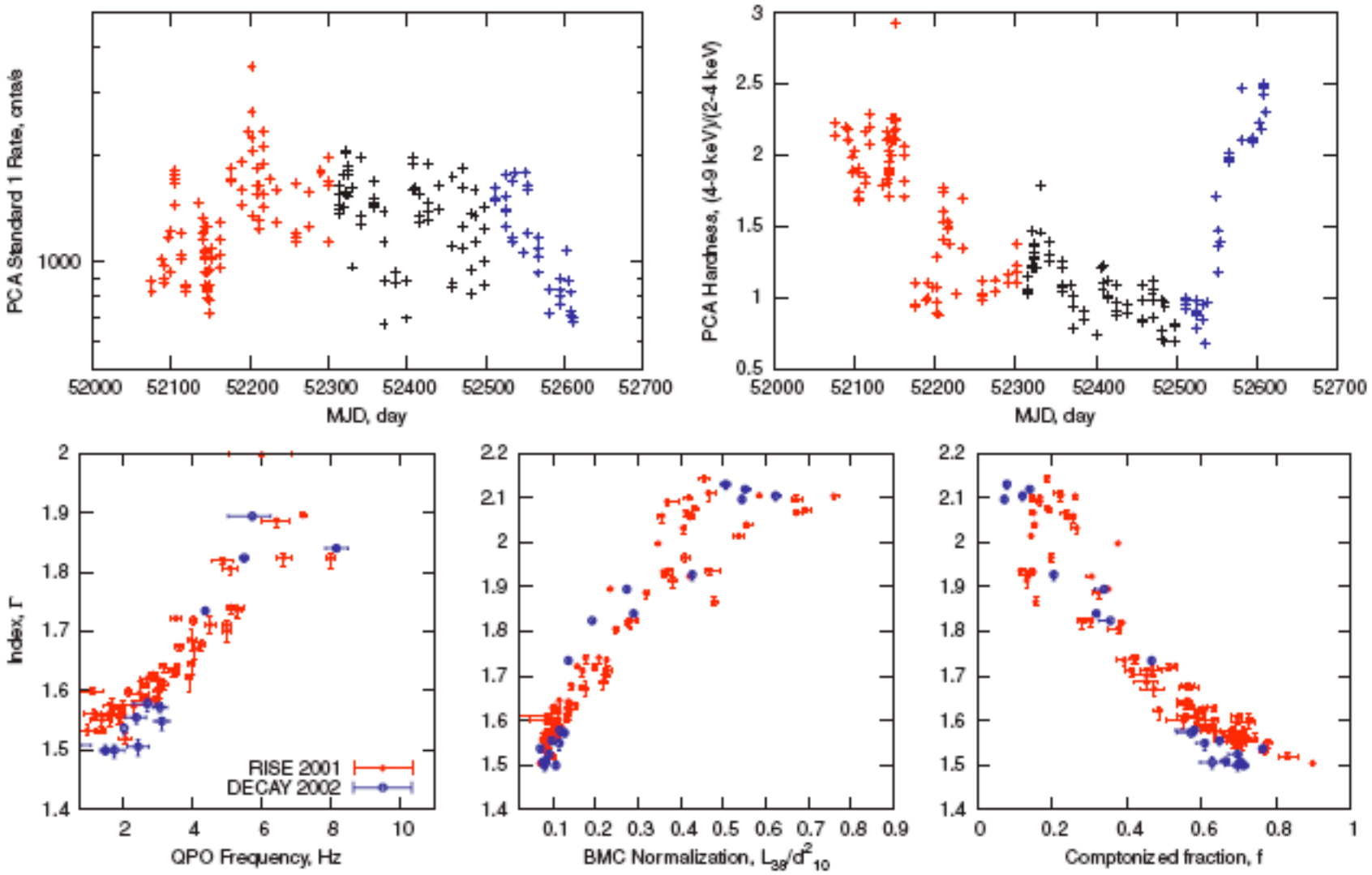

Figure 6. Top: PCA Standard 1 light curve (left) and hardness (right) for Cyg X-1 during 2001–2002. Red points indicate soft-to-hard transition while blue points show hard-to-soft transition. Observations during the HS are shown in black color. Bottom: photon index vs. QPO (left), BMC normalization (middle), and Comptonized fraction (right) during 2001–2002 state transitions in Cyg X-1.

Black hole mass determination

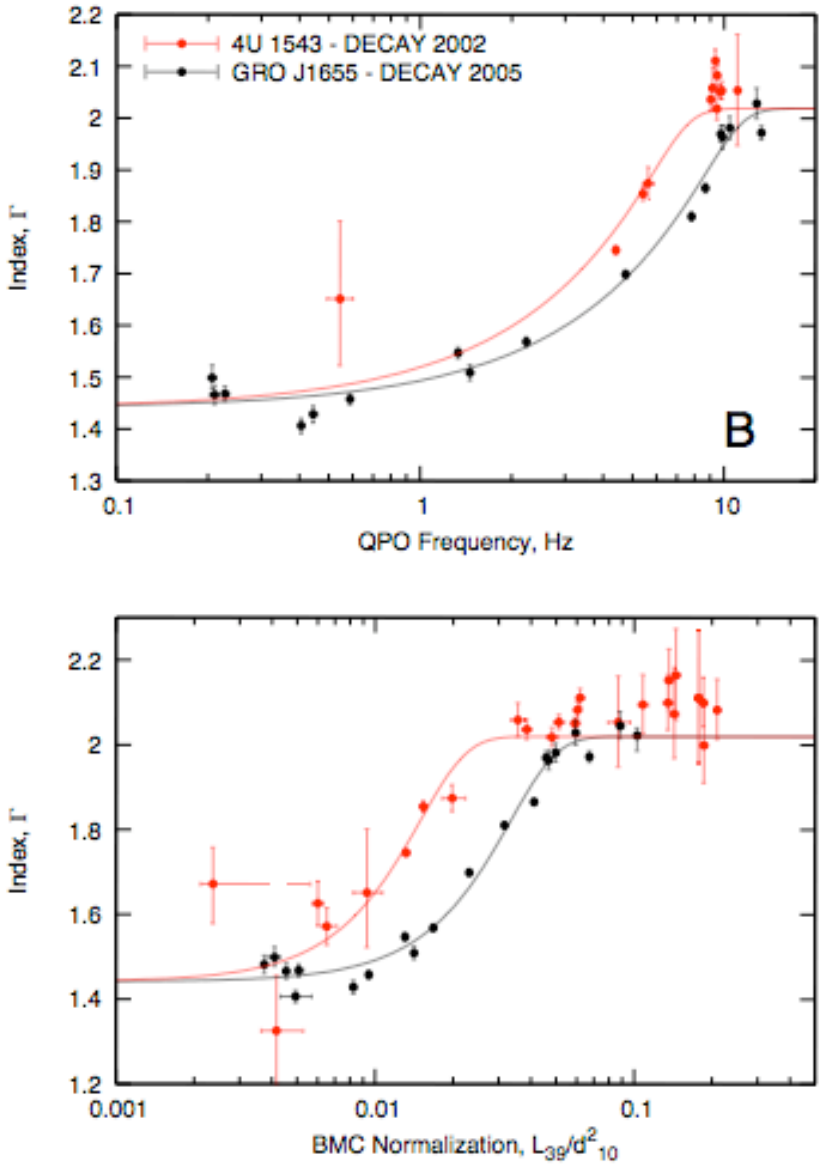

Shaposhnikov & T (2009)

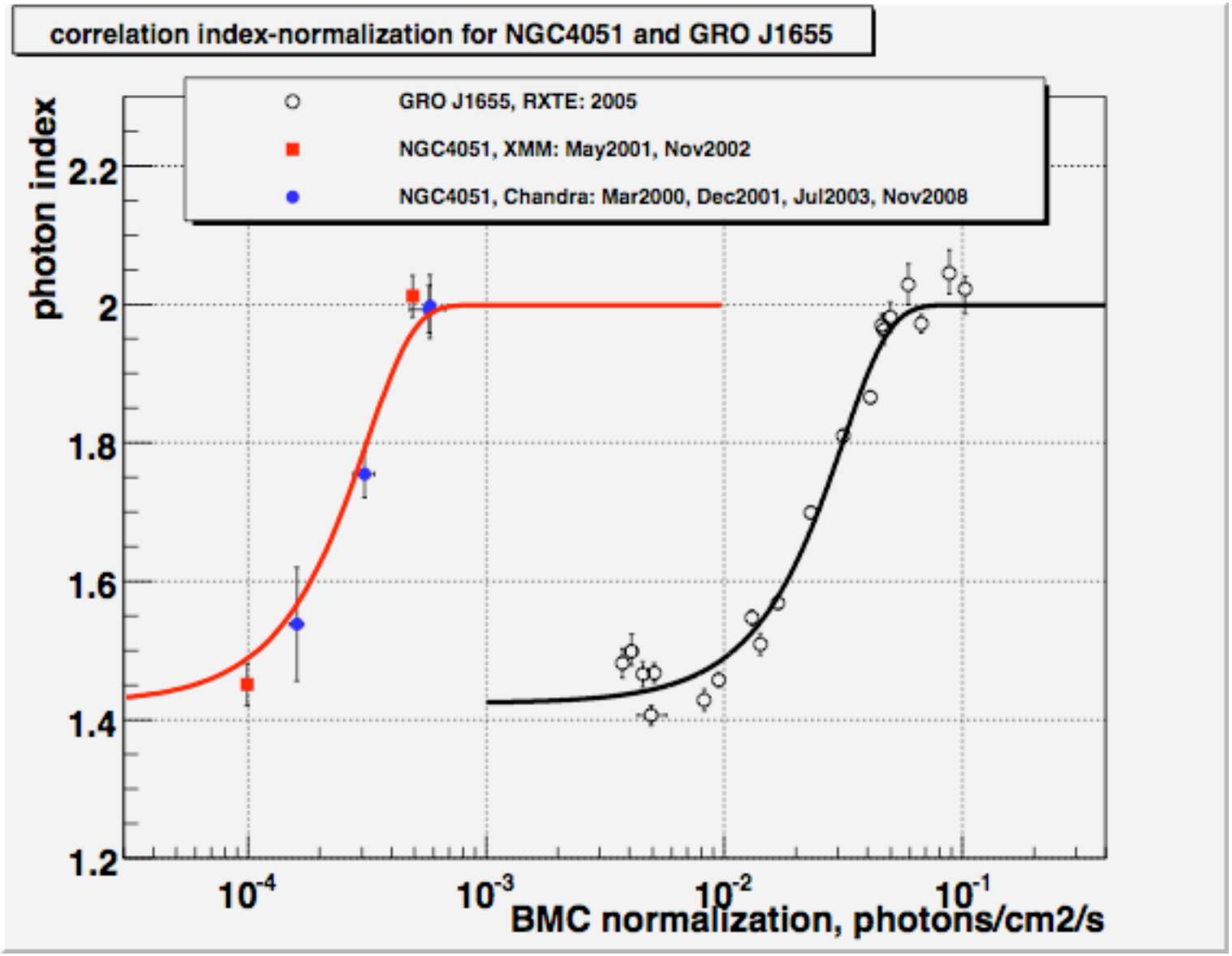

Shekhtman & T, 2010

The scaling method vs other methods BH masses and distances

Source	M_{dyn}[a], $M_\odot$	i,[a] deg	d,[b] kpc	M_{ST03}[c] $M_\odot$	M_{scal} $M_\odot$	d_{scal}, kpc	Refs.
GRO J1655-40[d]	6.3±0.3	70±1	3.2±0.2				1,2
GX 339-4	> 6	-	7.5±1.6	9.0±3.8(4)	12.3±1.4	5.75±0.8	5,6
4U 1543-47	9.4±1.0	20.7± 1.5	7.5±1.0	14.8±1.6 (6.4)	9.4±1.4	9.4±1.8	7,8
XTE J1550-564	9.5±1.1	72±5	∼2.5,∼6	9.4±2.1 (5)	10.7±1.5	3.3±0.5	9,10,11
XTE J1650-500	$2.7 - 7.3$	> 50	2.6±0.7	10.6±4.0 (5)	9.7±1.6	3.3±0.7	12,13
H 1743-322	∼11	~ 70	∼10	-	13.3±3.2	9.1±1.5	14
XTE J1859-226	7.6 - 12.0	-	11	12.3±1.7 (11)	7.7±1.3	4.2±0.5	15,16
Cygnus X-1	6.8 - 13.3	35± 5	2.5±0.3	-	7.9±1.0	2.2±0.3	3,4

[a]Dynamically determined BH mass and system inclination

[b]Source distances found in literature

[c]$M_i = M \cos_i$. Source distances used by ST03 are given in paranthesis.

[d]GRO J1655-40 is a primary reference source. All masses and distances given in columns 9 and 10 are determined with respect to the best measured parameters for this source.

References. — [1]Green, Bailyn & Orosz (2001),[2]Hjellming & Rupen (1995),[3]Herrero et al. (1995),[4]Ninkov et al. (1987),[5]Muñoz-Darias et al. (2008),[6]Hynes et al. (2004),[7]Orosz (2003),[8]Park et al. (2004),[9]Orosz et al. (2002),[10]Sánchez-Fernández et al. (1999),[11]Sobczak et al. (1999),[12]Orosz et al. (2004),[13]Homan et al. (2006),[14]McClintock et al. (2007),[15]Filippenko & Chornock (2001),[16]Zurita et al. (2002)

- What is the nature of the observed correlations?
  - Observed properites
    - QPO requency is correlated with power law index
    - Index saturates for high values of QPO frequency
    - QPO frequency is correlated with source luminosity (~dM/dt)
  - Physics: first principles
    - QPO frequency is inversely proportional to size
    - Index is inverse proportional to Comptonization efficiency (parameter)
    - Photon trapping effect in the converging flow suppresses the Comptonization efficiency for higher dM/dt
- What does it mean?
  - Correlation curves should scale as $1/M_{BH}$
  - Saturation is a BH signature

Summary

1. A new method for evaluation of the BH mass using this observable index-QPO frequency [mass accretion rate (Mdot)] correlation is demonstrated.

2. In the soft state this index-QPO and Mdot correlations show the saturation to the photon index at high values of the low frequency which are identified as a black hole signature. This index saturation is an observational evidence of existence of the converging flow in BH sources.

3. On the other hand in the soft state of NS sources the index is not saturated with QPO frequency (Mdot). It monotonically increases when QPO frequency increases. Finally the emergent spectrum is a sum of two BB components, one is related to NS and another one to disk.

Likely scenario

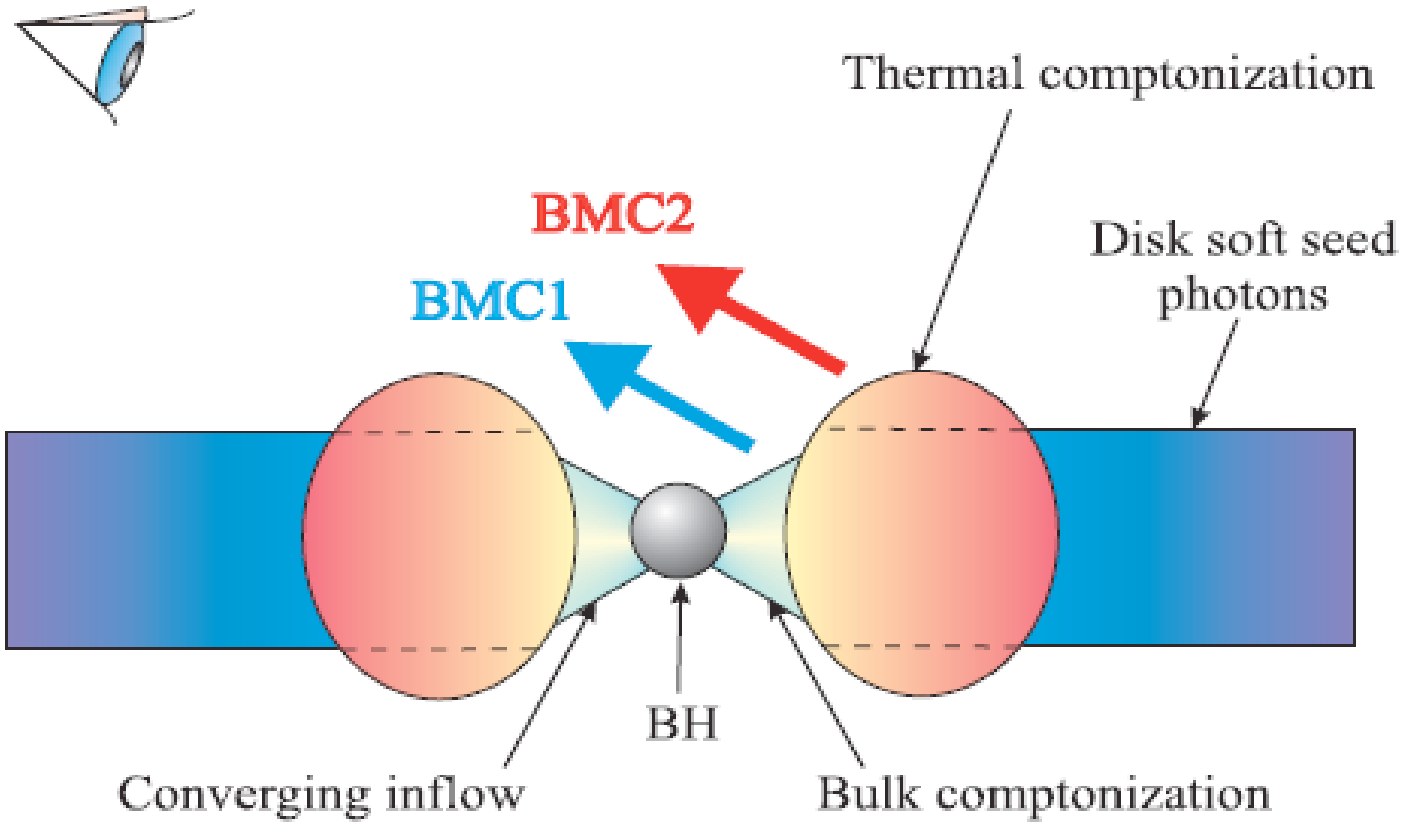

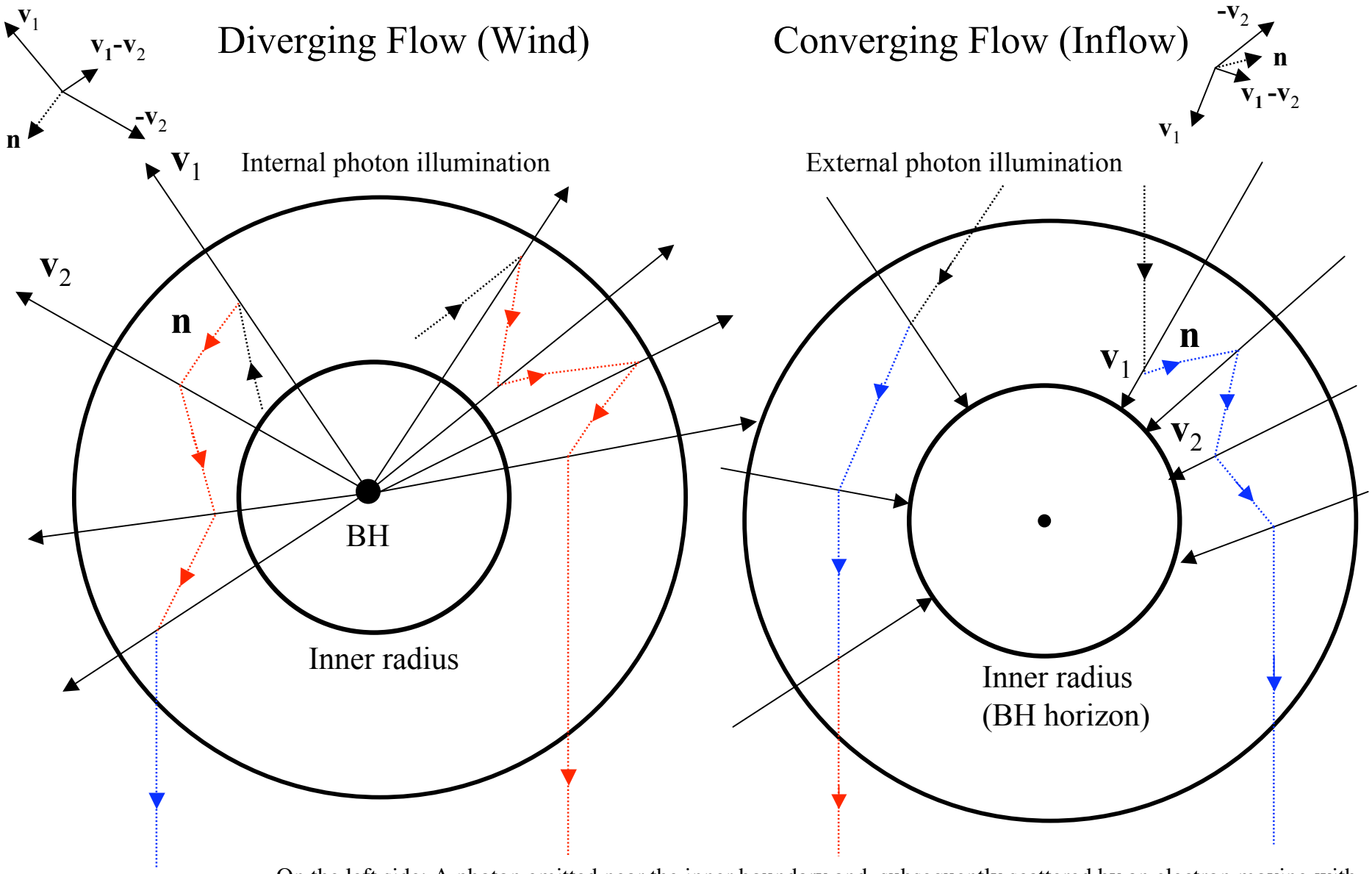

On the left side: A photon emitted near the inner boundary and subsequently scattered by an electron moving with velocity $\mathbf{v}_1$, impinges on an electron moving with velocity $\mathbf{v}_2$ as shown. The change in frequency is $\nu_2 = \nu_1 [1 + (\mathbf{v}_1 - \mathbf{v}_2) \bullet \mathbf{n}/c]$. In a diverging flow $(\mathbf{v}_1 - \mathbf{v}_2) \bullet \mathbf{n}/c < 0$ and photons are successively redshifted, until scattered to an observer at infinity. The color of photon path indicates the frequency shift in the rest frame of the receiver (electron or the Earth observer). On the right side: In a converging flow $(\mathbf{v}_1 - \mathbf{v}_2) \bullet \mathbf{n}/c > 0$ and photons are blueshifted.

Transition Layer. Scaling method I.

The radial motion in the disk is controlled by friction and the angular momentum exchange between adjacent layers, resulting in the loss of the initial angular momentum by accreting matter. The corresponding radial transport of the angular momentum in a disk is described by the following equation [see e.g. Shakura & Sunyaev (1973)]:

$$\dot{M}\frac{d}{dR}(\omega R^2) = 2\pi\frac{d}{dR}(W_{r\varphi}R^2), \tag{1}$$

where $\dot{M}$ is the accretion rate in the disk and $W_{r\varphi}$ is the component of a viscous stress tensor that is related to the gradient of the rotational frequency $\omega = 2\pi\nu$, namely,

$$W_{r\varphi} = -2\eta H R\frac{d\omega}{dR}, \tag{2}$$

where H is a half-thickness of a disk and η is turbulent viscosity. The nondimensional parameter that is essential for equation (1) is the Reynolds number for the accretion flow,

$$\gamma = \dot{M}/4\pi\eta H = RV_r/D, \tag{3}$$

where V_r is a characteristic velocity, and D is the diffusion coefficient. D can be defined as $D = V_t l_t/3$ using the turbulent velocity and the related turbulent scale, respectively or as $D = D_M = c^2/\sigma$ for the magnetic case where σ is the conductivity [e.g. see details of the D-definition in Lang (1998)].

Transition Layer. Scaling method II.

Equations $\omega = \omega_0$ at $R = R_{in} = bR_S$ (at the inner TL radius), $\omega = \omega_K$ at $R = R_{out}$ [the radius where the transition layer adjusts to the Keplerian motion for which $\omega_K = (GM/R^3)^{1/2}$], and $d\omega/dR = d\omega_K/dR$ at $R = R_{out}$ were assumed by TLM98 to be the boundary conditions. Note that here we set the inner boundary at $R_{in} = bR_S$ with b of 3. This value of R_{in} can valid for a BH which spin a is less than 0.8.

Thus, the profile $\omega(R)$ and the outer radius of the transition layer are uniquely determined by the boundary conditions and the angular momentum equation (1-2) for a given value of the Reynolds number γ (see Eq. 3).

The solution of angular momentum equation (1-2) satisfying the above boundary conditions is equation (10) in TLM98 and the equation (see TLM98, Eq. 11)

$$3\theta_{out}/2 = D_1\gamma r_{out}^{-\gamma} + 2(1 - D_1)r_{out}^{-2} \tag{4}$$

determines $r_{out} = R_{out}/R_{in}$ as a function of $\gamma-$parameter, where $\theta_{out} = \omega_k(r_{out})/\omega_0$ and $D_1 = (\theta_{out} - r_{out}^{-2})/(r_{out}^{-\gamma} - r_{out}^{-2})$. The adjustment of the Keplerian disk to the sub-Keplerian inner boundary creates conditions favorable for the formation of a hot plasma outflow at the outer boundary of the transition layer (TLM98), because the Keplerian motion (if it is followed by sub-Keplerian motion) must pass through a super-Keplerian centrifugal barrier region.

Angular velocity profile in transition layer

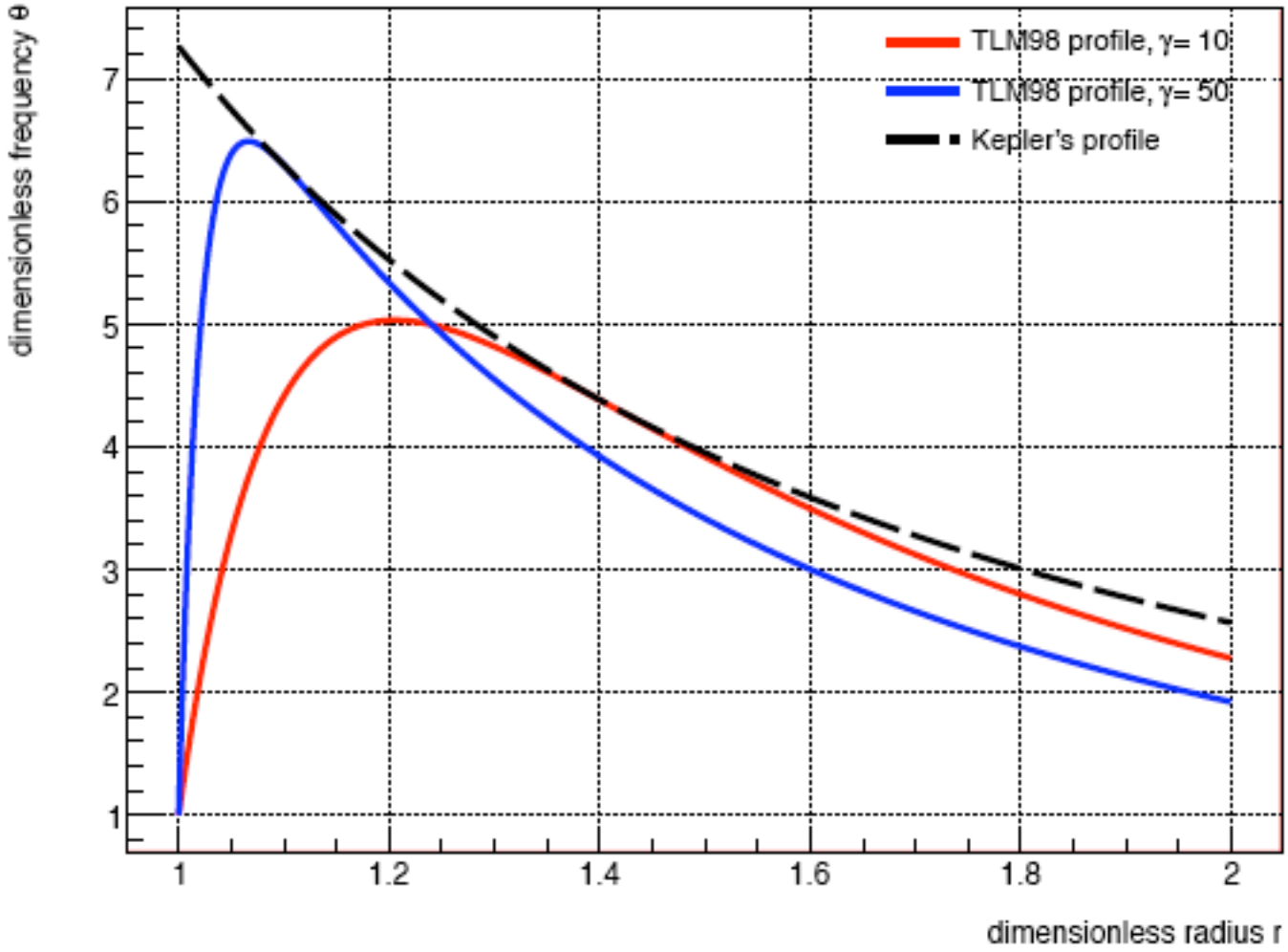

Transition Layer. Scaling method III.

The TLM98 numerical calculations of Eq. (4) (see Fig. 2 there) showed that the value of dimensionless outer radius r_{out} strongly depends on $\gamma-$parameter ($Re-$number) and independent of θ_{out} for $\theta_{out} >> 1$, i.e when the rotational velocity of central of object ω_0 is less of that at the TL outer boundary $\omega_{\rm K}$. In fact, one can see that the right hand side of Eq. (4) is linearly proportional to θ_{out} if $\theta_{out} \gg 1$ because $D_1 \propto \theta_{out}$ and $|D_1/r_{out}^2| \gg 1$ for $\theta_{out} \gg 1$ and $\gamma > 2$. As a result θ_{out} can be canceled from left and hand sides of Eq. (4) when $\theta_{out} \gg 1$.

It implies the CC dimensionless size $l_{cc} = (R_{out} - R_{in})/R_{in} = r_{out} - 1$ is a function $\gamma-$parameter ($Re-$number) only in the case of $\theta_{out} \gg 1$. Namely, given that $Re-$number determines the spectral state (see TLM98 and TL04) *that CC dimensionless size l_{cc} is the same for any given spectral state of BH even if BH masses differ by orders of magnitude.* Thus the CC dimensional size $L_{cc} = bR_{\rm S}l_{cc}(\gamma) \approx 9l_{cc}(\gamma)m$ km is just proportional to BH mass $m = M/M_\odot$ for a given spectral state (or γ).

It is worth noting that in the general case of non-dimensional frequency θ $(= \omega_{\rm K}/\omega_0)$ the size l_{cc} is a function of γ and ω_0 (or a BH spin a) too. The direct scaling of $L_{cc} = bR_{\rm S}l_{cc}(\gamma, a)$ with BH mass m is not possible anymore. There is a systematic shift of the values of $l_{cc}(\gamma, a)$ for a given γ because of BH spin a.

BH mass and distance determinations

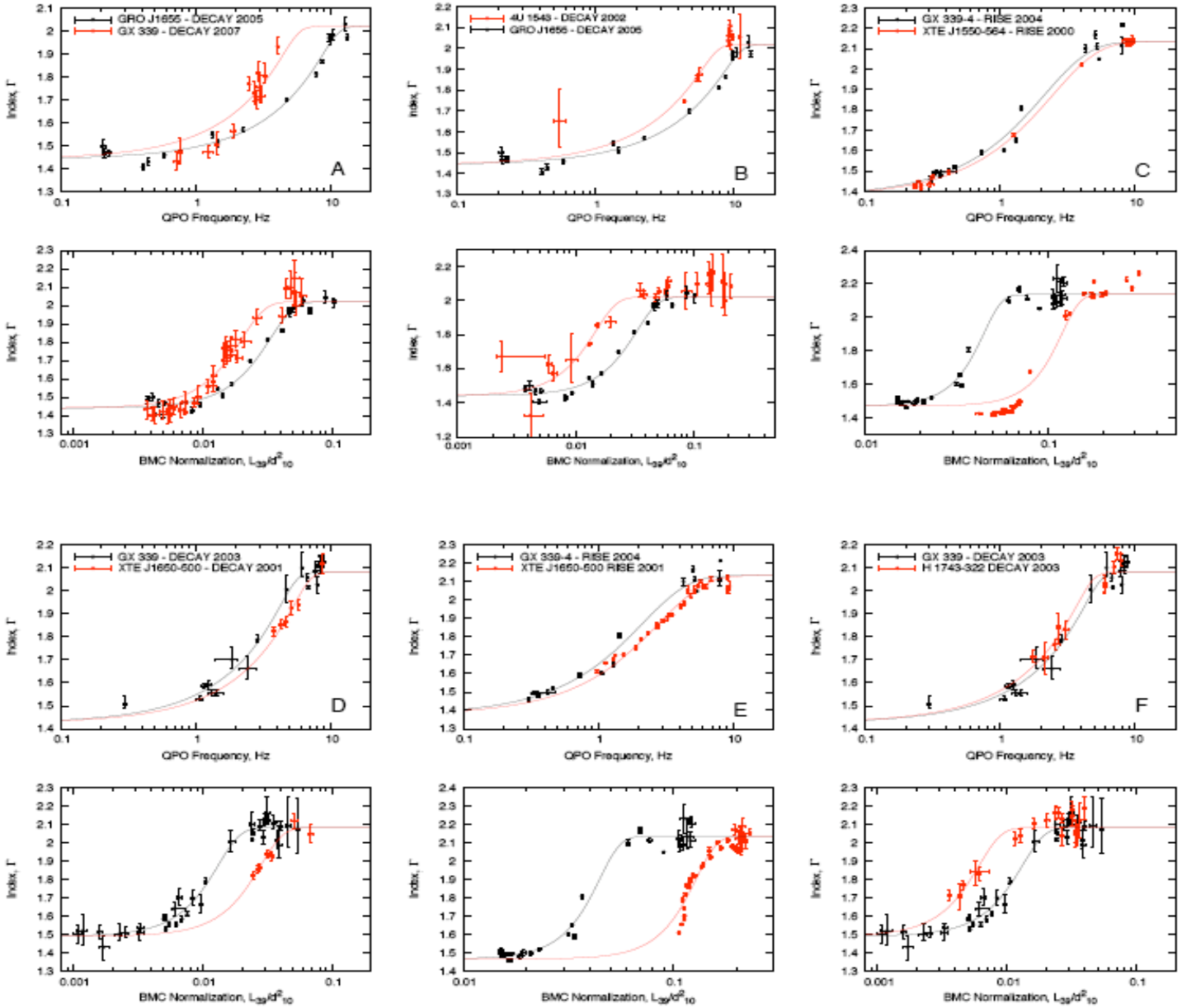

Shaposhnikov &T (2008)

PDS - harder part (blue) and softer part (red) of Hard State of XTE-J1650 (TOO1)

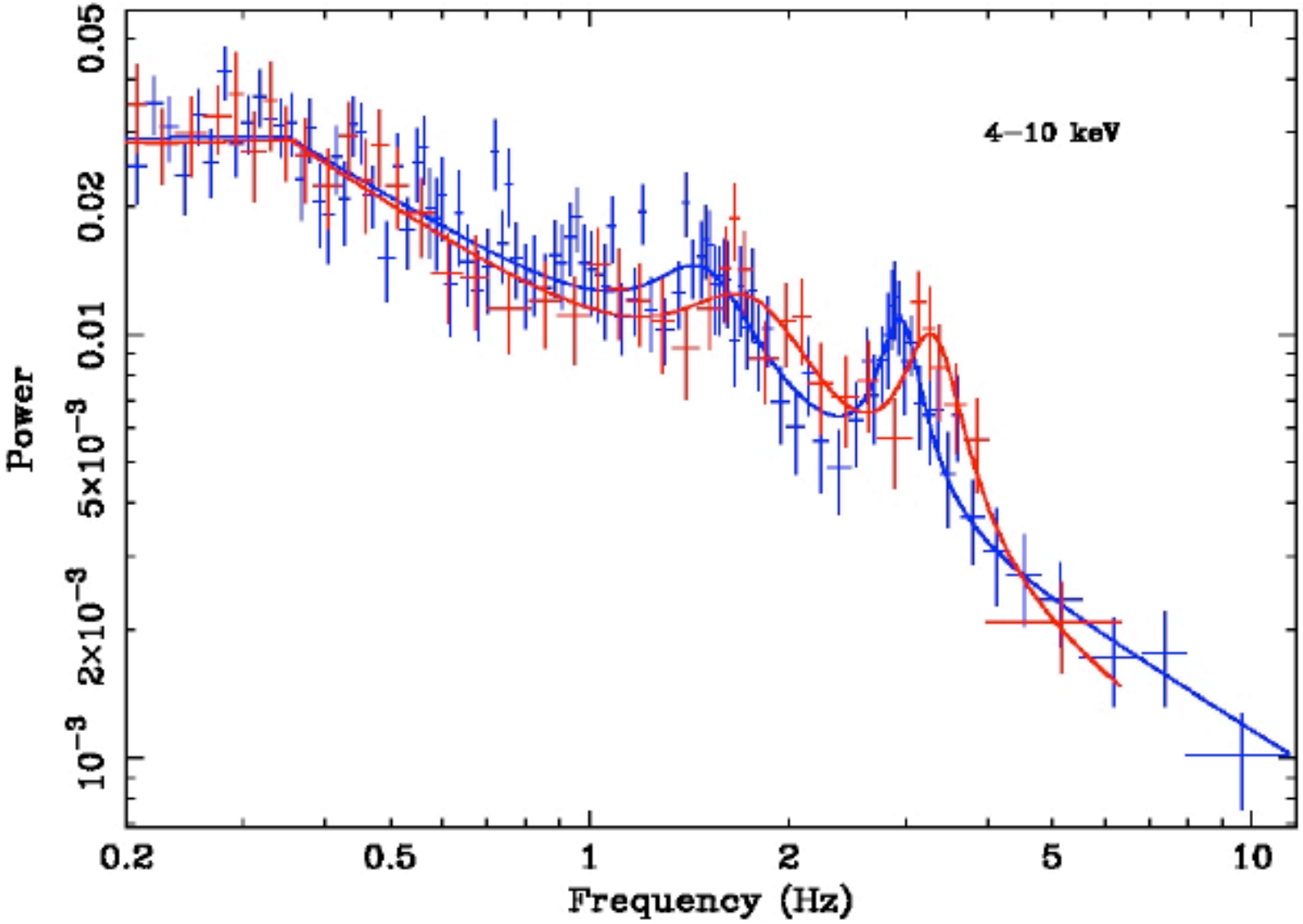

Montanari, T & Frontera 2006

BH XTE J1650-500. BeppoSAX

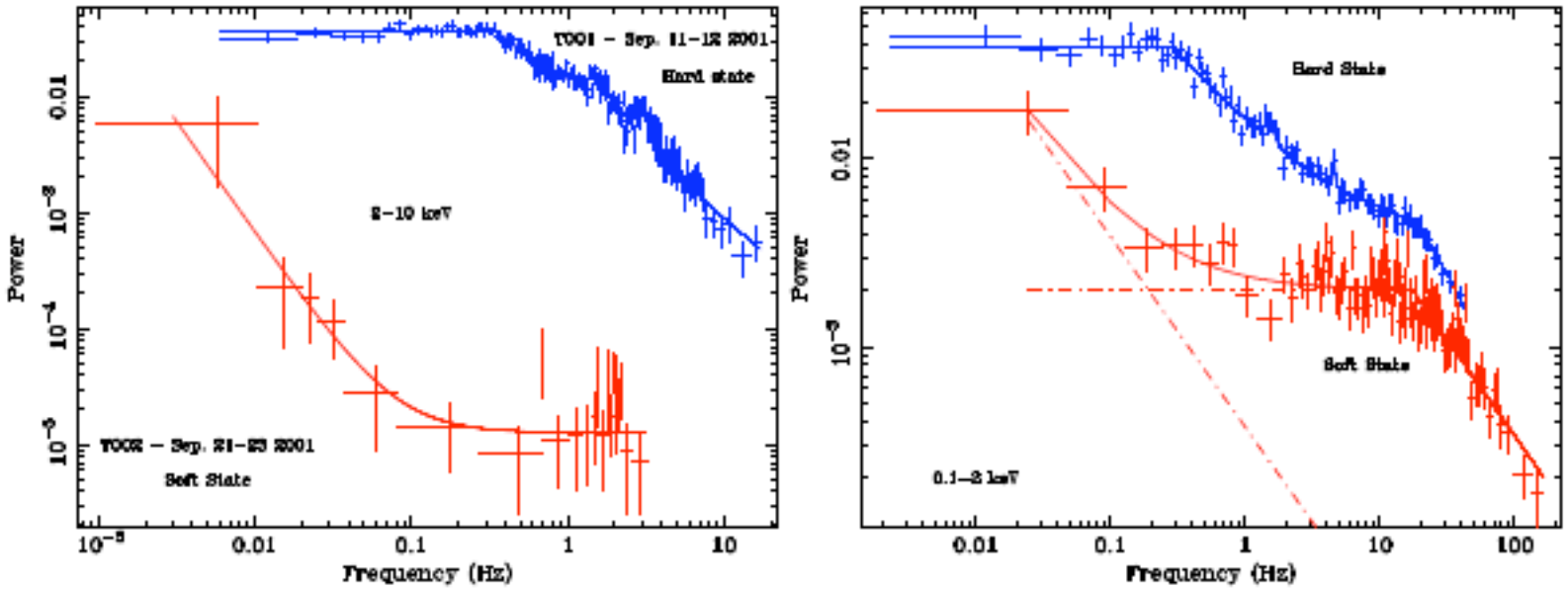

Fig. 7.— LHS PS (blue) vs that of HSS PS (red) for two different energy bands: 2-10 keV (*left panel*) and 0.12-2 keV (*right panel*). The HSS PS are fit with the sum of two broken power–laws in the case of the 0.1–2 keV energy band, while it is fit with the sum of a power-law and a constant in the 2-10 keV energy band. It is apparent that the relative power of the HSS PS (with respect to LHS PS) strongly depends on the energy band.

Montanari, T & Frontera 2008

Simultaneous Power and energy spectra evolution

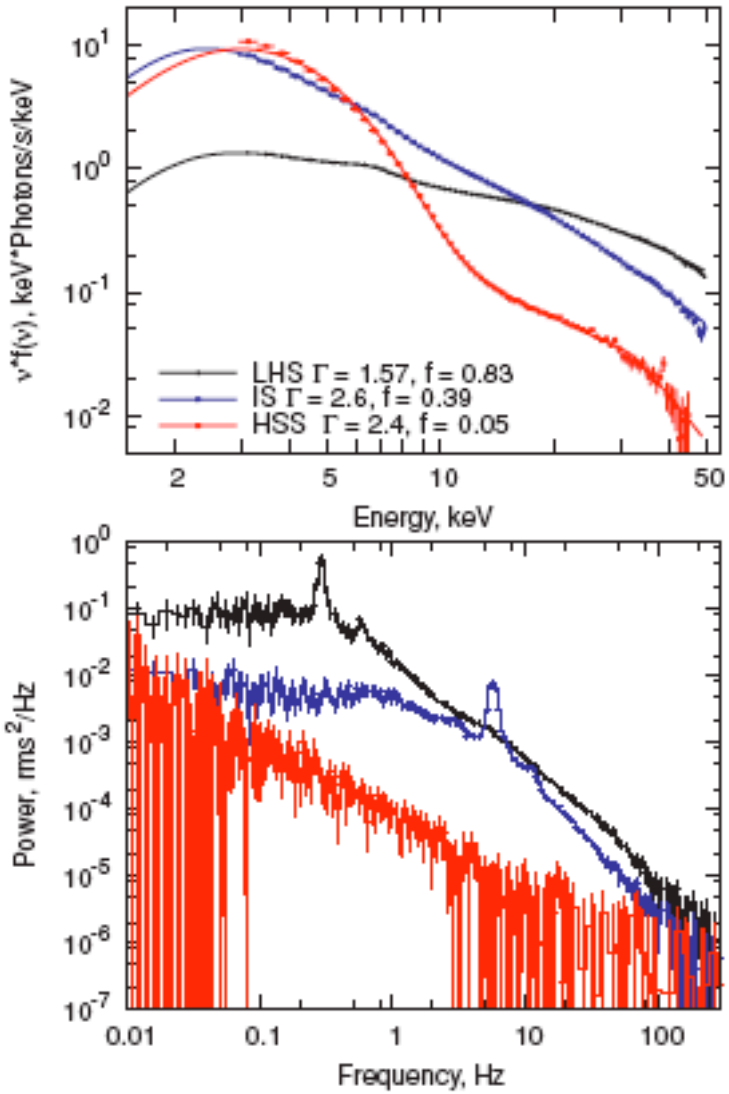

Figure 1. Three representative energy (top) and power (bottom) spectra during the rise part of the 1998 outburst of XTE J1550−564. Data are taken from *RXTE* observations 30188-06-01-00 (red), 30188-06-01-00 (blue), and 30191-01-05-00 (black). In the top panel, the solid curves correspond to the best-fit model spectra.

NASA PRESS RELEASE

NASA Scientists Pioneer Technique for "Weighing" Black Holes
05.09.07

Two astrophysicists at NASA's Goddard Space Flight Center in Greenbelt, Md., Nikolai Shaposhnikov and Lev T, have successfully tested a new method for determining the masses of black holes.

This elegant technique, which Lev T. first suggested in 1998, shows that the black hole in a binary system known as Cygnus X-1 contains 8.7 times the mass of our sun, with a margin of error of only 0.8 solar mass.

Working independently, Tod Strohmayer and Richard Mushotzky of Goddard and four colleagues used T's technique to estimate that an ultra-luminous X-ray source in the small, nearby galaxy NGC 5408 harbors a black hole with a mass of about 2,000 suns.

BH SPECTRUM OF CONVERGING FLOW

1. INTRODUCTION

Do black holes interact with an accretion flow in such a way that a distinct observational signature that is entirely different from those associated with any other compact object exists? In other words, can the existence of a black hole be solely inferred from the radiation observed at infinity?

The distinct feature of black hole spacetime, as opposed to the spacetimes due to other compact objects, is the presence of the event horizon. Near the horizon, the strong gravitational field is expected to dominate the pressure forces and thus to drive the accreting material into a free fall.

We investigate the particular case of a nonrotating Schwartzschild black hole powering the accretion, leaving the case of a rotating black hole.

We demonstrate that the power-law spectra are produced when low- frequency photons are scattered in the Thomson regime.

Radiative Transfer Formalism and photon trajectories in the Schwarzchild background

We consider background geometry described by the following line element:

$$ds^2 = -f dt^2 + dr^2 / f + r^2 d\Omega^2$$

where $f = 1 - r_s / r.$

We can write the full relativistic kinetic equation for occupation number N(**r,**E) in the Lab frame of reference which operator form is

$$\mu\sqrt{f}\frac{\partial N}{\partial r} - E\mu\frac{\partial\sqrt{f}}{\partial r}\frac{\partial N}{\partial E} - (1-\mu^2)\left(\frac{\partial\sqrt{f}}{\partial r} - \frac{\sqrt{f}}{r}\right)\frac{\partial N}{\partial \mu} = S(N)$$

This equation assumes the separation of variables for Thomson regime of scattering $N=E^{-(3+\alpha)}J(\mathbf{r})$. The photon trajectories can be found as characteristics of the integrodifferential equation for J:

$$\frac{x(1-\mu^2)^{1/2}}{(1-x^{-1})^{1/2}} = p$$

It is seen from here that for p=6.75 and x=3/2

$$\mu = 0.$$

Namely we deal with a perfect circular orbits at x=3/2 (3M).

2. THE MAIN EQUATION

We begin by considering background geometry, described by the following line element:

$$ds^2 = -f\,dt^2 + \frac{dr^2}{f} + r^2\,d\Omega^2 \ , \tag{1}$$

where, for the Schwarzschild black hole, $f = 1 - r_s/r$, $r_s = 2GM/c^2$, and t, r, θ, and φ are the event coordinates with $d\Omega^2 = d\theta^2 + \sin^2\theta\,d\varphi^2$. G is the gravitational constant, and M is the mass of a black hole.

Taking into account only Compton scattering of photons off the background electrons, one may covariantly write the transfer equation

$$p^\alpha \frac{DN}{dx^\alpha} = \int N(r, P')\kappa(x, \boldsymbol{p}')\zeta(x; \boldsymbol{p}' \to \boldsymbol{p})dP' - N(r, P)\int \kappa(x, \boldsymbol{p}')\zeta(x; \boldsymbol{p} \to \boldsymbol{p}')dP' \ . \tag{2}$$

By rewriting for the orthonormal frame of equation (1) we obtain the following kinetic equation:

$$\mu\sqrt{f}\,\frac{\partial N}{\partial r} - \nu\mu\,\frac{\partial\sqrt{f}}{\partial r}\,\frac{\partial N}{\partial \nu} - (1-\mu^2)\left(\frac{\partial\sqrt{f}}{\partial r} - \frac{\sqrt{f}}{r}\right)\cdot\frac{\partial N}{\partial \mu}$$

$$= \int_0^\infty dv_1 \int_{4\pi} d\Omega_1 \left[\left(\frac{v_1}{v}\right)^2 \sigma_s(v_1 \to v, \xi) N(v_1, \mu_1, r) - \sigma_s(v \to v_1, \xi) N(v, \mu, r)\right]. \quad (3)$$

3. THE METHOD OF SOLUTION

3.1. *Separation Variables*

As long as the ejected low-energy photons satisfy $z_0 = h\nu_0/m_e c^2\gamma \ll 1$, the integration over incoming frequencies, ν_0, is trivially implemented provided that the explicit function of $N(r, \nu_0, \nu, \mathbf{\Omega})$ is known. Thus, we need to describe the main properties of Green's function, $N(r, \nu_0, \nu, \mathbf{\Omega})$, in a situation where the low-energy photons are injected into the atmosphere with the bulk motion.

$$N(r,\ v,\ \mathbf{\Omega}) = v^{-(3+\alpha)} J(r,\ \mu)\ . \tag{4}$$

Then we can formally get from equation (3) that

$$\mu\sqrt{f}\frac{\partial J}{\partial r} + (\alpha + 3)\mu\frac{\partial\sqrt{f}}{\partial r}J - (1-\mu^2)\left(\frac{\partial\sqrt{f}}{\partial r} - \frac{\sqrt{f}}{r}\right)\frac{\partial J}{\partial \mu}$$

$$= n_e \sigma_{\mathrm{T}}\left[-J + \frac{1}{4\pi}\int_{-1}^{1} d\mu_1 \int_{0}^{2\pi} d\varphi R(\xi) J(\mu_1,\ \tau)\right]. \tag{5}$$

Here the phase function, $R(\xi)$, is as follows:

$$R(\xi) = \frac{3}{4}\int_0^{\pi} \sin\ \theta\, d\theta \int d^3\boldsymbol{v}\ \frac{F(r,\ P_e)}{\gamma^2}\left(\frac{D_1}{D}\right)^{\alpha+2}\frac{1}{D_1} \tag{6}$$

$$\times\ [1 + (\xi')^2]\ ,$$

where ξ' is the cosine of the scattering angle between photon incoming and outgoing directions in the electron rest frame. The reduced integrodifferential equation is two dimensional, and it can be treated and solved much more easily than the original equation (eq. 3). The whole problem is reduced to the eigenvalue problem for equation (5). We can not claim that the kinetic equation allows a power-law solution (eq. 4) unless first α is found and $J(r, \mu)$ is specified.

3.2. *Photon Trajectories and the Characteristics of the Space Operator, ℓ*

The characteristics of the differential operator, ℓ, are determined by the following differential equation:

$$\left[-\frac{1}{2x^2(1-x^{-1})} + x^{-1} \right] dx = d[\ln(1-\mu^2)^{-1/2}] , \tag{7}$$

where $x = r/r_s$ is a dimensionless radius. The integral curves of this equation (the characteristic curves) are given by

$$\frac{x(1-\mu^2)^{1/2}}{(1-x^{-1})^{1/2}} = \frac{x_0(1-\mu_0^2)^{1/2}}{(1-x_0^{-1})^{1/2}} = p , \tag{8}$$

We can resolve equation (8) with respect to μ to get

$$\mu = \pm(1-p^2/y^2)^{1/2} , \tag{9}$$

where $y = x^{3/2}/(x-1)^{1/2}$. The graph of y as a function of x is presented in Figure 1, which allows us to comprehend the possible range of radii for the given impact parameter, p, through the inequality $p \leq y$. For example, if $p \leq (6.75)^{1/2}$, then the photon can escape from the inner boundary (the black hole horizon) toward the observer or vice versa; all photons going toward the horizon having these impact parameters are gravitationally attracted by the black hole.

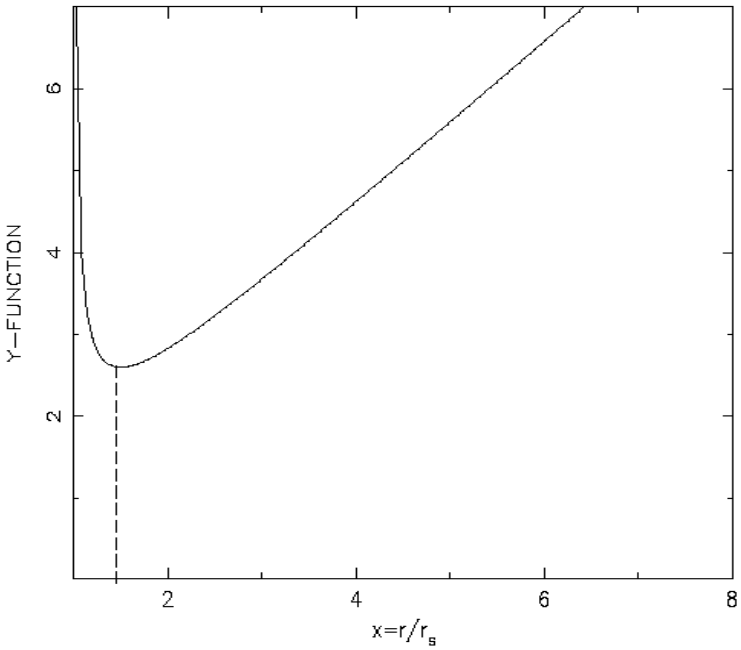

FIG. 1.—Plot of the photon trajectory phase space: the phase-space function, y, vs. the dimensionless radius, $x = r/r_s$.

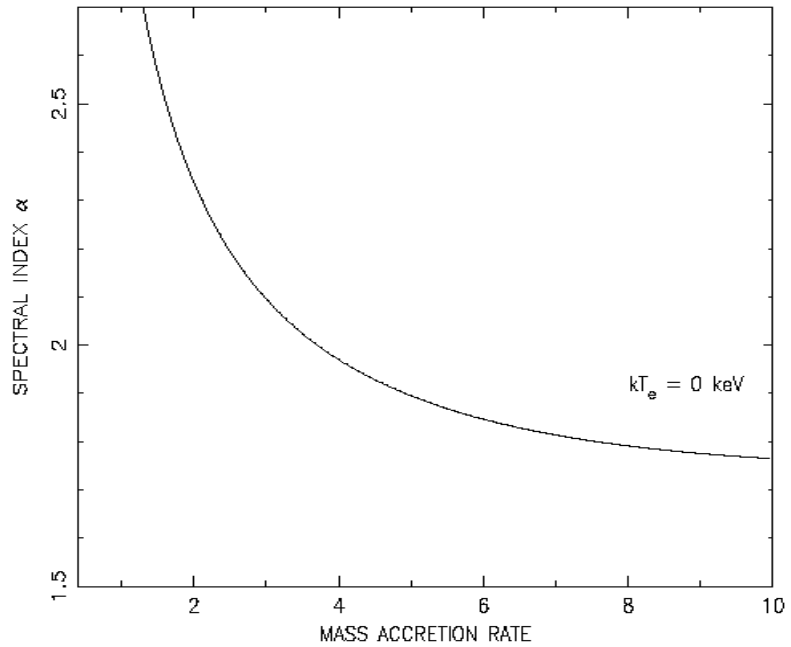

FIG. 2.—Plot of the energy spectral index (photo index — 1) vs. the total mass accretion rate.

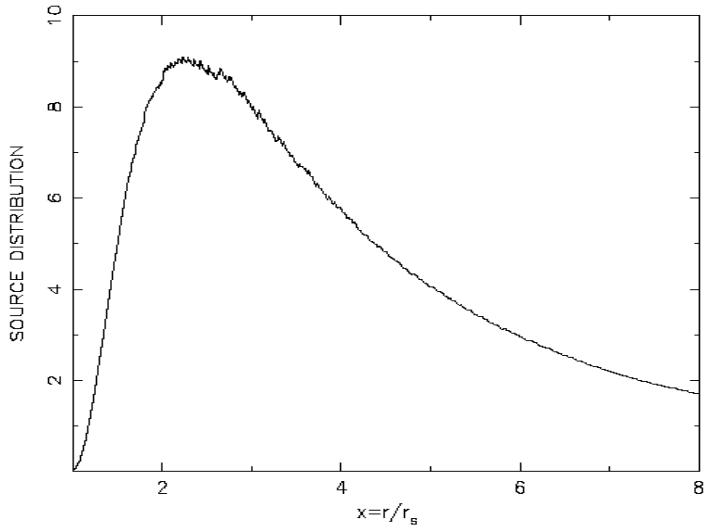

FIG. 3.—Plot of the source function distribution, eq. (B1), in arbitrary units vs. the dimensionless radius, $x = r/r_s$, for the dimensionless mass accretion rate, $\dot{m} = 4$, and $\mu = 0$.

T & Zannias (1998)

Soft State Model Picture: The "Drain"

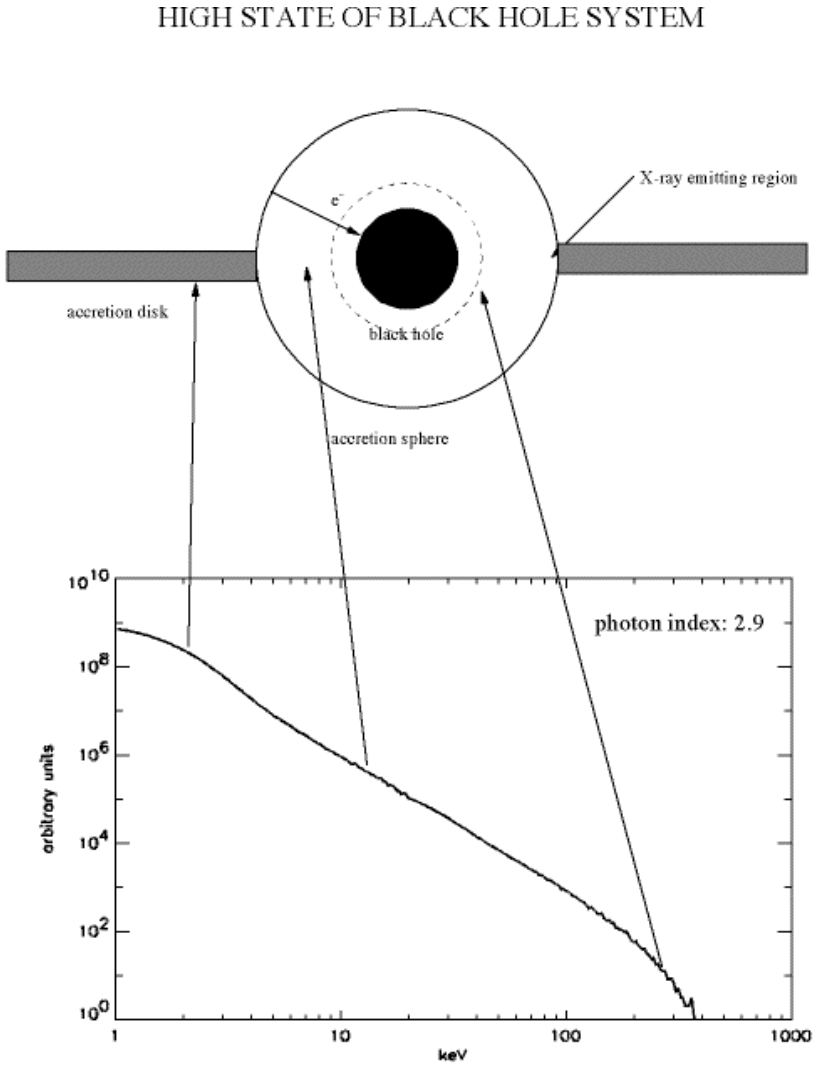

From: Laurent & T, 2001

- Gravitational attraction of BH in presence of plenty of accreting mass develops mass accretion flow rate of order of Eddington.
- At such a high mass accretion rate a specific X-ray spectrum is formed as a result of the photon trapping effect.
  - Photon is trapped by the accretion flow, as it attempts to diffuse out of the hot accreting plasma
  - Result: steep spectrum, low Compton upscatter efficiency.

The photon index varies from 2.5-2.8 depending on the temperature of the flow. The soft photon component is characterized by blackbody-like spectrum that temperature is around 1 keV (for galactic sources) and 10-50 eV for extragalactic sources – UV bump.

Scattering events in the flow

Doppler effect

$$\frac{\nu'}{\nu} = \frac{1 - \mu_1 V/c}{1 - \mu_2 V/c}$$

where $\mu_1 = \bar{\Omega}_1 \bullet (\bar{V}/V)$ and $\mu_2 = \bar{\Omega}_2 \bullet (\bar{V}/V)$

For highly relativistic speeds

$$\theta_2 = \arccos \mu_2 \approx 1/\gamma, \quad V/c = 1 - 1/2\gamma^2$$ and

$$\frac{\nu'}{\nu} = (1 - \mu_1)\gamma^2$$

Source Photon Spatial Distribution in CI Atmosphere

Our Monte Carlo simulations (Laurent & T 2001) reproduce the source function spatial distribution: 2-5 keV (curve a), 5-13 keV (curve b), 19-29 keV (curve c), and 60-150 keV (curve d).

- We confirm the analytical results that the density of the highest energy X-ray photons is concentrated near the BH horizon.

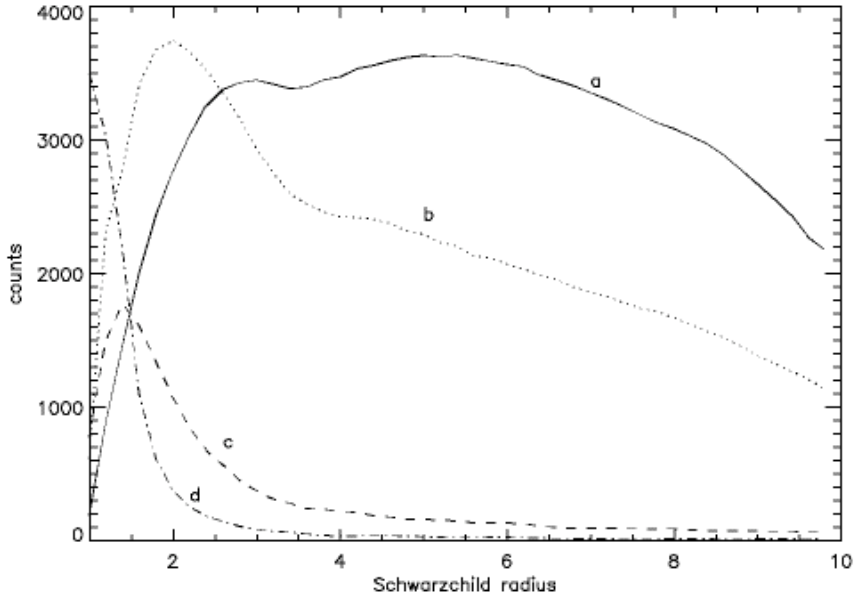

BH QPO feature

Upper panel: Distribution of soft photons over disk radius, which upscatters to energies 10 keV and higher in the atmosphere.
Lower panel : PDS for photon energies higher then 10 keV. It is assumed that any disk annulus oscillates with Keplerian frequency (Laurent & T 2001).

- **There is a striking similarity between the QPO frequency of the MC results and real observation of BH.**

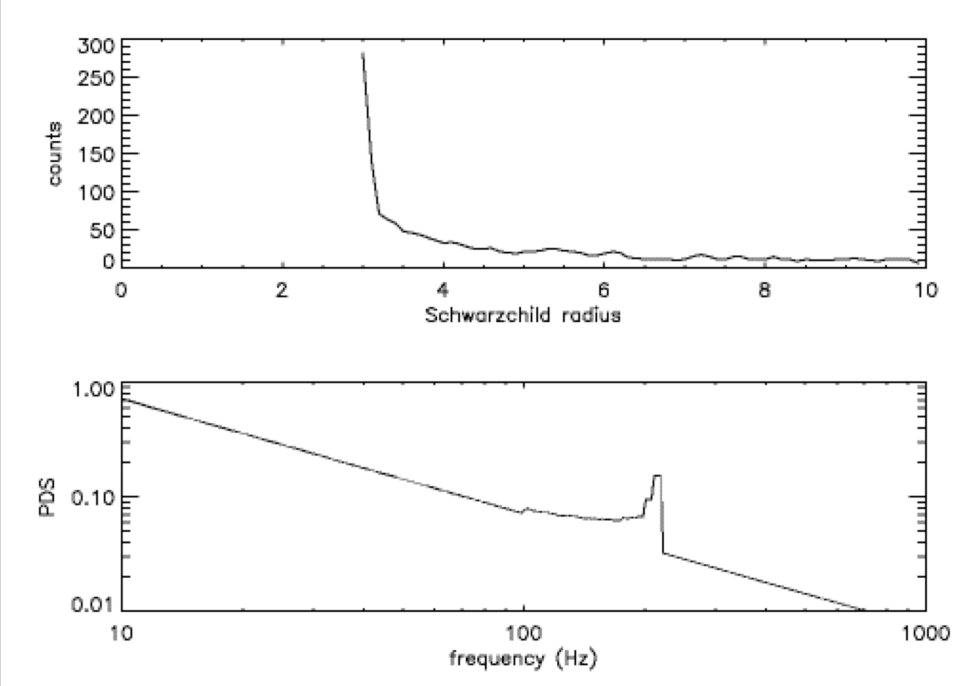

Photon trajectories in the converging flow

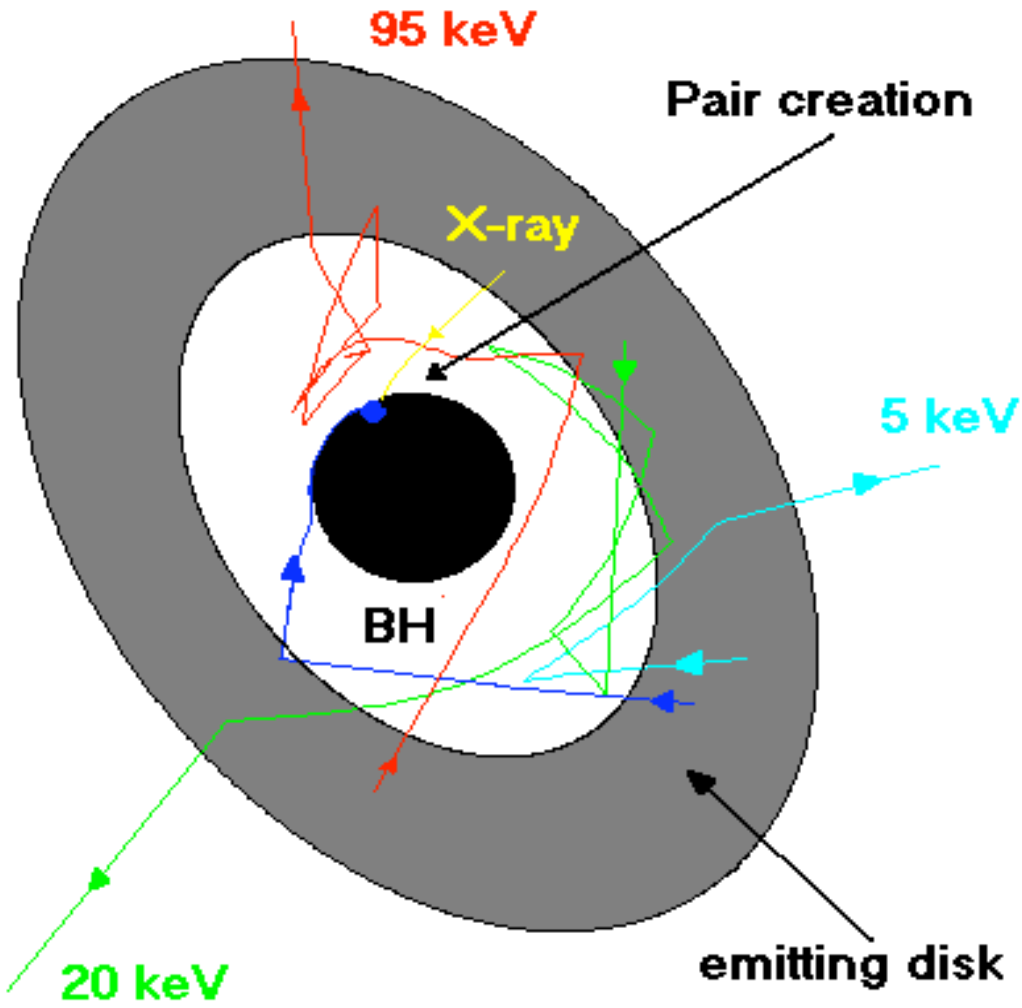

Space distribution of created pairs

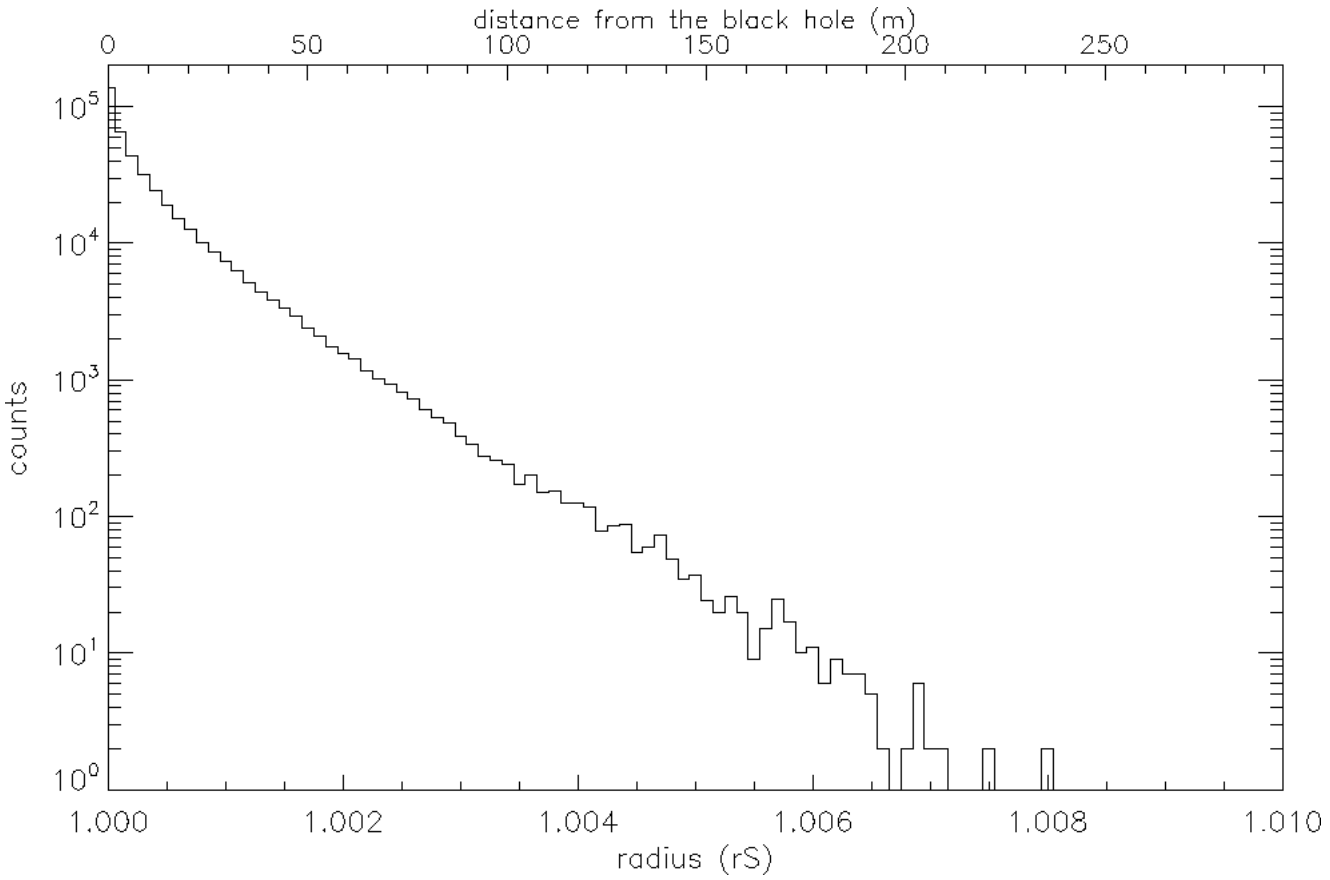

Emergent spectrum in high/soft state of BHs

kT_{seed}=1 keV

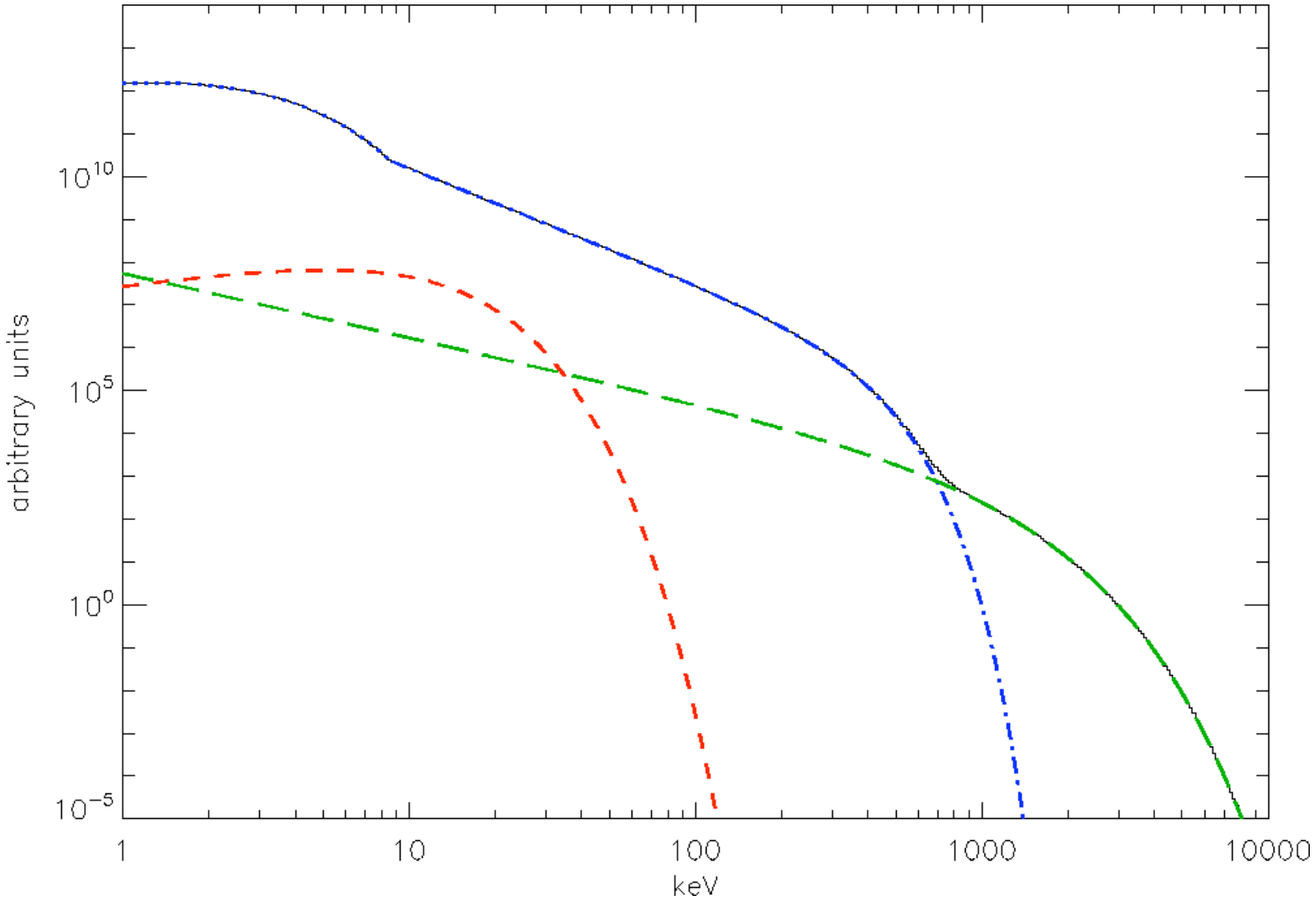

Gravitationally redshifted annihilation line feature

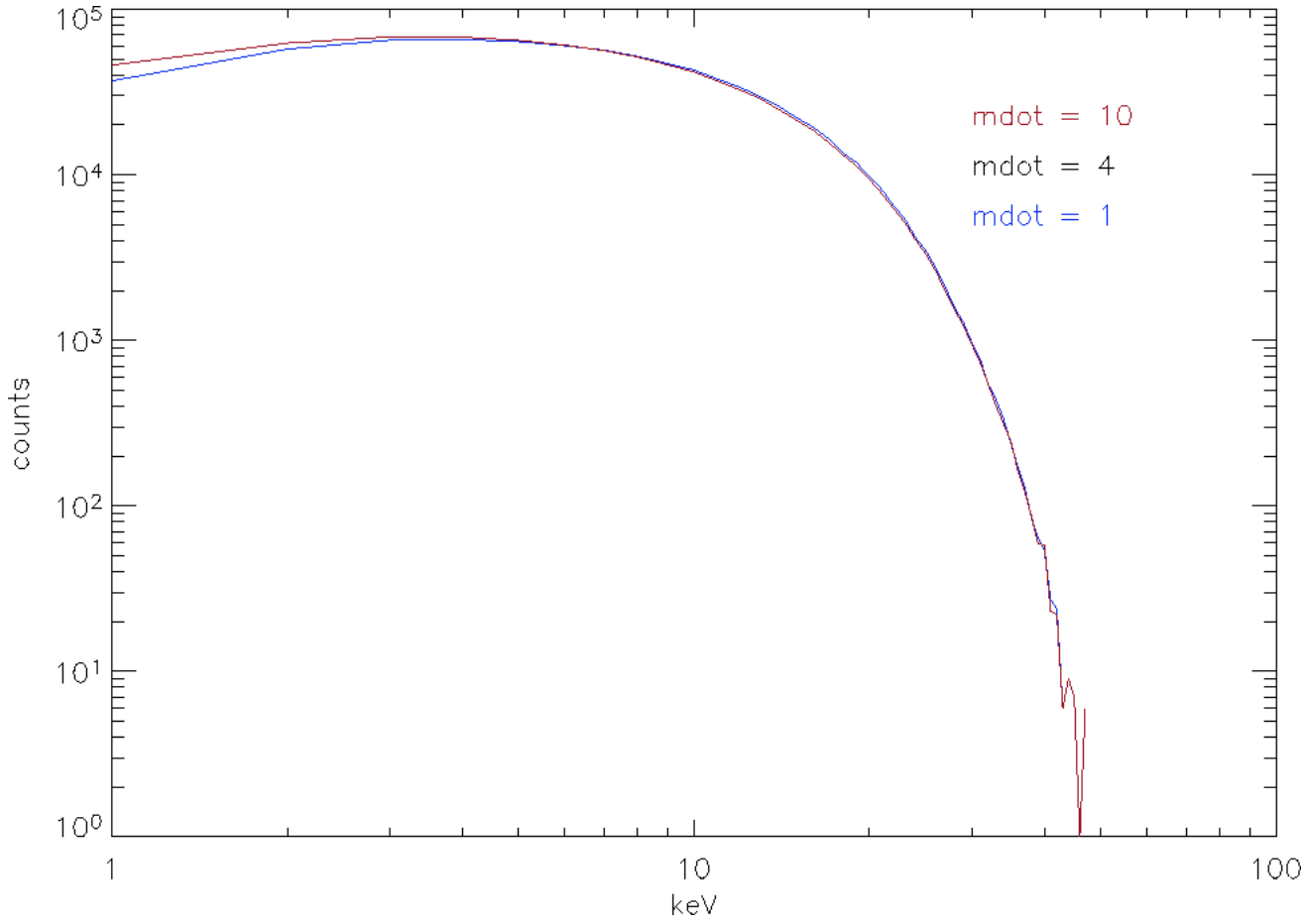

Laurent & T (2006)

GRS 1915+105 spectrum of intermediate state

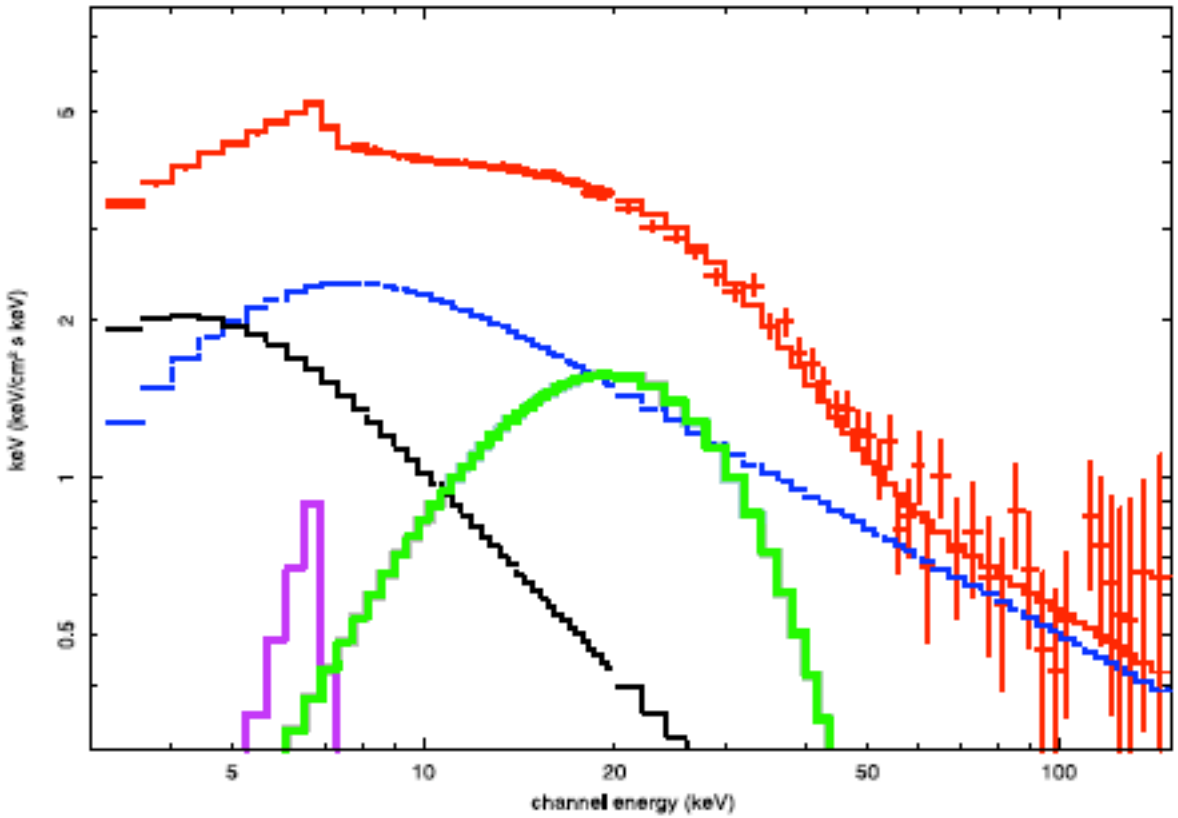

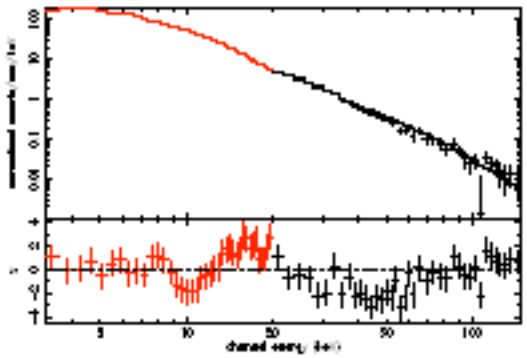

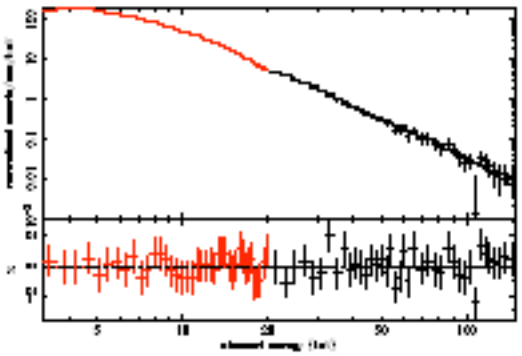

Summary – Main Points

The black hole sources are usually in two phases (states):

•The soft phase (state) is related to the very compact region where soft energy photons of the disk are upscattered forming the steep power law with the photon index around 2.7, the low QPO frequencies are above 10 Hz and high QPO frequencies are of order 100 Hz. In the soft state sometimes we see a transient feature of the redshifted annihilation line. The spectrum of the BHC soft state is a particular signature of the black hole *and it is completely different from that in NSs.*

•The hard phase (state) is related to an extended Compton cloud (cavity) characterized by the photon index around 1.5 and the low QPO frequencies below 1 Hz.

All these observational appearances of BHs and difference between BHs and NSs are consistently explained in the frameworks of the BMC model: the bulk inflow is present in BH when the high mass accretion is high *but not in NS.* **The presence of the firm surface leads to the high radiation pressure which stops the accretion. The bulk inflow and all its features are absent in NSs.**

The observable index-frequency correlation in BHC can be used for evaluation of the mass of the central object

Diffusion of matter in a Keplerian accretion disk

The basic equation which governs the time evolution of surface density in a Keplerian accretion disk due to viscous processes is given, for example, in Bath & Pringle (1981), hereafter BP81,

$$\frac{\partial \Sigma}{\partial t} = \frac{3}{R}\frac{\partial}{\partial R}\left[\sqrt{R}\frac{\partial}{\partial R}(\nu \Sigma \sqrt{R})\right]. \tag{1}$$

The exact nature of the parameter ν, kinematic viscosity, $[\mathrm{cm}^2/\mathrm{s}]$, is unknown. Up to date the most commonly accepted prescription for ν is the $\alpha-$prescription of Shakura & Sunyaev (1973)

$$\nu = \alpha c_{\mathrm{S}} 2H, \tag{2}$$

where $\alpha \leq 1$, c_{S} is the speed of sound, $2H$ is the disk thickness. Disk viscosity ν, in general, can be a function of local variables Σ, R, and t, resulting in a nonlinear equation for Σ.

Diffusion equation (1) can be derived from the fundamental gas dynamics equations, namely the continuity equation and the equation of conservation of angular momentum. Consider a thin cylindrical shell of disk material of radius R, thickness $\triangle R \ll R$, height $2H$. The mass-continuity equation reads

$$\frac{\partial \rho}{\partial t} + \mathrm{div}(\rho \mathbf{v}) = 0. \tag{3}$$

Writing (3) in cylindrical coordinates (R, φ, z) we have

$$\frac{\partial \rho}{\partial t} + \frac{1}{R}\frac{\partial}{\partial R}(R\rho v_{\mathrm{R}}) + \frac{1}{R}\frac{\partial v_\varphi}{\partial \varphi} + \frac{\partial v_z}{\partial z} = 0.$$

The φ-derivative is zero, under our assumption of azimuthal symmetry. Integrating the entire equation vertically from 0 to $2H$, we obtain

$$\frac{\partial}{\partial t}\int_0^{2H} \rho(z)dz + \frac{1}{R}\frac{\partial}{\partial R}\left(R v_{\mathrm{R}} \int_0^{2H} \rho(z)dz\right) + \int_0^{2H} \frac{\partial v_z}{\partial z}dz = 0.$$

The third integral (a perfect differential), contributes zero, since $v_z(0) = v_z(2H) = 0$, yielding

$$\frac{\partial \Sigma}{\partial t} + \frac{1}{R}\frac{\partial}{\partial R}(R v_{\mathrm{R}} \Sigma) = 0. \tag{4}$$

Likewise, the conservation of angular momentum is expressed as follows: its rate of change is given by the net flow of angular momentum through the shell's surfaces at R and $R + \triangle R$ plus the net torque N_{visc} on a ring of gas between R and $R + \triangle R$

$$\frac{\partial L}{\partial t} = -\mathrm{div}(L\mathbf{v}) + N_{\mathrm{visc}}, \tag{5}$$

or rewriting in cylindrical coordinates

$$\frac{\partial L}{\partial t} = -\left[\frac{1}{R}\frac{\partial}{\partial R}(R L v_{\mathrm{R}}) + \frac{1}{R}\frac{\partial}{\partial \varphi}(L v_\varphi) + \frac{\partial}{\partial z}(L v_z)\right] + N_{\mathrm{visc}}. \tag{6}$$

The cylindrical shell of gas has mass $M_{\mathrm{sh}} = 4\pi R \triangle R H \rho$ and angular momentum $L_{\mathrm{sh}} = M v_\varphi R = M \Omega R^2 = 4\pi R \triangle R H \rho \Omega R^2$. Substitution of L_{sh} into (6) gives, after dropping the φ-derivative term

$$\frac{\partial}{\partial t}(4\pi R \triangle R H \rho \Omega R^2) = -\left[\frac{1}{R}\frac{\partial}{\partial R}(R v_{\mathrm{R}} 4\pi R \triangle R H \rho \Omega R^2) + \frac{\partial}{\partial z}(4\pi R \triangle R H \rho \Omega R^2 v_z)\right] + N_{\mathrm{visc}}.$$

Dividing through by a constant quantity $4\pi R \triangle R H$ we have

$$\frac{\partial}{\partial t}(\rho \Omega R^2) = -\left[\frac{1}{R}\frac{\partial}{\partial R}(R v_{\mathrm{R}} \rho \Omega R^2) + \frac{\partial}{\partial z}(\rho \Omega R^2 v_z)\right] + \frac{1}{4\pi R \triangle R H} N_{\mathrm{visc}}.$$

Performing vertical integration from $z = 0$ to $z = 2H$, using the assumption that the angular frequency Ω does not vary along z-axis for given radius R, gives

$$\frac{\partial}{\partial t}(\Sigma \Omega R^2) = -\frac{1}{R}\frac{\partial}{\partial R}(R v_{\mathrm{R}} \Sigma \Omega R^2) + \frac{1}{2\pi R \triangle R} N_{\mathrm{visc}},$$

where the net viscous torque on a shell of gas between R and $\triangle R$ is given by

$$N_{\rm visc} = G(R+\triangle R) - G(R) = \left.\frac{dG}{dR}\triangle R\right|_{\triangle R\to 0}, \text{ with } G = 2\pi R\nu\Sigma\frac{d\Omega}{dR}R^2 \tag{7}$$

being the torque exerted by the outer ring of gas on the inner ring [see Pringle (1981)]. Thus the angular momentum conservation is expressed by equation

$$\frac{\partial}{\partial t}(\Sigma\Omega R^2) = -\frac{1}{R}\frac{\partial}{\partial R}(Rv_{\rm R}\Sigma\Omega R^2) + \frac{1}{2\pi R}\frac{\partial G}{\partial R}. \tag{8}$$

Using the continuity equation (4) and the fact that for orbits in a fixed gravitational potential $\dfrac{\partial\Omega}{\partial t} = 0$, the conservation equation for angular momentum simplifies to

$$Rv_R\Sigma\left(\Omega R^2\right)' = \frac{1}{2\pi}\frac{\partial G}{\partial R}. \tag{9}$$

Elimination of v_R from combination of equations (4) and (9) yields

$$R\frac{\partial\Sigma}{\partial t} = -\frac{\partial}{\partial R}(Rv_R\Sigma) = -\frac{\partial}{\partial R}\left[\frac{1}{2\pi(\Omega R^2)'}\frac{\partial G}{\partial R}\right].$$

For the Keplerian angular velocity profile $\Omega_K = \sqrt{GM_{\rm CO}}R^{-\frac{3}{2}}$, substituting expression (7) for the torque $G(R,t)$, we immediately obtain (1).

For a complete formulation of the diffusion problem the appropriate initial and boundary conditions need to be specified. In BP81, for example, any matter at the inner radius $R = R_{\rm in}$, is allowed to be accreted on to the central object such that $\Sigma = 0$. At the outer edge $R = R_{\rm out}$ the angular momentum is removed from the disk material due to tidal effects of a companion star, which also limit the disk radius to about $0.8 - 0.9$ of the size if the primary's Roche lobe. It is reasonable, therefore, to fix the outer radius $R_{\rm out}$ and set $\dfrac{\partial\Sigma}{\partial R} = 0$ at $R = R_{\rm out}$, i.e.

$$\begin{cases} \Sigma = 0, & \text{at } R = R_{\rm in} \\ \dfrac{\partial\Sigma}{\partial R} = 0, & \text{at } R = R_{\rm out}. \end{cases} \tag{10}$$

Diffusion equation (1) is applied to flows within thin accretion disks, but paradigm is universal in disk accretion models.

Diffusive propagation of the perturbation in the disk

Formulation of the problem

The diffusion equation for the time variable quantity $W(R,t)$, related to the surface density perturbations $\Delta\Sigma(R,t)$, $W(R,t) = \Delta\Sigma(R,t)$, can be written in an operator form

$$\frac{\partial W}{\partial t} = \mathbf{\Lambda_R} W + \varphi(t) f(R) \tag{2}$$

where R is a radial coordinate in the disk and $\mathbf{\Lambda_R}$ is the space diffusion operator. Equation (2) should be combined with the appropriate boundary conditions at $R = 0$, $R = R_0$ and initial conditions at $t = 0$. For homogeneous initial conditions, namely for $W(R,0) = 0$ the solution at any R and t can be presented as a convolution

$$W(R,t) = \int_0^t \varphi(t') X(R, t-t') dt'. \tag{3}$$

The kernel of convolution (3), $X(R,t-t')$ is a solution of the initial value problem for the homogeneous equation

$$\frac{\partial X}{\partial t} = \mathbf{\Lambda_R} X \tag{4}$$

with the following initial conditions

$$X(R,t-t')_{t=t'} = X(R,0) = f(R) \tag{5}$$

The power spectrum $||F_W(\omega)||^2$ of $W(R,t)$ can be presented as a product of the power spectra $||F_\varphi(\omega)||^2$ and $||F_X(\omega)||^2$ of $\varphi(t)$ and $X(R,t)$ respectively:

$$||F_W(\omega,R)||^2 = ||F_\varphi(\omega)||^2||F_X(\omega,R)||^2, \tag{6}$$

The X-ray resulting variable signal is determined by the fluctuations of the luminosity $\Delta L_x(t)$. We assume that the mass accretion rate variations $\Delta\dot{M}(0,t)$ is converted with efficiency ε_{eff} into the variations of the X-ray luminosity, i.e. $\Delta L_x(t) = \varepsilon_{eff}\Delta\dot{M}(0,t)$.

W01 show that for the function $\mathcal{W}(x,t) = x\hat{\nu}W(x^2,t)$ using a new variable $x = R^{1/2}$ the diffusion equation (2) can be presented in the form

$$\frac{\partial\mathcal{W}}{\partial t} = \frac{3\hat{\nu}(x)}{4x^2}\frac{\partial^2\mathcal{W}}{\partial x^2} + \varphi(t)\mathcal{F}(x)$$

where $\hat{\nu}(x)$ is viscosity in the disk, $\mathcal{F}(x) = x\hat{\nu}(x)f(x^2)$. The convolution, similar to Eq. (3), presents the solution $\mathcal{W}(x,t)$

$$\mathcal{W}(x,t) = \int_0^t \varphi(t')\mathcal{X}(x,t-t')dt'$$

where $\mathcal{X}(x,t)$ is a solution of the initial value problem (compare with Eqs. 4, 5)

$$\frac{\partial\mathcal{X}}{\partial t} = \frac{3\hat{\nu}(x)}{4x^2}\frac{\partial^2\mathcal{X}}{\partial x^2}$$

with the following initial conditions

$$\mathcal{X}(x,0) = \mathcal{F}(x).$$

The boundary condition at the outer boundary $\dfrac{\partial \mathcal{X}}{\partial x} = 0 \quad \text{at} \quad x = x_0$

Assumed that at the inner boundary $x_{\rm in} \ll x_0,\ W = \Delta\Sigma = 0,$ *which is equivalent to*

$$\mathcal{X} = 0 \quad \text{at} \quad x = x_{\rm in}.$$

We assume that perturbations of the mass accretion rate at the inner disk edge is converted with efficiency $\varepsilon_{\rm eff}$ *into perturbations of the X-ray luminosity, i.e.*

$$\Delta L(t) = \varepsilon_{\rm eff} \Delta \dot{M}(t, R_{in})$$

Because $\Delta \dot{M} = 3\pi \dfrac{\partial \mathcal{X}}{\partial x}$ *then* $Y(t) \propto \Delta L_x(t) \propto \dfrac{\partial \mathcal{X}}{\partial x}(t, 0).$

Now we consider a general case of problems where $\hat{\nu}(x) = (\hat{\nu}_0 / x_0^{\psi}) x^{\psi}.$

a. Viscosity linearly distributed over radius: $\psi = 2$

$$Y(t) \propto \sum_{k=1}^{\infty} \exp[-\pi^2 (2k-1)^2 t / 4t_0].$$

where the viscous time scale $t_0 = 4x_0^4 / 3\hat{\nu}_0 = 4R_0^2 / 3\hat{\nu}(R_0).$

Then the power spectrum of Y(t) *is:* $||F_Y(\nu)||_\nu^2 \propto \sum_{k=0}^{\infty} \dfrac{1}{(8t_0\nu/\pi)^2 + (2k+1)^4}.$

The series in the right hand side of this equation can be calculated exactly

$$||F_Y(\nu)||^2_\nu \propto \frac{\pi}{2^{3/2}a^{3/2}} \frac{\sinh 2^{1/2}\pi a^{1/2} + \sin 2^{1/2}\pi a^{1/2}}{\cosh 2^{1/2}\pi a^{1/2} - \cos 2^{1/2}\pi a^{1/2}} -$$

$$- \frac{\pi}{2^{5/2}a^{3/2}} \frac{\sinh \pi a^{1/2}/2^{1/2} + \sin \pi a^{1/2}/2^{1/2}}{\cosh \pi a^{1/2}/2^{1/2} - \cos \pi a^{1/2}/2^{1/2}}$$

where $a = 8t_0\nu/\pi.$

As it follows from this formula that

$$||F_Y(\nu)||^2_\nu = C_N \times \pi^4/96 \qquad \text{when} \quad \nu \ll \pi/8t_0$$

and $$||F_Y(\nu)||^2_\nu = C_N \times \frac{1}{2^7\pi^{1/2}t_0^{3/2}} \frac{1}{\nu^{3/2}} \qquad \text{when} \quad \nu \gg \pi/8t_0.$$

General case

Although the series of power spectrum

$$||F_Y(\nu)||^2_\nu \propto \sum_{k=1}^{\infty} \frac{[2k-(10-3\psi)/2(4-\psi)-\varepsilon_k/\pi]^{2\delta}}{(8t_0\nu/\pi)^2+[2k-(10-3\psi)/2(4-\psi)-\varepsilon_k/\pi]^4}$$

has to be calculated numerically the asymptotic form of PDS can be easily evaluated analytically:

$$||F_Y(\nu)||^2_\nu = C_N \times \mathcal{A}_L \qquad \text{when} \quad \nu \ll \pi/8t_0$$

$$||F_Y(\nu)||^2_\nu = C_N \times \frac{\mathcal{A}_H(\nu)}{\nu^{(3-2\delta)/2}} \qquad \text{when} \quad \nu \gg \pi/8t_0$$

where

$$\mathcal{A}_H(\nu) = \frac{1}{2(8t_0\pi)^{(3-2\delta)/2}} \int_{x_1(\nu)}^{\infty} \frac{x^{2\delta}dx}{1+x^4},$$

$$\alpha = \frac{3}{2} - \delta = \frac{16-5\psi}{2(4-\psi)} \quad \text{for} \quad \psi > 0$$

and $\alpha = 2$ for $\psi < 0.$

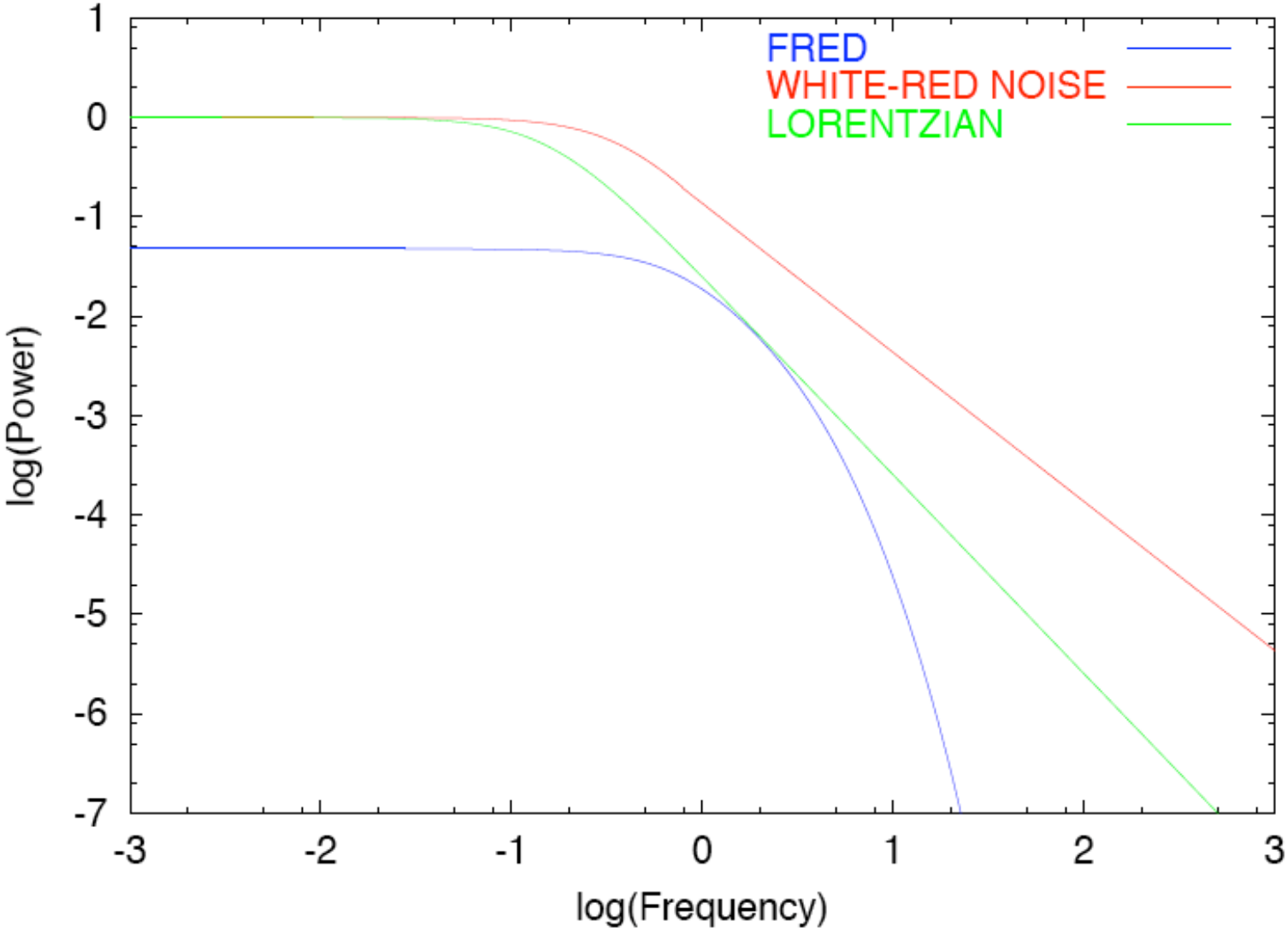

Fig. 1.— Examples of PDS models: PDS of fast rise and exponential decay (FRED) (blue line), PDS of white-red noise (red line) and Lorentzian PDS (green line).

Integrated Power of X-ray emission vs total integrated power of the disk configuration

We obtain that the integrated total power of X-ray resulting signal

$$P_x = \int_0^\infty ||F_x(\omega)||^2 d\omega \sim \frac{1}{D\mathcal{Q}} \frac{P_{dr}}{\omega_{dr} t_0}.$$

We arrive to the conclusion that the resulting integrated power P_x, which is related to the perturbation amplitude at the inner disk edge, is much less than the total integrated power of the driving oscillation in the disk P_{dr}

$$\frac{P_x}{P_{dr}} \sim (D\mathcal{Q}\omega_{dr} t_0)^{-1} \ll 1.$$

Evolution of Power density spectrum and energy spectrum

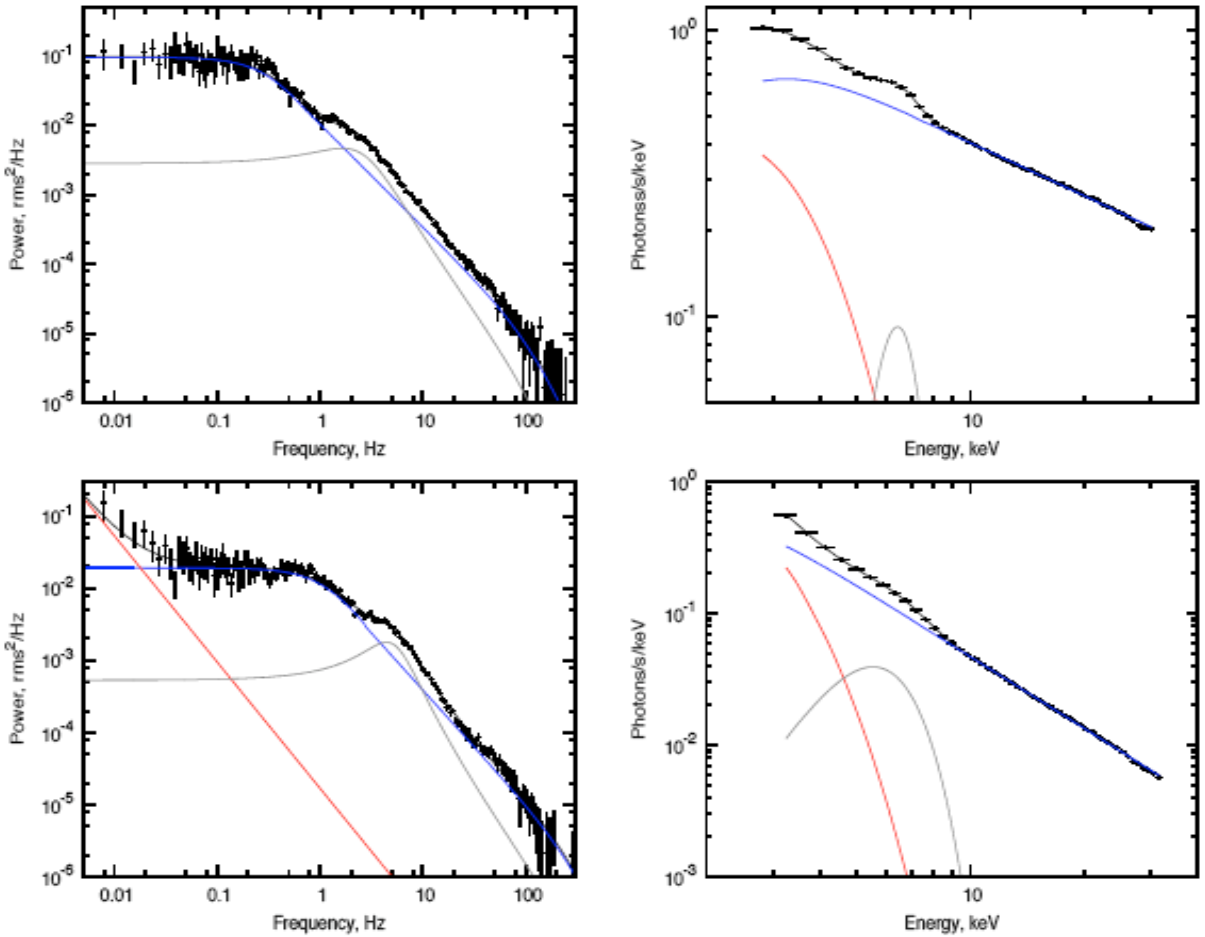

Cyg X-1: Observable power spectrum (PDS) (left panel) vs photon spectrum (right panel). The first observation is a pure low/hard state with no LF WRN component in the PDS. During the second observation the source energy spectrum is still hard, but LF WRN is already detectable.

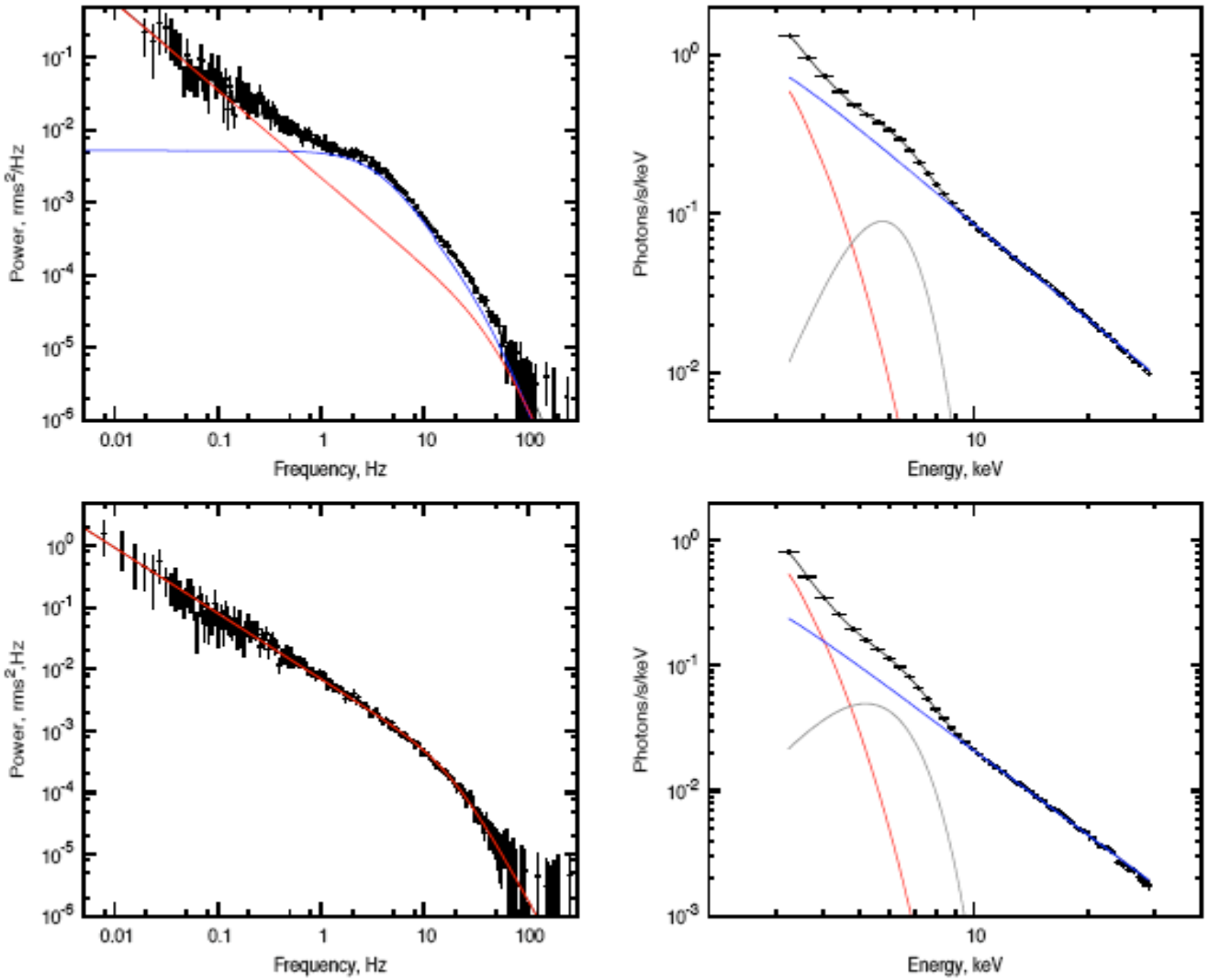

The first observation is taken during the intermediate state just before the transition to high/soft state, which is presented by the second observation.No HF WRN is present in PDS during high/soft state.

Power spectra of Cyg X-1: Hard and intermediate states

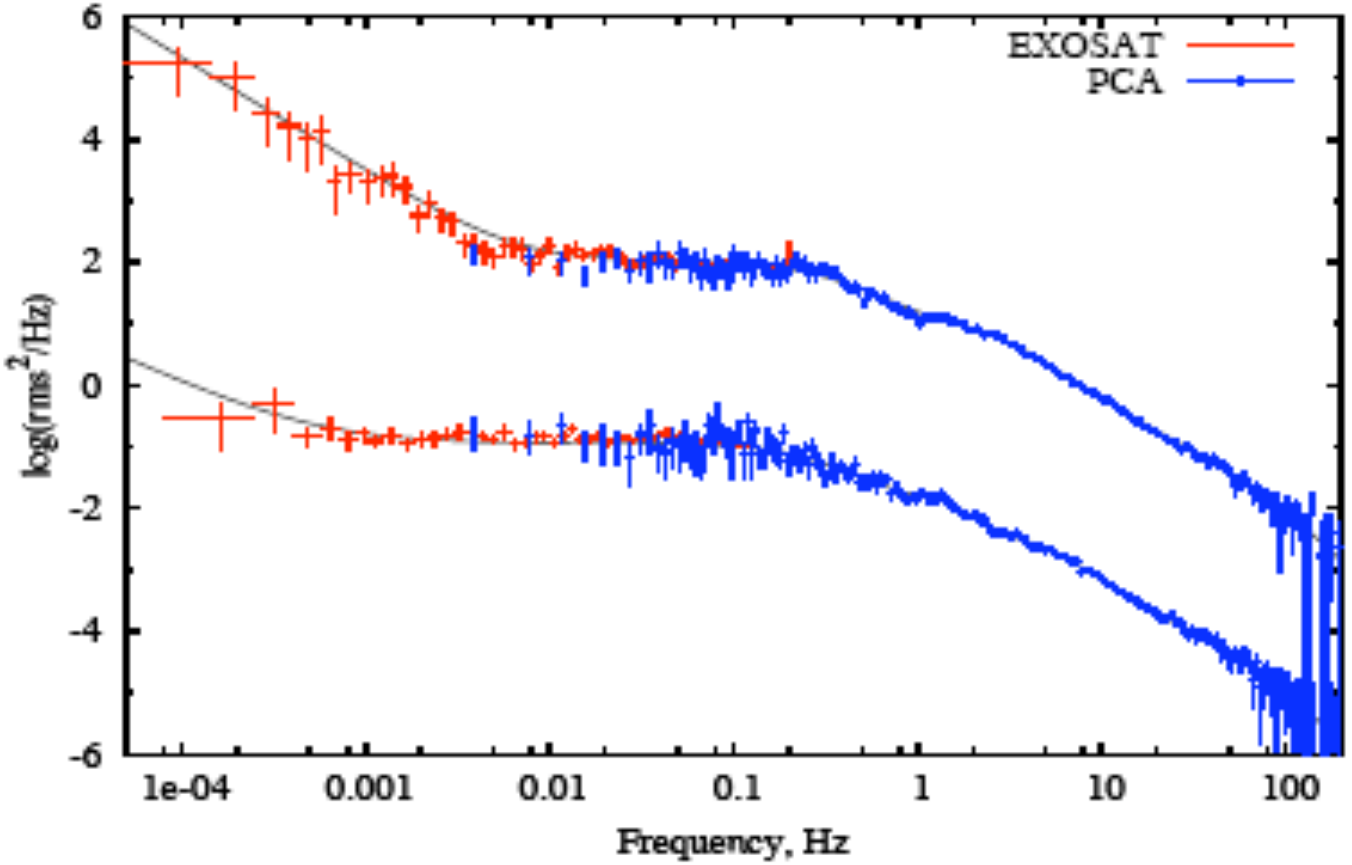

Two composite PDSs: EXOSAT spectra with matching high frequency PCA PDS. Data are fitted by LF-HF diffusion model:
χ_2/N_{dof} = 250.1/267 = 0.94, ψ_{corona} = 2.32 ± 0.12, $t_{0,C}$ = 1.8 ± 0.3, ψ_D = 2.5 and
χ_2/N_{dof} = 278.5/267 = 1.04, ψ_{corona} = 2.07 ± 0.7, $t_{0,C}$ = 1.24 ± 0.12, ψ_D= 0.3 ± 0.3.

Reynolds number of the flow and Shakura-Sunyaev disk - alpha parameter as observable quantities

Using the best-fit parameters of the PDS model we can infer the evolution of the physical parameters of the source such the disk diffusion time t_0, magnetoacoustic QPO frequency and Reynolds number of the accretion flow Re, with the change of photon index. We can relate t_0 with Re and magnetoacoustic QPO frequency ν_{MA}

$$t_0 = \frac{4}{3}\frac{4}{(4-\psi)^2}\left[\frac{V_{MA}R_0}{\hat{\nu}(R_0)}\right]\left(\frac{R_0}{V_{MA}}\right) = \frac{4}{3}\frac{4}{(4-\psi)^2}\frac{\mathrm{Re}}{a_{MA}\nu_{MA}},$$

because

$$\nu_{MA} = V_{MA}/(a_{MA}R_0)$$

These formulas leads to equation

$$\mathrm{Re} = a_{AM}\frac{3}{4}\frac{(4-\psi)^2}{4}(\nu_L t_0)$$

that allows us to infer a value of Re using the best-fit model parameters t_0 and the QPO low frequency ν_L ***presumably equals to*** ν_{MA} **.**

Determination of Reynolds number of accretion flow from Observations I

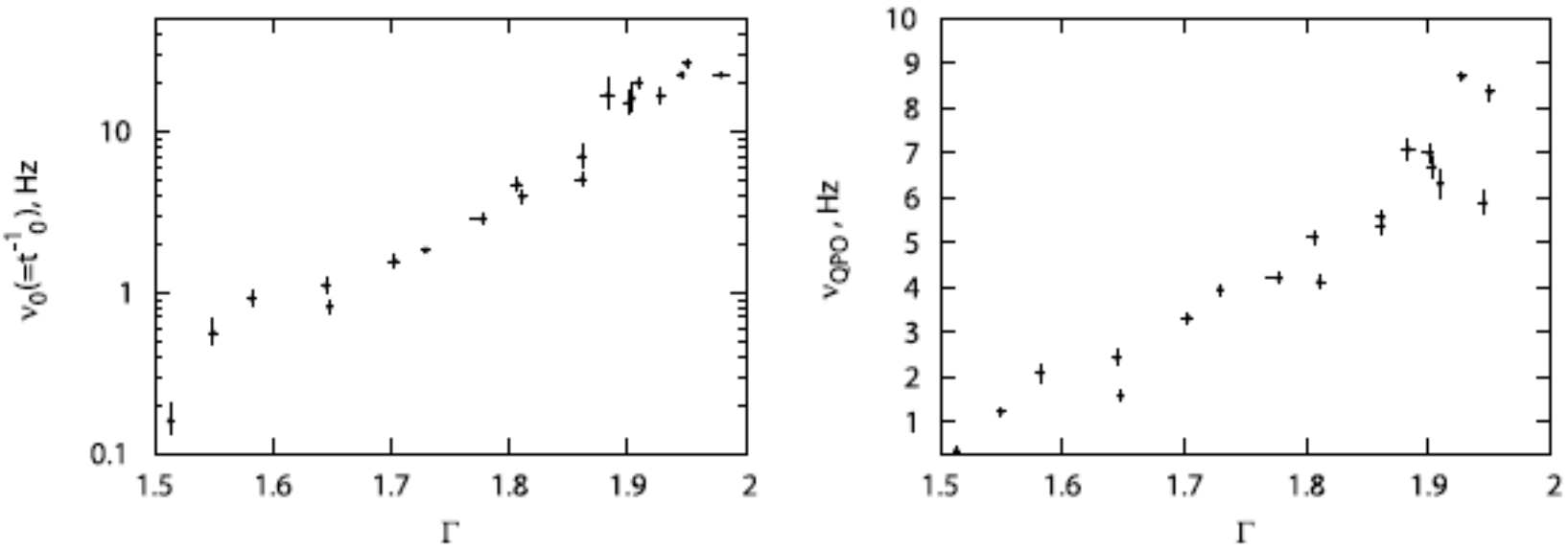

Fig. 8.— Cyg X-1: HF white-red noise component: the best-fit diffusion frequency $\nu_0 = t_0^{-1}$ vs Γ (upper left panel), QPO low frequency ν_{QPO} (ν_L) vs Γ (right upper panel)

T, Shaposhnikov & Arefiev 2007

Determination of Reynolds number of accretion flow from Observations II

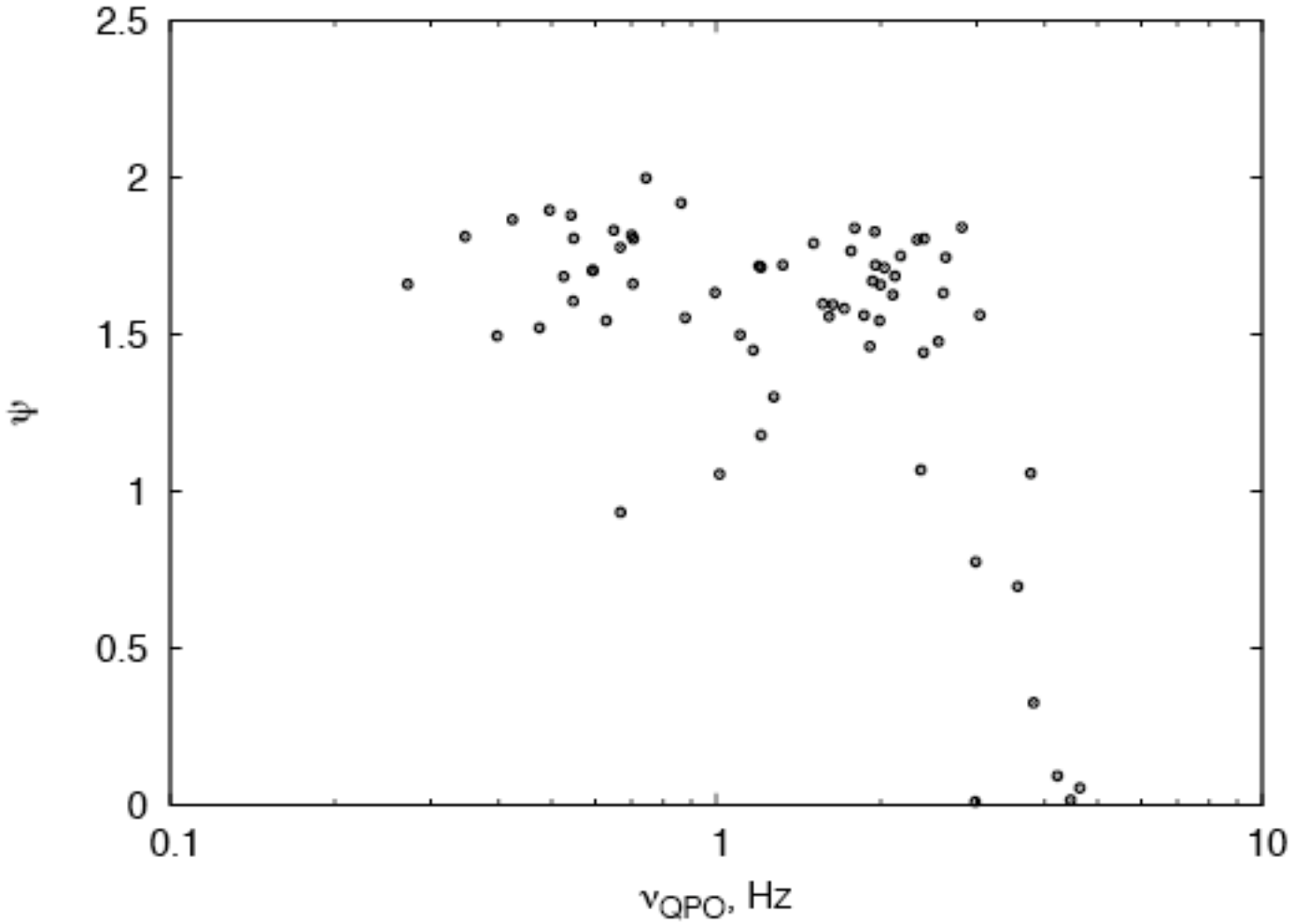

Determination of Reynolds number of accretion flow from Observations III

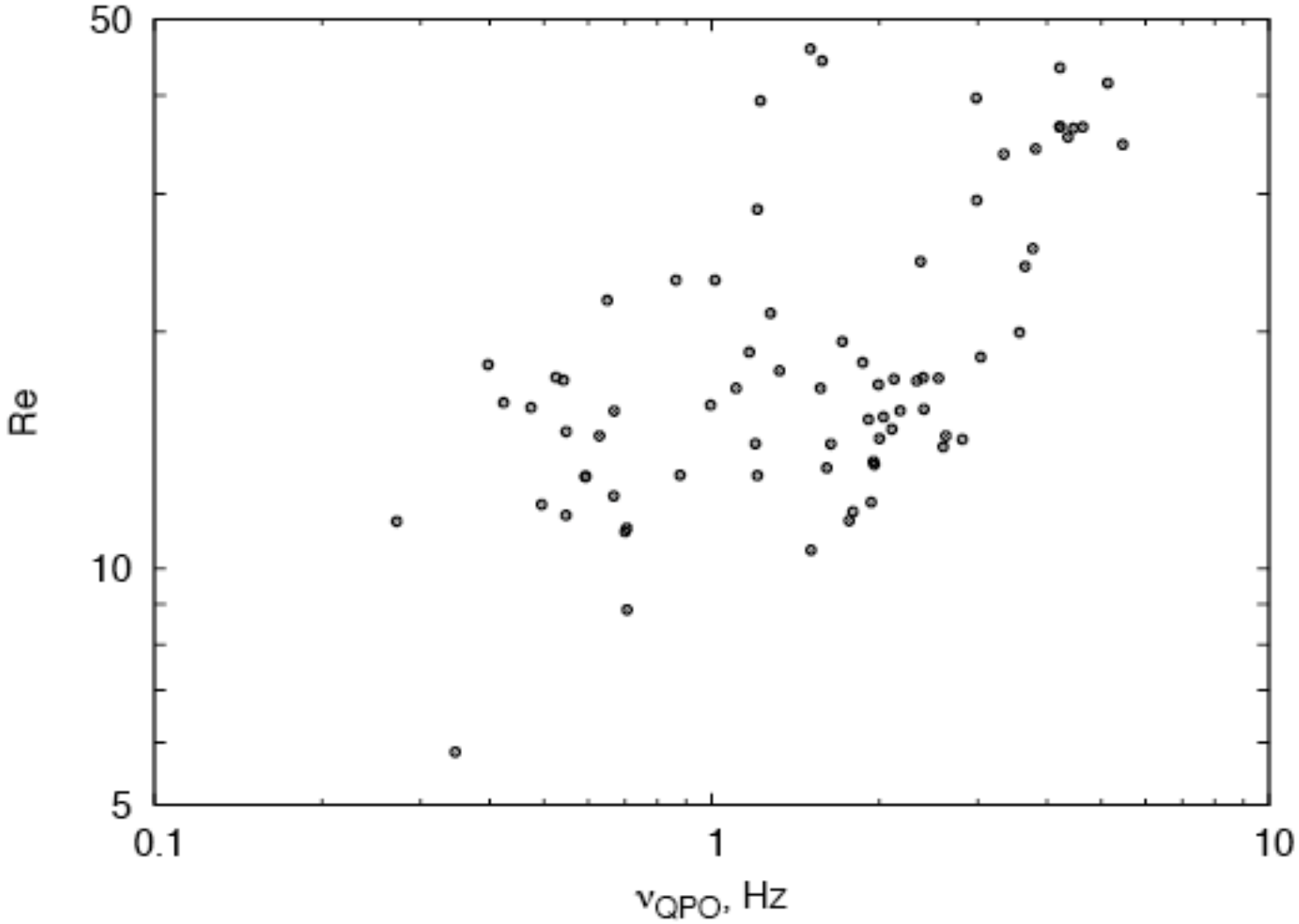

Observational Evidence of Compton Cloud Contraction

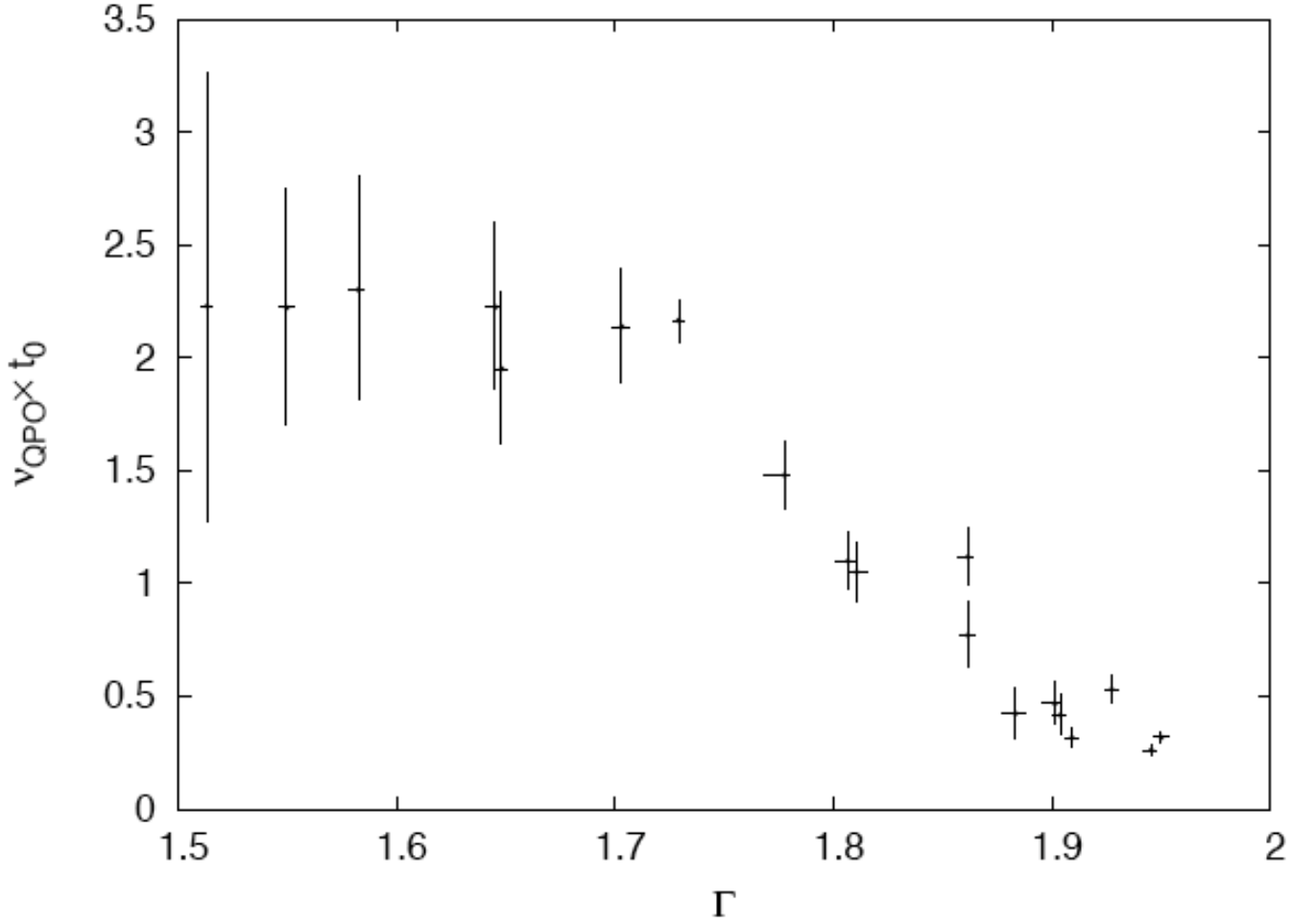

Cyg X-1: a product of QPO low frequency $\nu_{QPO}(\nu_L)$ and the best-fit diffusion time of HF WRN t_0 vs Γ. Decrease of $\nu_{QPO} \times t_0$ with Γ implies that Compton cloud contracts when the source evolves to the softer states.

Driving QPOs in the observed power spectra

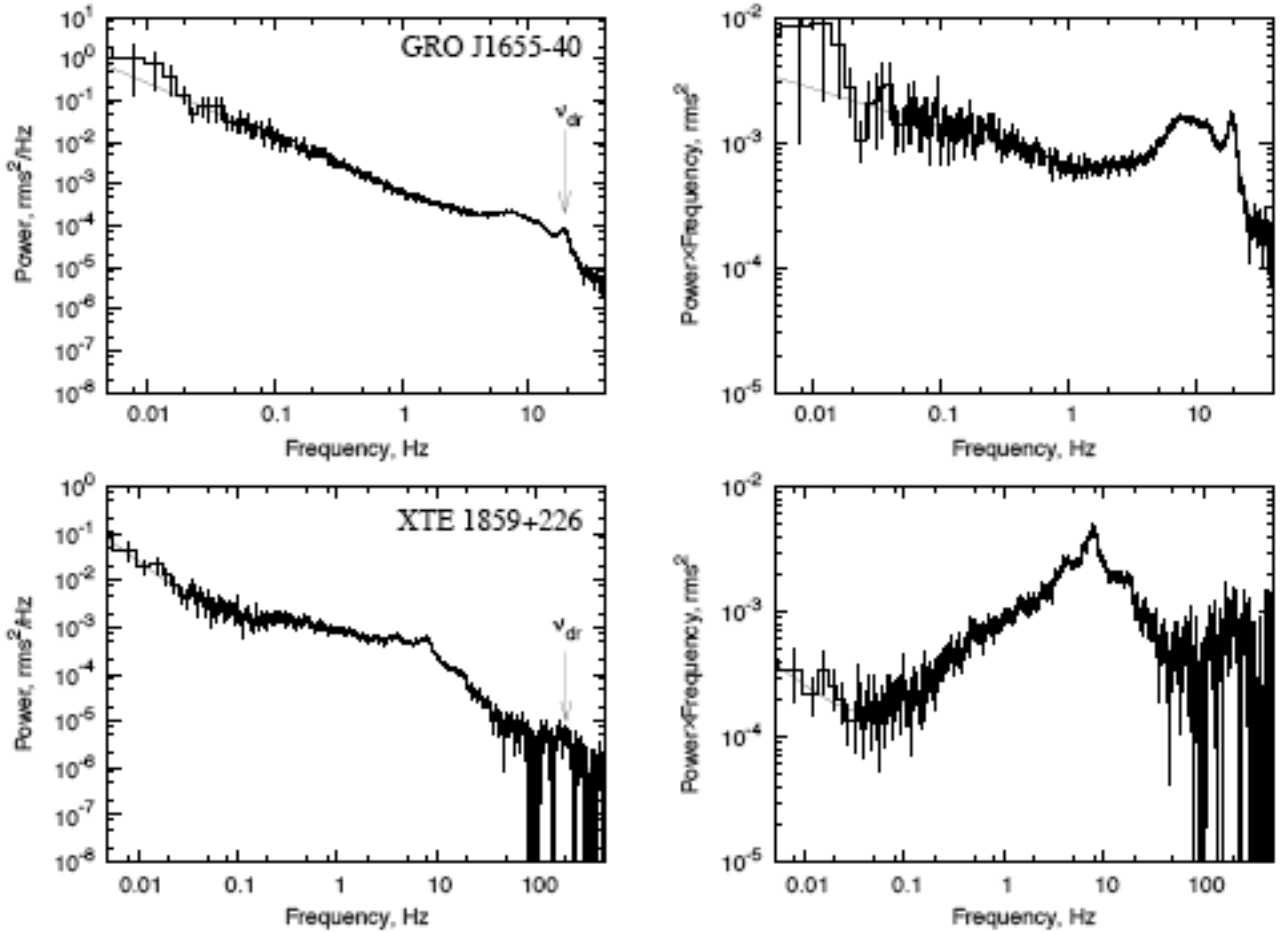

RXTE/PCA power spectra (left panels) and power×frequency diagrams (right panels) of GRO J1655-40 (top) and XTE 1859+226 (bottom). One can clearly see QPO frequencies dr at 10 – 20 Hz for GRO J1655-40 and 185 Hz for XTE 1859+226 before a high-frequency cut-off. The rms^2 power at ν_{dr} is comparable (GRO J1655-40) or higher (XTE 1859+226) than that at low frequencies (see right panels).

Power vs Driving QPO frequency

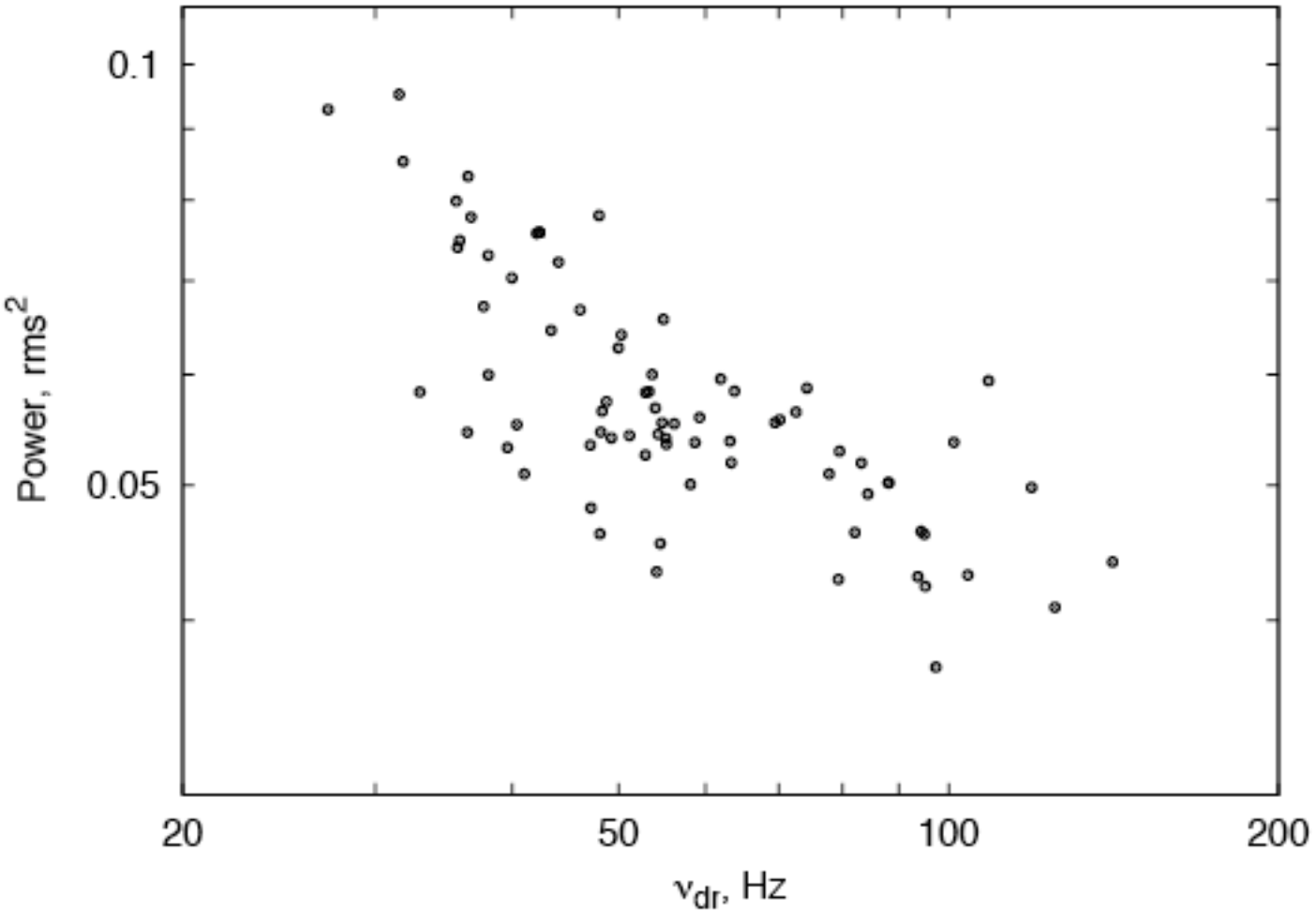

Low QPO frequency vs Driving QPO frequency

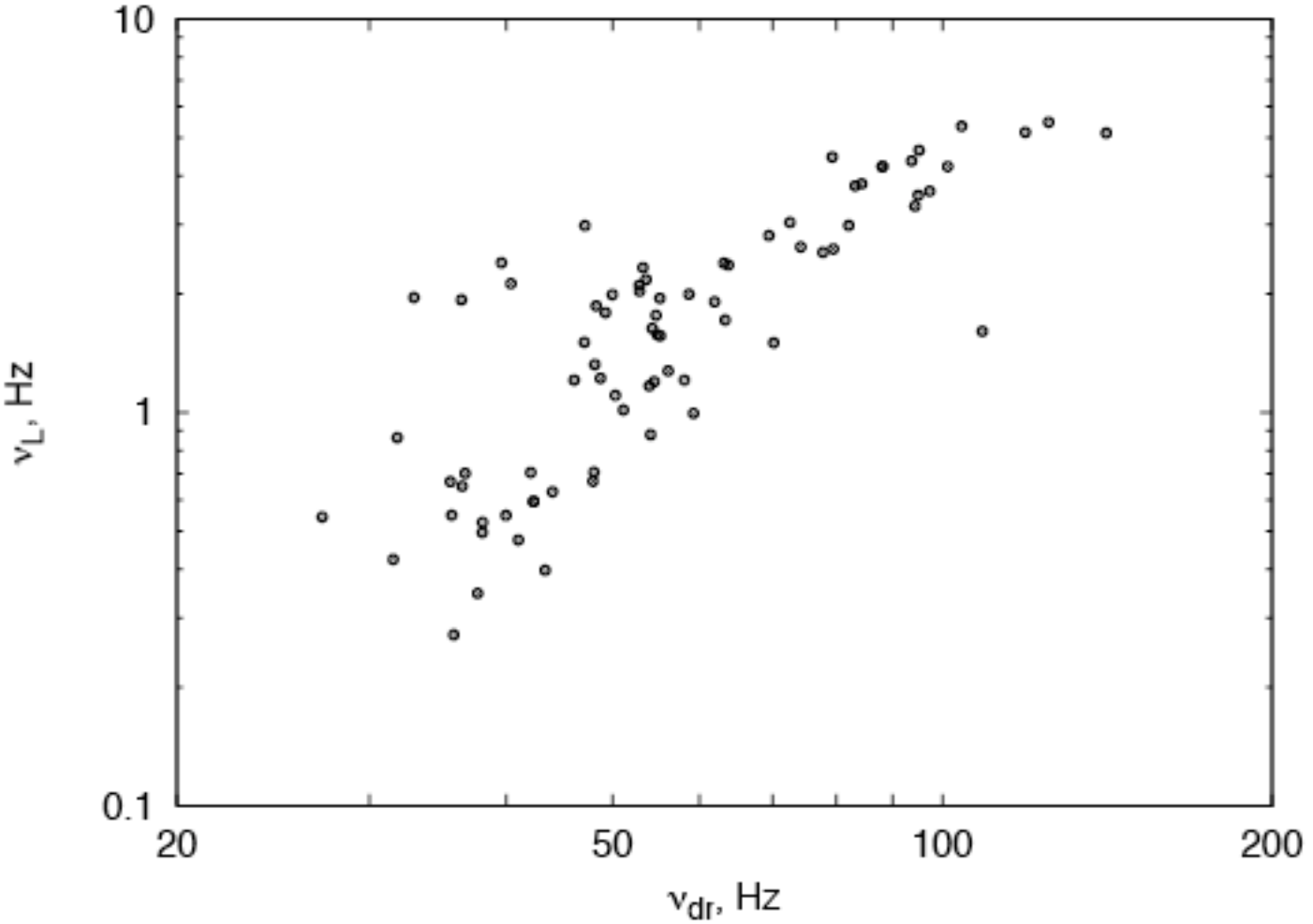

Summary I.

We present a model of Fourier Power Density Spectrum (PDS) formation in accretion powered X-ray binary systems derived from the first principles of the diffusion theory.

The resulting PDS continuum is a sum of two components, a low frequency (LF) component is presumably originated in an extended accretion disk and a high frequency (HF) component is originated in the innermost part of the source (Compton cloud).

Summary II.

The LF PDS component has a power law shape with index about 1.5 at higher frequencies (“red” noise) and a flat spectrum below a characteristic (break) frequency (“white” noise).

This white-red noise (WRN) continuum spectrum holds information about physical parameters of bounded extended medium, diffusion time scale and dependence of viscosity vs radius.

We offer a method to measure an effective Reynolds number, Re using the basic PDS parameters (PDS index and characteristic frequencies).
We obtain that the inferred Re increases from 8 in low/hard state to 70 high/soft state.

K_α line formation in the wind.

Direct component

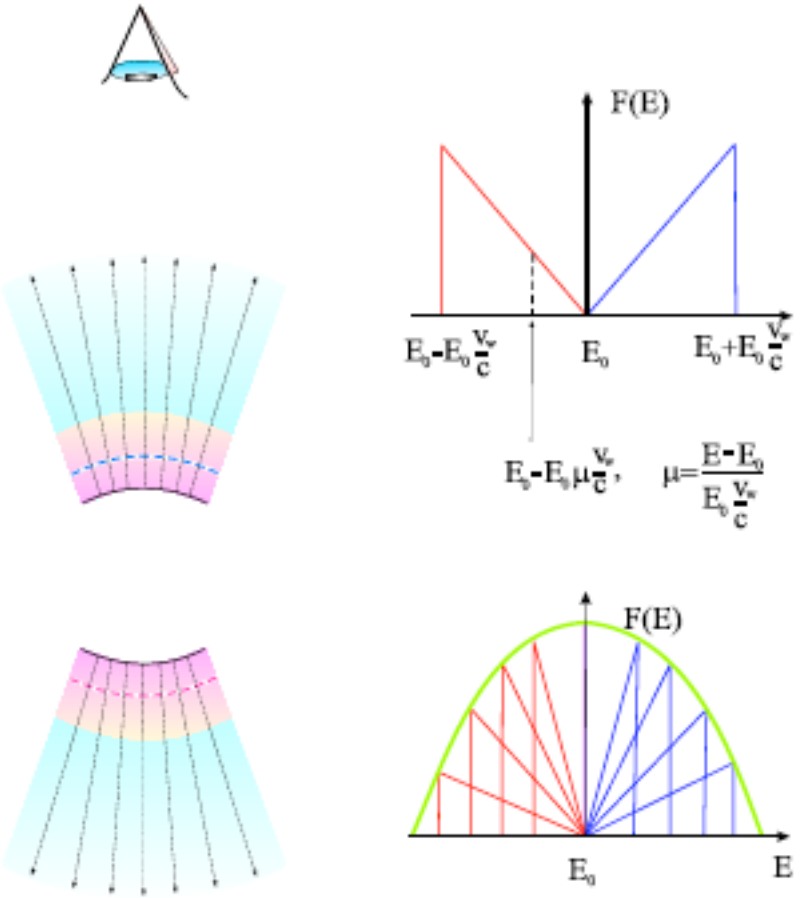

Fig. 9.— Spherical wind geometry and wind line profiles of direct component.

Observational evidence of wind.
I. Main idea of smearing out a pulsed signal

The emergent signal is a convolution

$$W(R,t) = \int_0^t \varphi(t')X(R,t-t')\,dt'$$

where $\varphi(t)$ is a pulsed signal and $X(R, t) \propto \exp(-t/t_0)$)
is a scattering reprocessing function

The resulting power spectrum

$$||F_W(\omega,R)||^2 = ||F_\varphi(\omega)||^2 ||F_X(\omega,R)||^2$$

II. POWER SPECTRUM

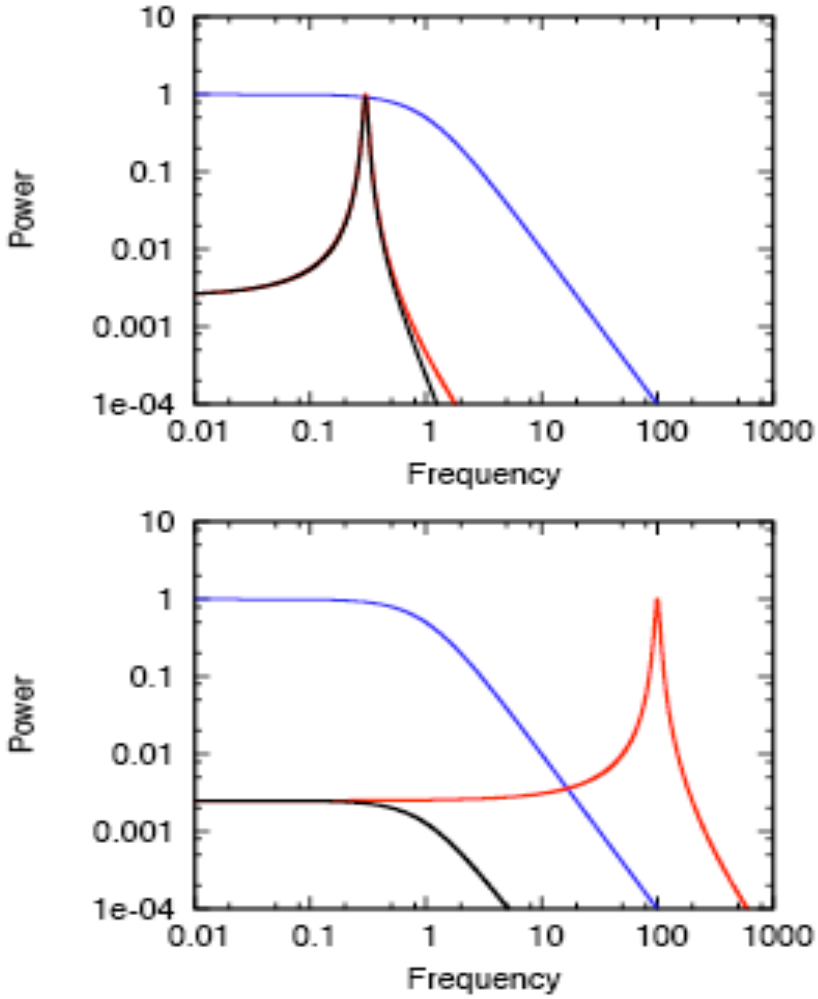

BLUE, RED AND BLACK LINES PRESENT POWER SPECTRA OF REPROCESSING FUNCTION, PULSED SIGNAL AND RESULTING PDS RESPECTIVELY

T, Laurent & shaposhnikov (2008)

Condition for supression of pulsed signal

$$||F_W(\omega_p)||^2 / ||F_W(\omega_p)||^2_{max} = [(\omega_p t_0)^2+1]^{-1} << 1$$

which leads to inequality

NS case:

$$0.7\tau_e^2(\nu_p/400\ \text{Hz})^2\,(L/10^7\ \text{cm})^2 >> 1$$

$$\text{or } \tau_e > 1$$

BH case:

$$(\tau_e/0.02)^2(\nu_p/100\ \text{Hz})^2\,(L/10^{11}\ \text{cm})^2 >> 1$$

$$\text{or } \tau_e > 0.02.$$

The above relations are for scattered component of the resulting signal. The direct component of the pulsed radiation is attenuated as exponential $\exp(-\tau_e)$.

T, Laurent & shaposhnikov (2008)

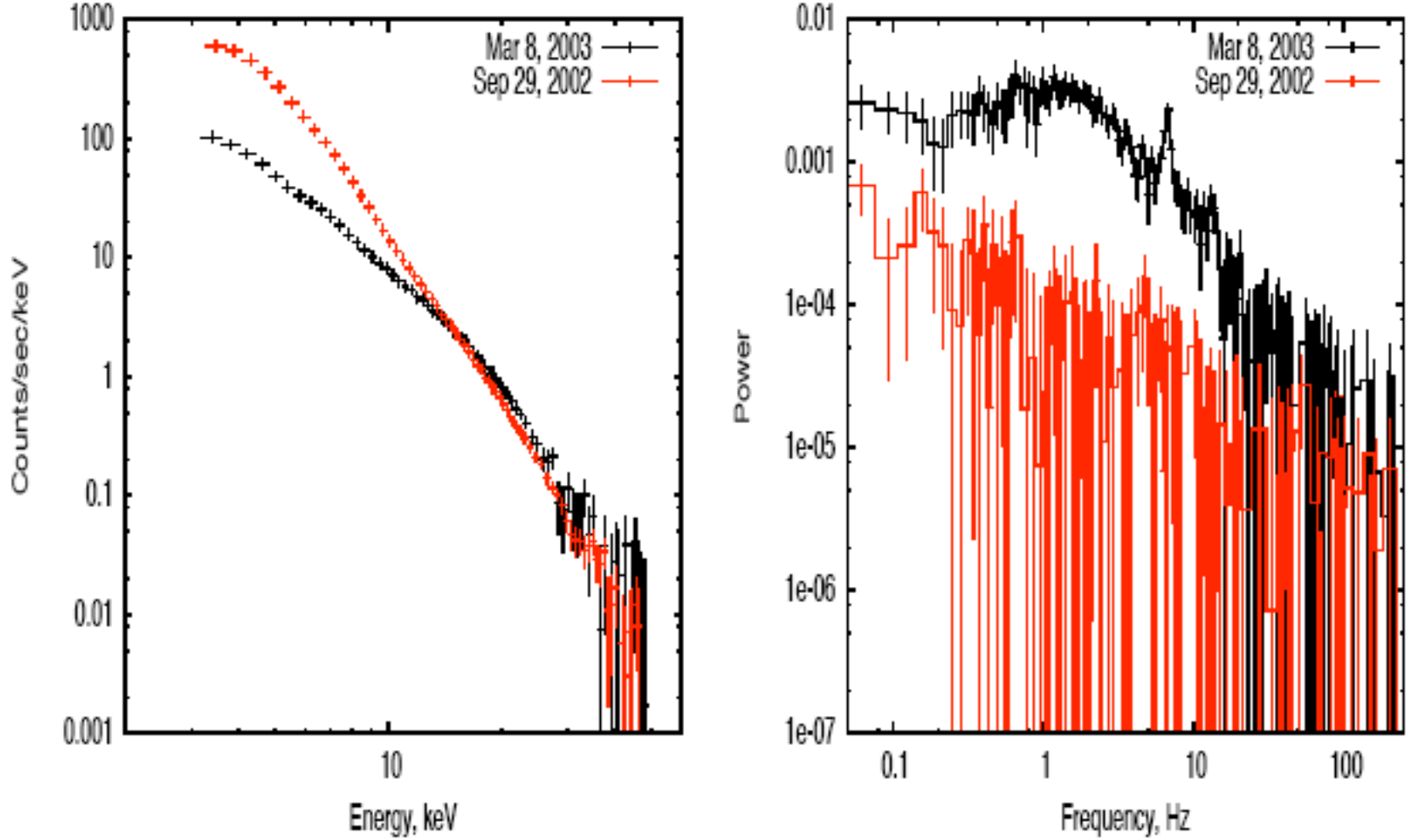

Fig. 7.— *Left:* X-ray continuum spectra of BH GX 339-4 observed with RXTE on September 29, 2002 related to XMM rev. 594 (black points) and that observed on March 8, 2003 related to XMM rev. 514 (red points). *Right:* RXTE power spectra (PDS) related to corresponding X-ray spectra. It is evident that PDS related to the strong iron line appearance (red) is featureless and noisy while in the case of the weak iron line the broken power-law continuum (white-red noise) and break frequency of 2 Hz and QPO frequency of 8 and 16 Hz are clearly seen in the PDS.

Red skewed line in GX 339-4 (rev. 514). XMM-RXTE observations

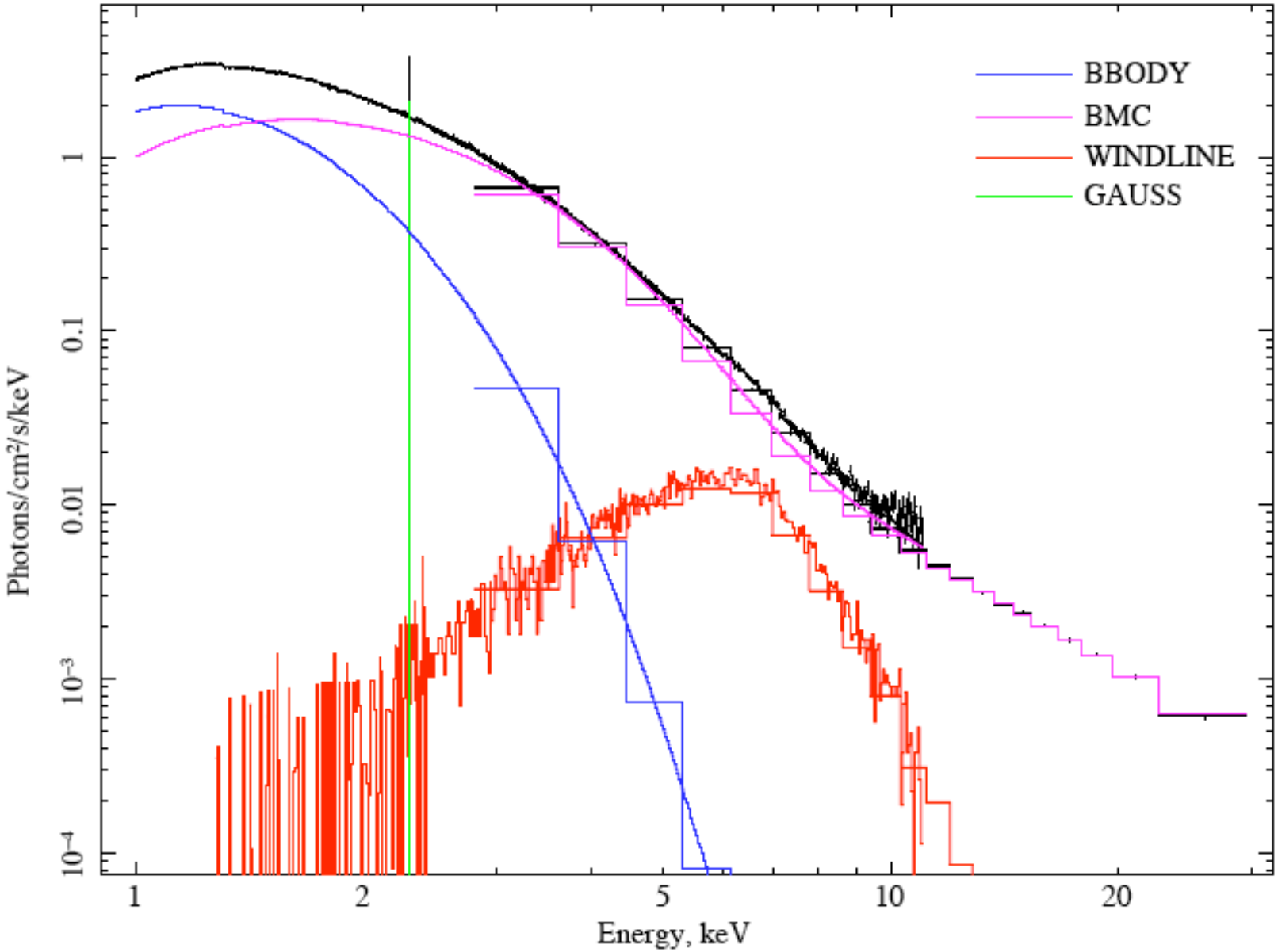

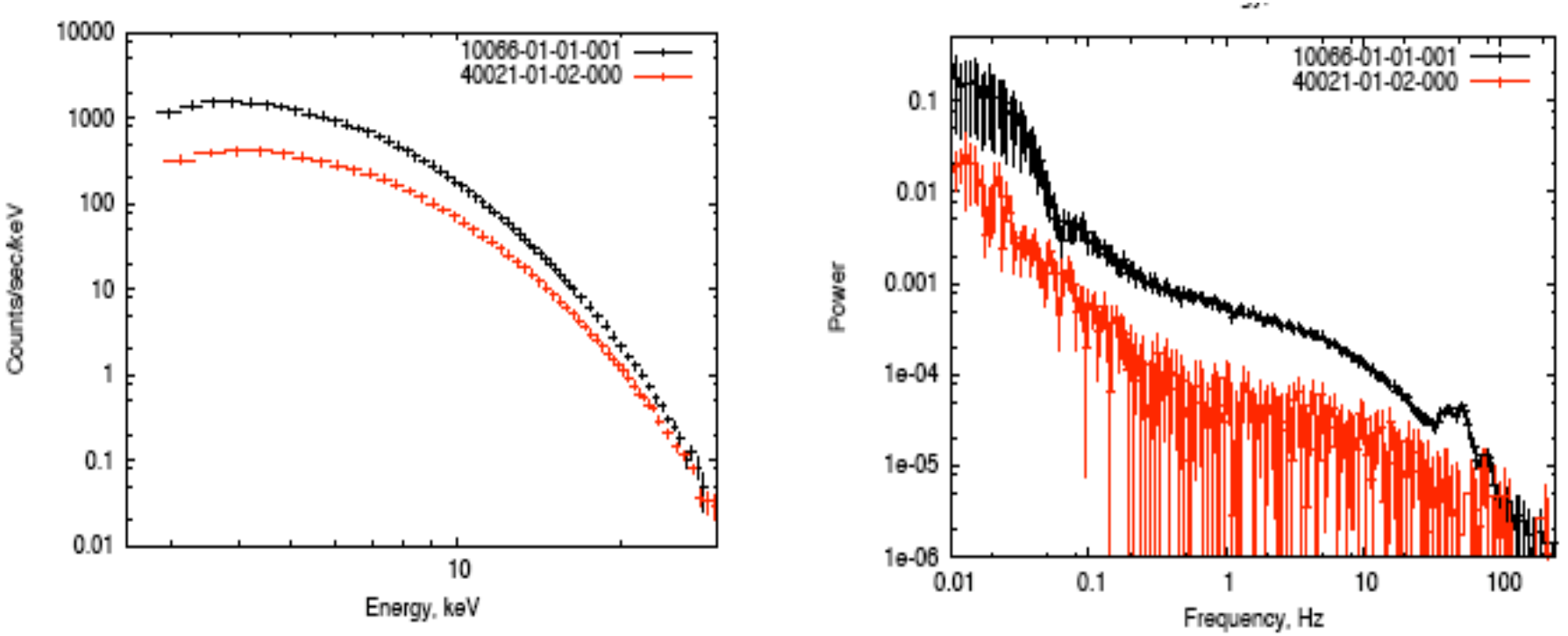

Fig. 2.— Energy and Power Density spectra as observed by *RXTE* during observation 10066-01-01-001 (black) and 40021-01-02-000 (red) . Spectral parameters during observation 40021-01-02-000 are similar to those measured during *Suzaku* observation. Timing analysis shows that high frequency variability during this particular observation is strongly suppressed.

Shaposhnikov, T & Laurent (2008)

Red skewed line in Cyg X-2. Suzaku observations

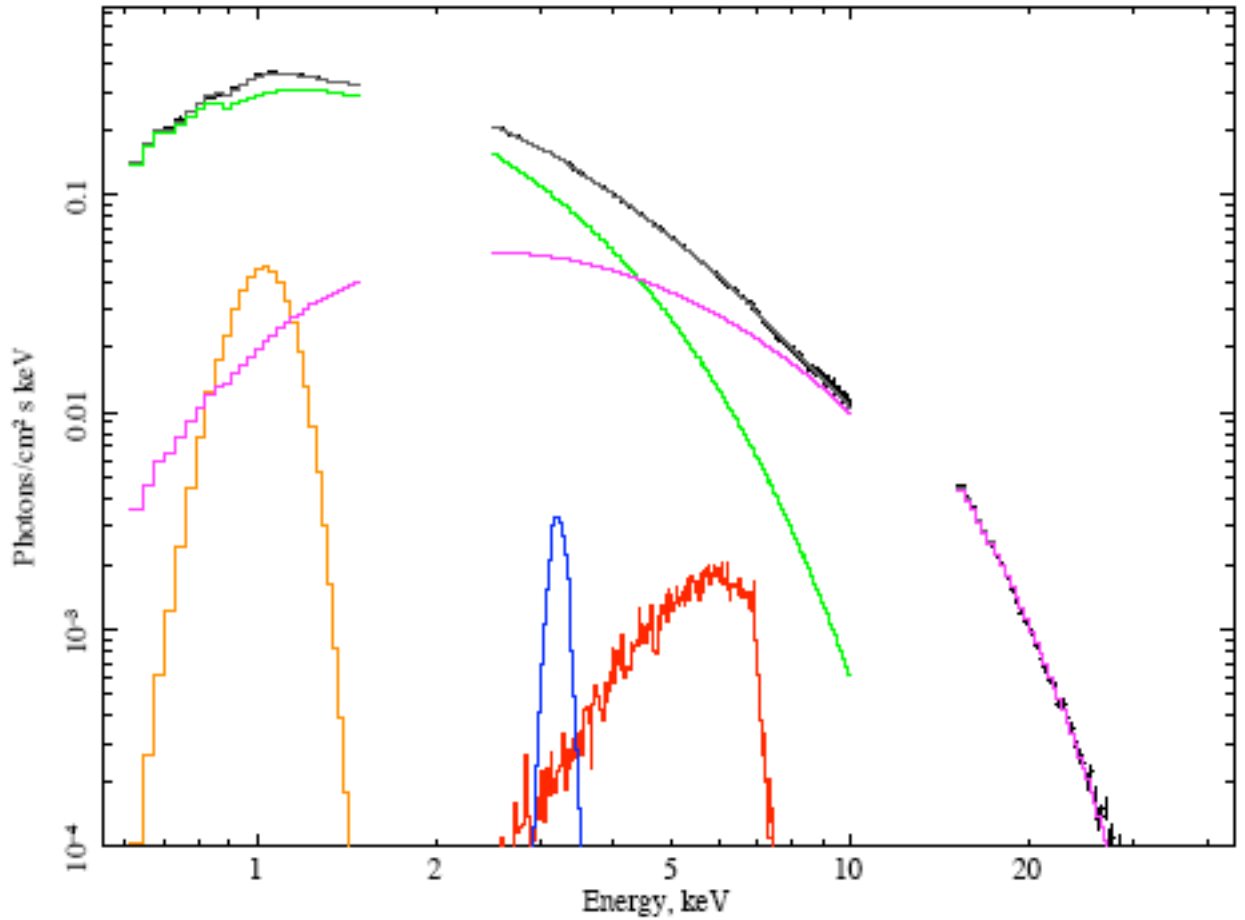

Fig. 2.— Unfolded model fit to the *Suzaku* Cyg X-2 spectrum with the Model 4. The best-fit model of the source spectrum consist of `comptt` (magenta), `diskbb` (green), `windline` (red) and two `gaussians` at 1 keV (brown) and 3.2 keV (blue).

Redskewed iron line profiles in CV (GK Per). Wind model

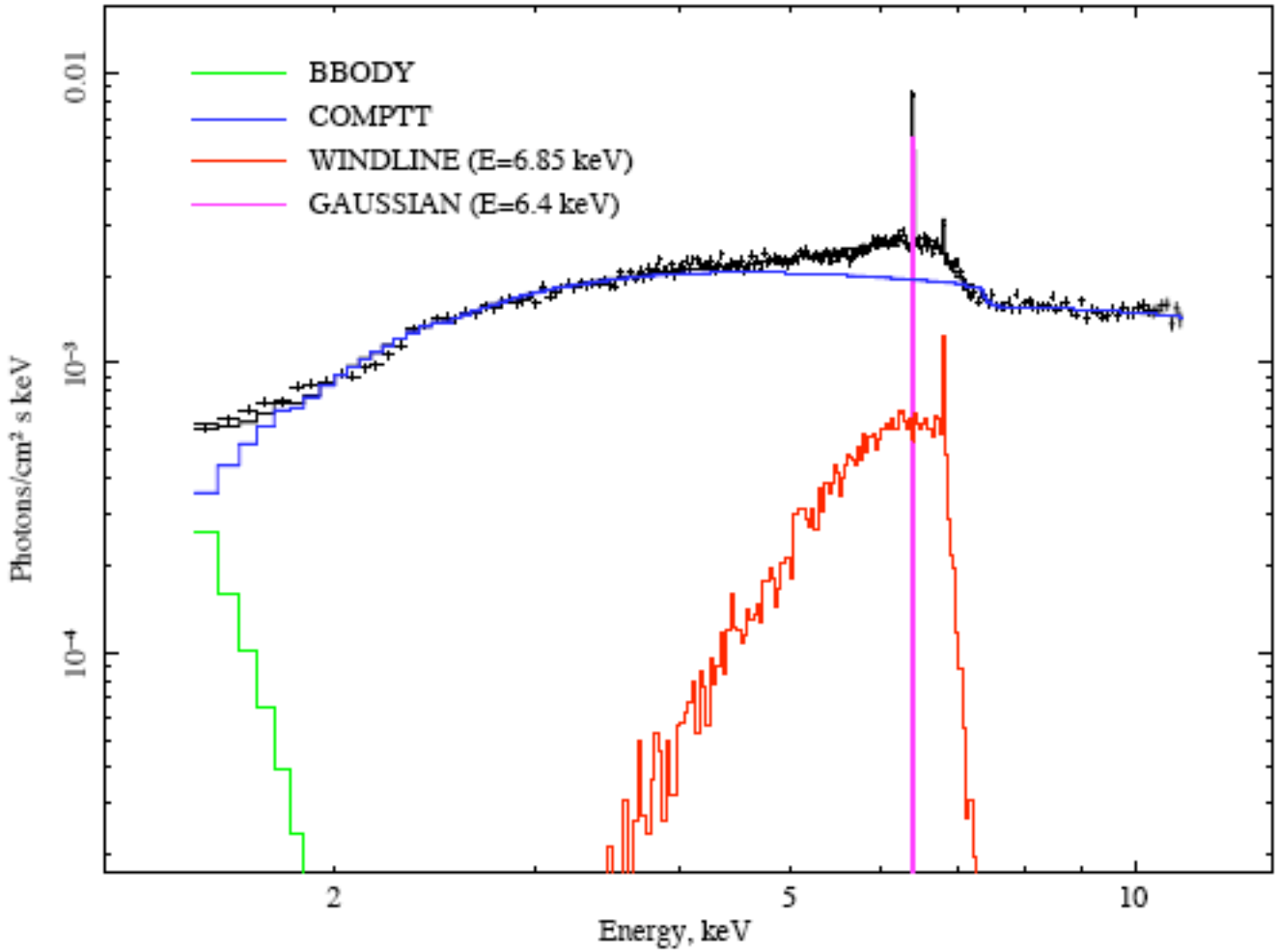

T, LAURENT & SHAPOSHNIKOV (2008)

Redskewed iron line profiles in CV (GK Per). ``Relativistic model''

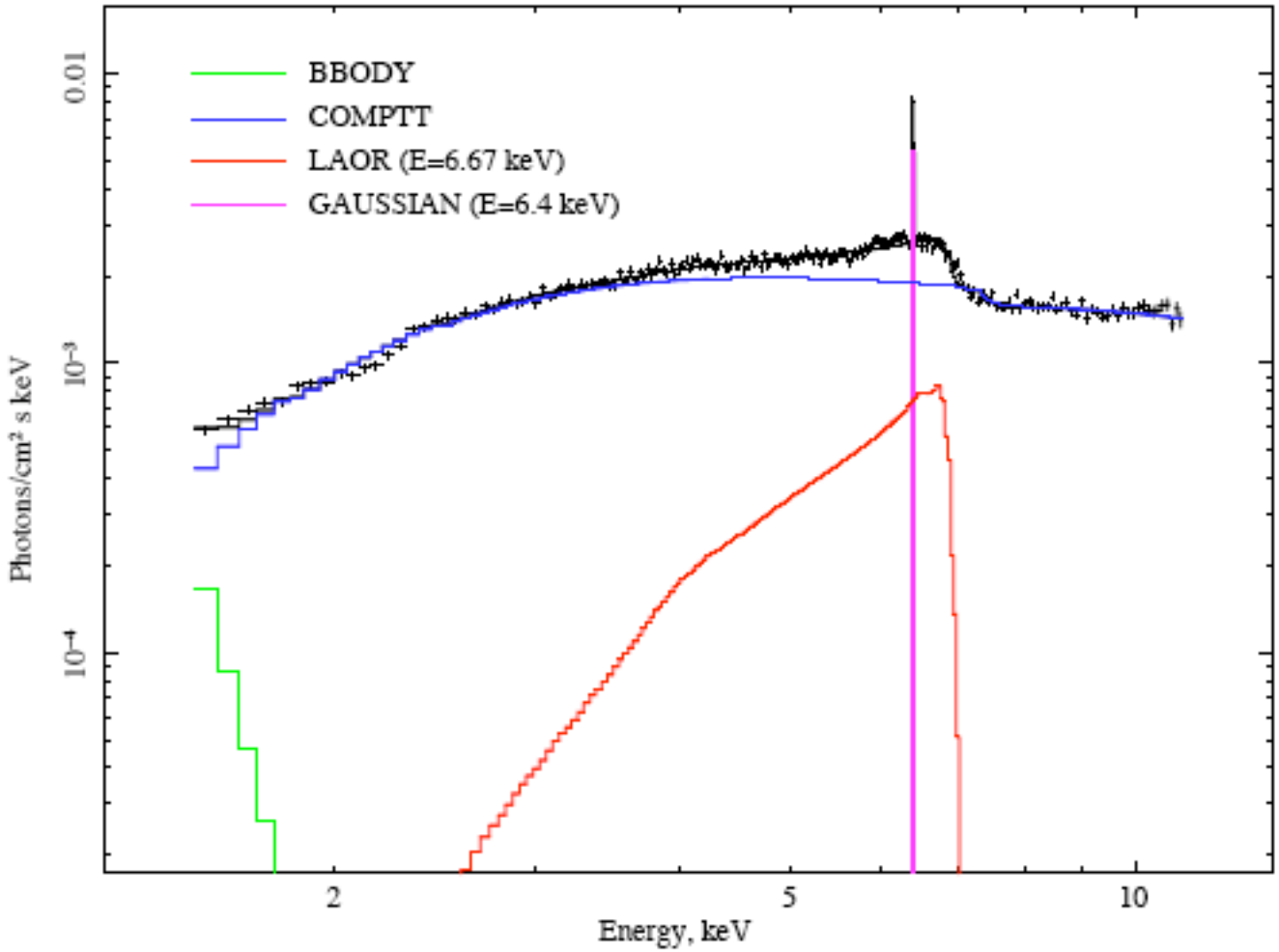

T, LAURENT & SHAPOSHNIKOV (2009)

Fit quality (GK Per). Wind model

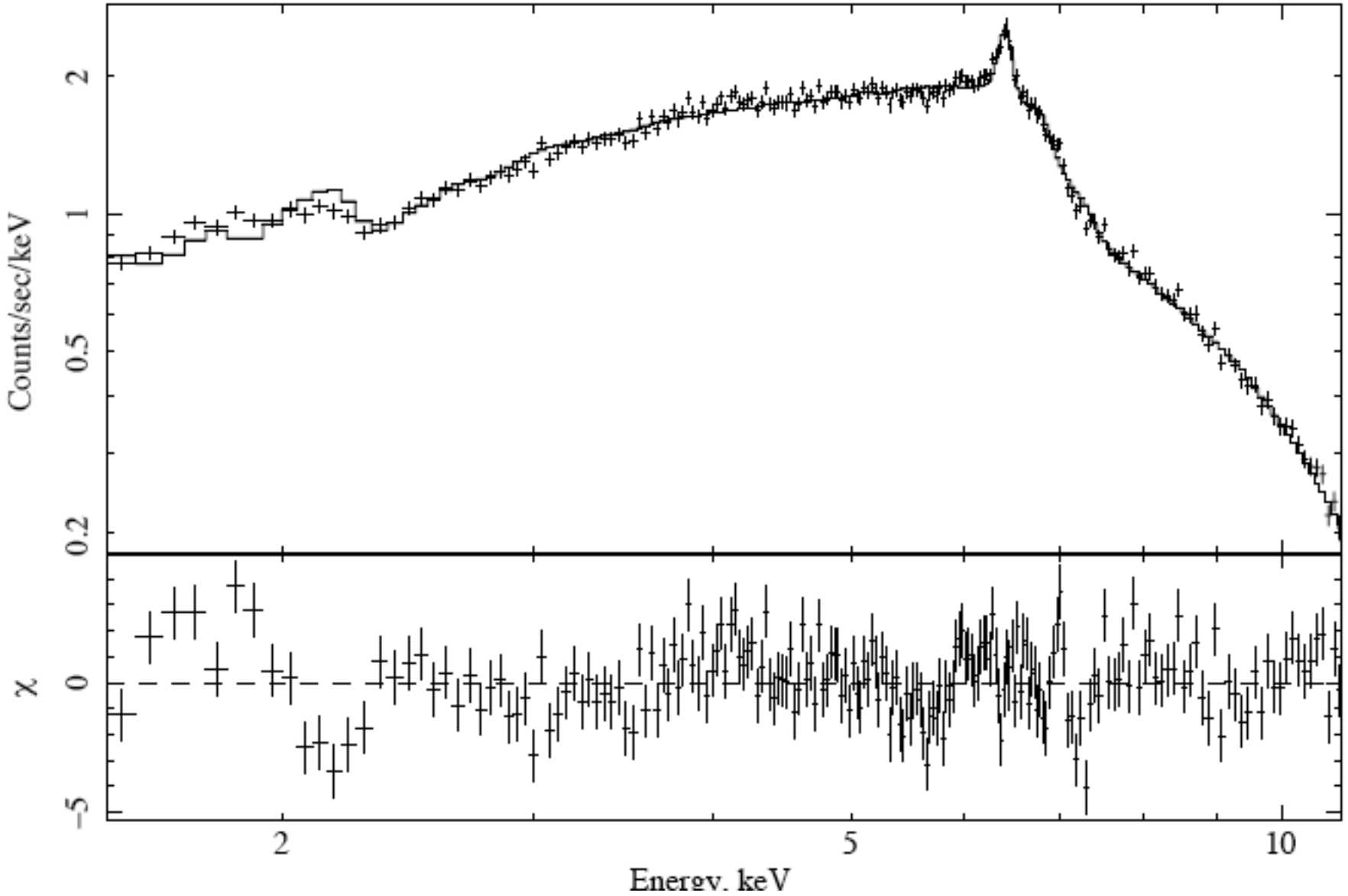

T, LAURENT & SHAPOSHNIKOV (2009)

Fit quality (GK Per). ``Relativistic model''

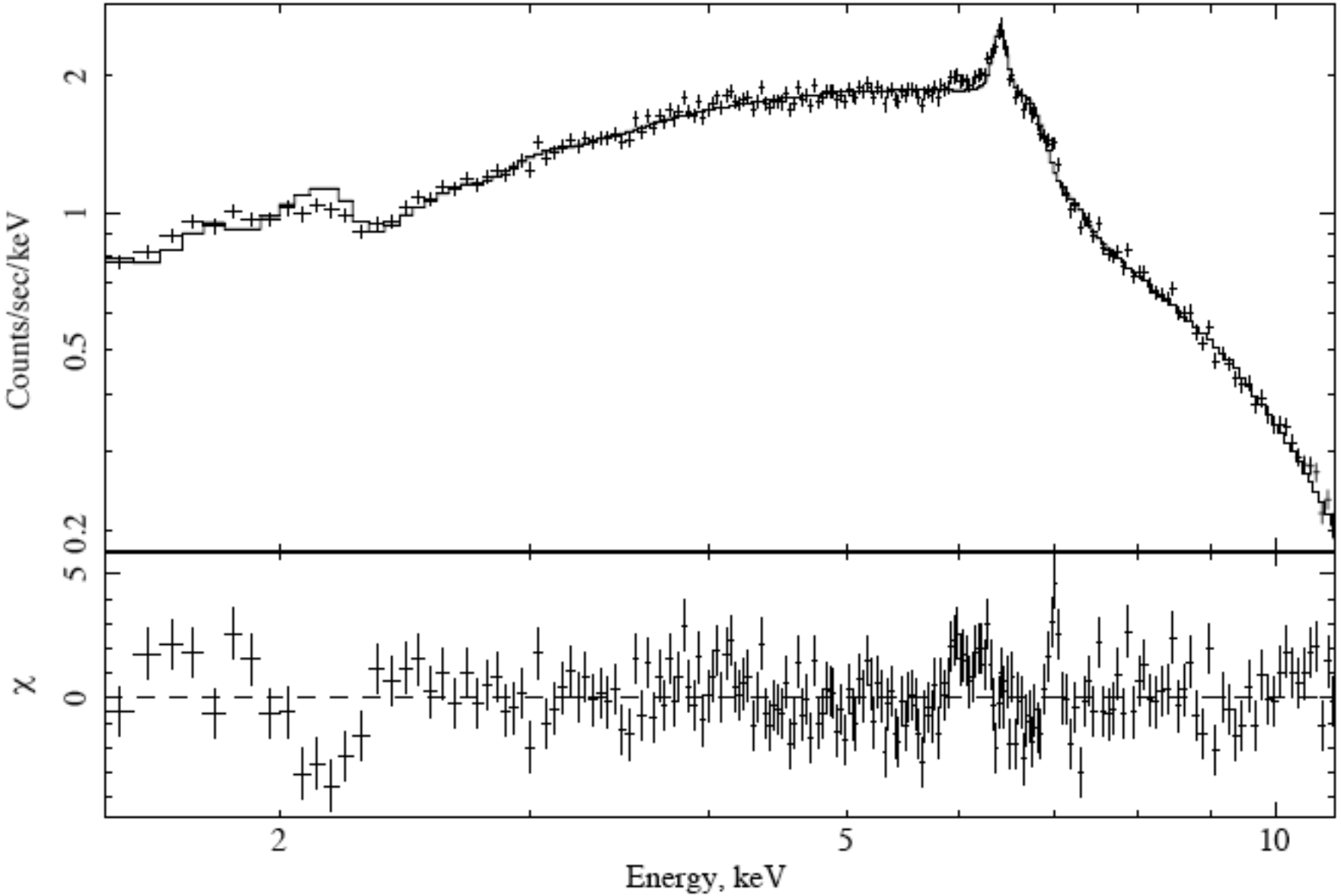

T, LAURENT & SHAPOSHNIKOV (2009)

GK Per XMM Spectrum

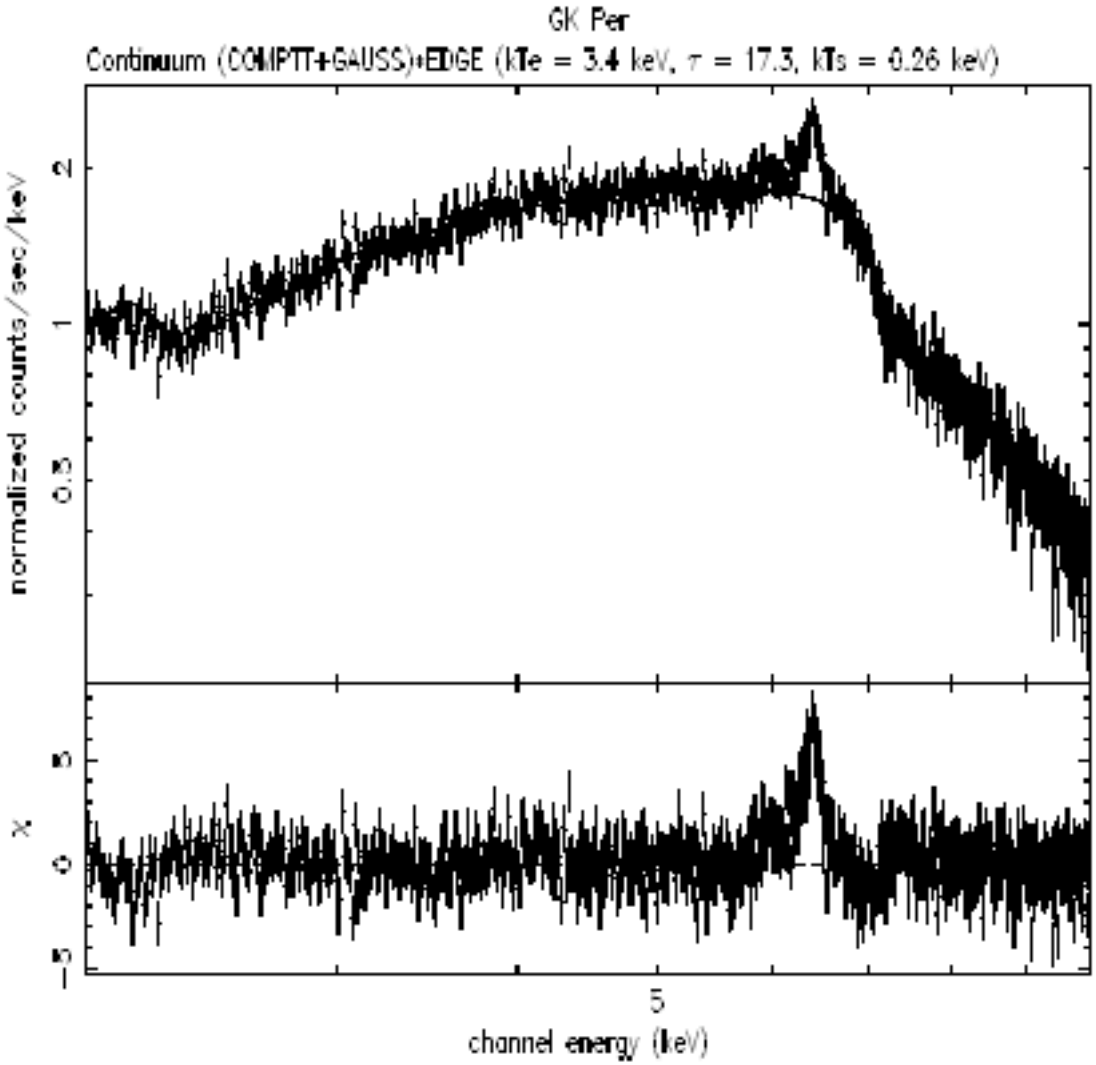

The XMM- *Newton* observation of GK Per on March 9 2002 (revolution 412)

T, LAURENT & SHAPOSHNIKOV (2008)

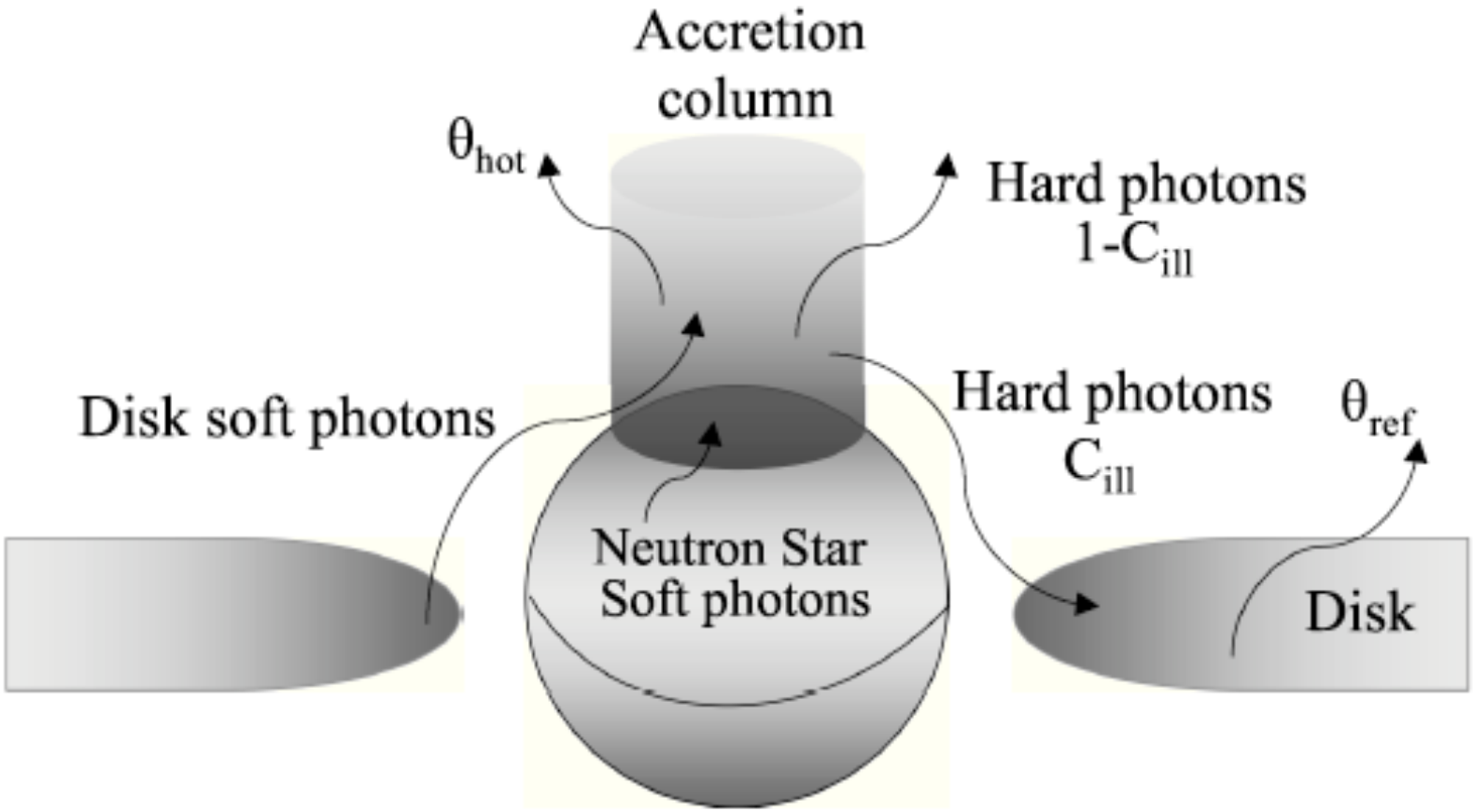

This cartoon illustrates the different emission patterns responsible for the time lags of the pulsed emission. Cill is the disk illumination fraction. Soft time lag of the pulsed emission is the result of downscattering of hard X-ray photons in the relative cold plasma of the disk. A fraction of hard X-ray photons 1- Cill that are upscattered soft disk photons coming from the disk and NS and directly are seen by the Earth Observer.

Time lags and density variations in compact objects

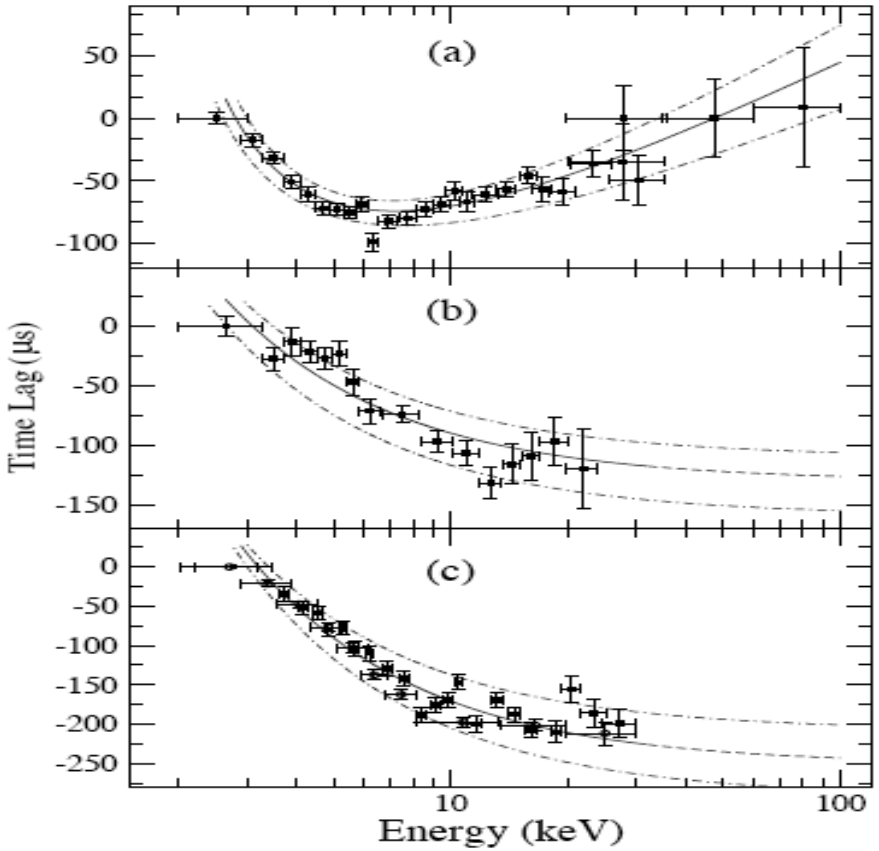

The measured soft time lag of the pulse profile versus energy (crosses) with respect to the first energy channel. The best- fit curve using the Comptonization model is shown with the solid line. The upper and lower limit of the electron number density of the Comptonization emission area, are given in dot-dashed line 1.6-2.6 x 10^{18} cm^{-3} . The panels corresponds (a) for IGR J00291+5934 including also the upper and lower limit of the electron number density of the reflector, 6.1-8 x 10^{18} cm^{-3}, and (b) that for XTE J1751-305, 6-6.6 x 10^{18} cm^{-3} and (c) that for SAX J1808.4-3658, 2.9-3.6 x 10^{18} cm^{-3}.

Time lag model

$$\Delta t = -\frac{C_{\rm ill}}{\sigma_{\rm T} n_{\rm e}^{\rm ref} c} \times$$

$$\left[\frac{1}{4\theta_{\rm ref}} \ln \frac{1 - 4\theta_{\rm ref}/z}{1 - 4\theta_{\rm ref}/z_*} - \frac{n_{\rm e}^{\rm ref}}{n_{\rm e}^{\rm hot}} \frac{1 - C_{\rm ill}}{C_{\rm ill}} \frac{\ln(z/z_*)}{\ln[1 + (3+\alpha)\theta_{\rm hot}]} \right] \quad (5)$$

where $n_{\rm e}^{\rm ref}$ is the electron number density of the reflector, $n_e^{\rm hot}$ is the electron number density of the Comptonization emission area (accretion column). $\theta_{\rm ref} = kT_e^{\rm ref}/(m_e c^2)$ is a dimensionless temperature of the reflector. We assume a typical value of $\theta_{\rm ref} < 0.7$ keV/511 keV. $kT_{\rm e}^{\rm hot}$ and α are the best-fit parameters for the hot plasma temperature and spectral index of the Comptonization spectrum, and $\theta_{\rm hot} = kT_e^{\rm hot}/(m_e c^2)$.

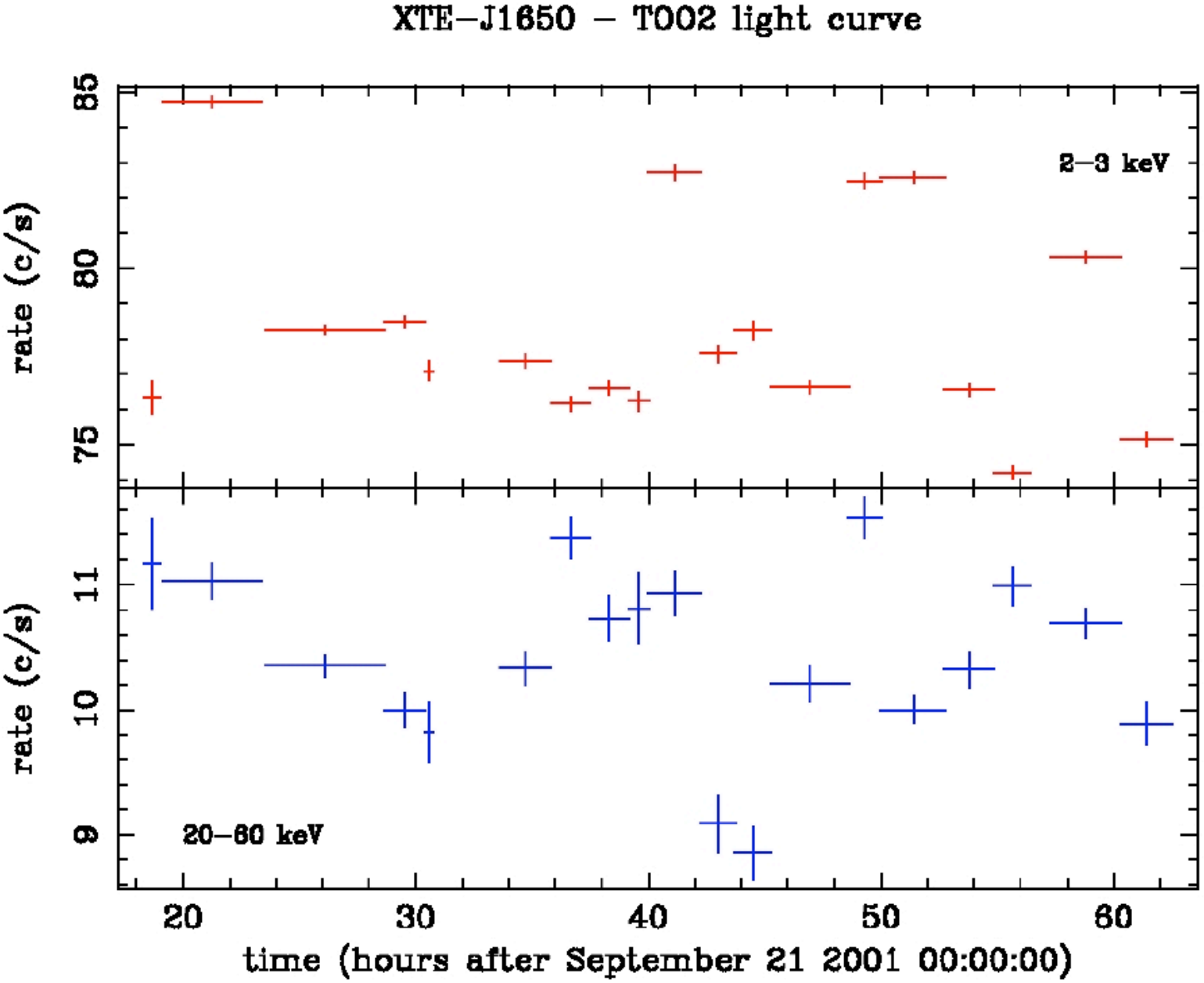
XTE−J1650 − T002 light curve
rate (c/s)
85
80
75
2−3 keV
rate (c/s)
11
10
9
20−60 keV
20
30
40
50
60
time (hours after September 21 2001 00:00:00)

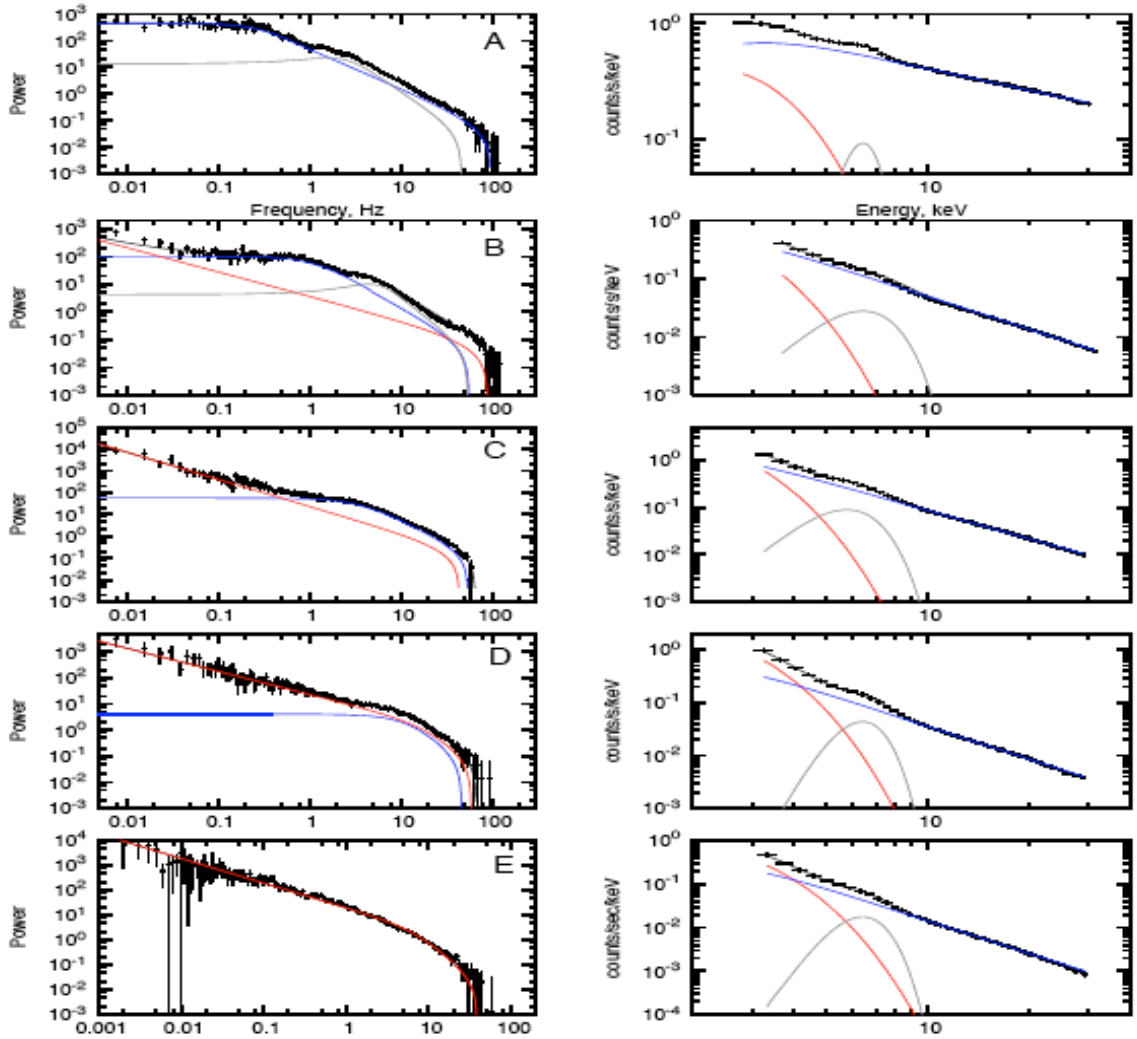

Fig. 2.— Cyg X-1: Observable power spectrum (PDS) (left panel) vs photon spectrum (right panel) from low/hard to soft state of Cyg X-1. Data points are shown with error bars. PDS is fitted by a product of sum of LF and HF white-red noise power spectra and Lorentzian (see formula 67). We also use Lorentzians to fit QPO features. Black line is for the resulting PDS as red and blue lines present LF and HF components respectively. Photon spectrum is fitted by BMC+GAUSSIAN model. Black line is for the resulting spectrum as red and blue lines present BMC blackbody and Comptonization components respectively. Grey line presents GAUSSIAN of K_α line located at 6.4 keV.

W01 demonstrated that the mass accretion rate in the disk $\dot{M}$ *can be calculated as*

$$\dot{M} = 3\pi \frac{\partial V}{\partial x}.$$

Furthermore, we assume that the mass accretion rate at the inner disk edge is converted with efficiency $\varepsilon_{\rm eff}$ *into the X-ray luminosity, L(t) i.e.*

$$L(t) = \varepsilon_{\rm eff} \dot{M}(t, R_{in})$$

and thus

$$X(t) = L(t) \propto \frac{\partial V}{\partial x}(t, 0).$$

Now we consider a general case of problems where $\hat{\nu}(x) = (\hat{\nu}_0 / x_0^{\psi}) x^{\psi}.$

a. Viscosity linearly distributed over radius: $\psi = 2$

$$X(t) \propto \sum_{k=1}^{\infty} \exp[-\pi^2 (2k-1)^2 t / 4t_0]$$

where the viscous time scale $t_0 = 4x_0^4 / 3\hat{\nu}_0 = 4R_0^2 / 3\hat{\nu}(R_0).$

Then the power spectrum of X(t) *is:*

$$||F_X(\nu)||^2 \propto \sum_{k=0}^{\infty} \frac{1}{(8t_0\nu/\pi)^2 + (2k+1)^4}.$$

where $F_X(\omega) = \int_0^{\infty} e^{-i\omega t} X(t) dt$

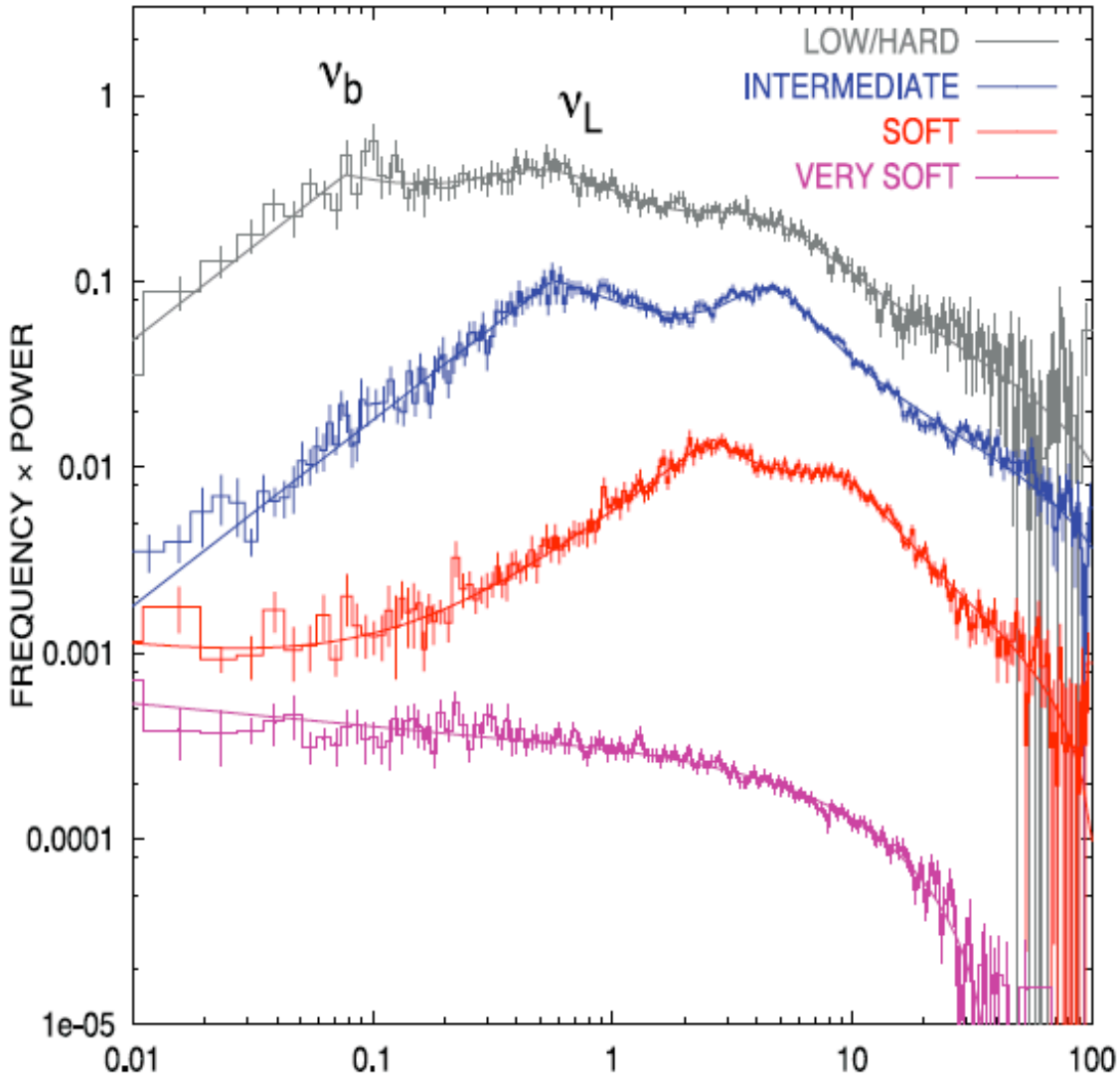

Shaposhnikov & T (2006)

FIG. 6.—Power spectrum (PDS) evolution of the source from the low/hard state (*gray lines*) through the intermediate state (*blue lines*) and soft state (*red lines*) to the very soft state (*purple lines*). The break frequency ν_b and the low QPO frequency are clearly seen in the low/hard, intermediate, and soft states. In the very soft state the power spectrum is featureless; neither QPO nor break are present. Any break and QPO features are washed out.

PDS for different energy ranges for TOO1

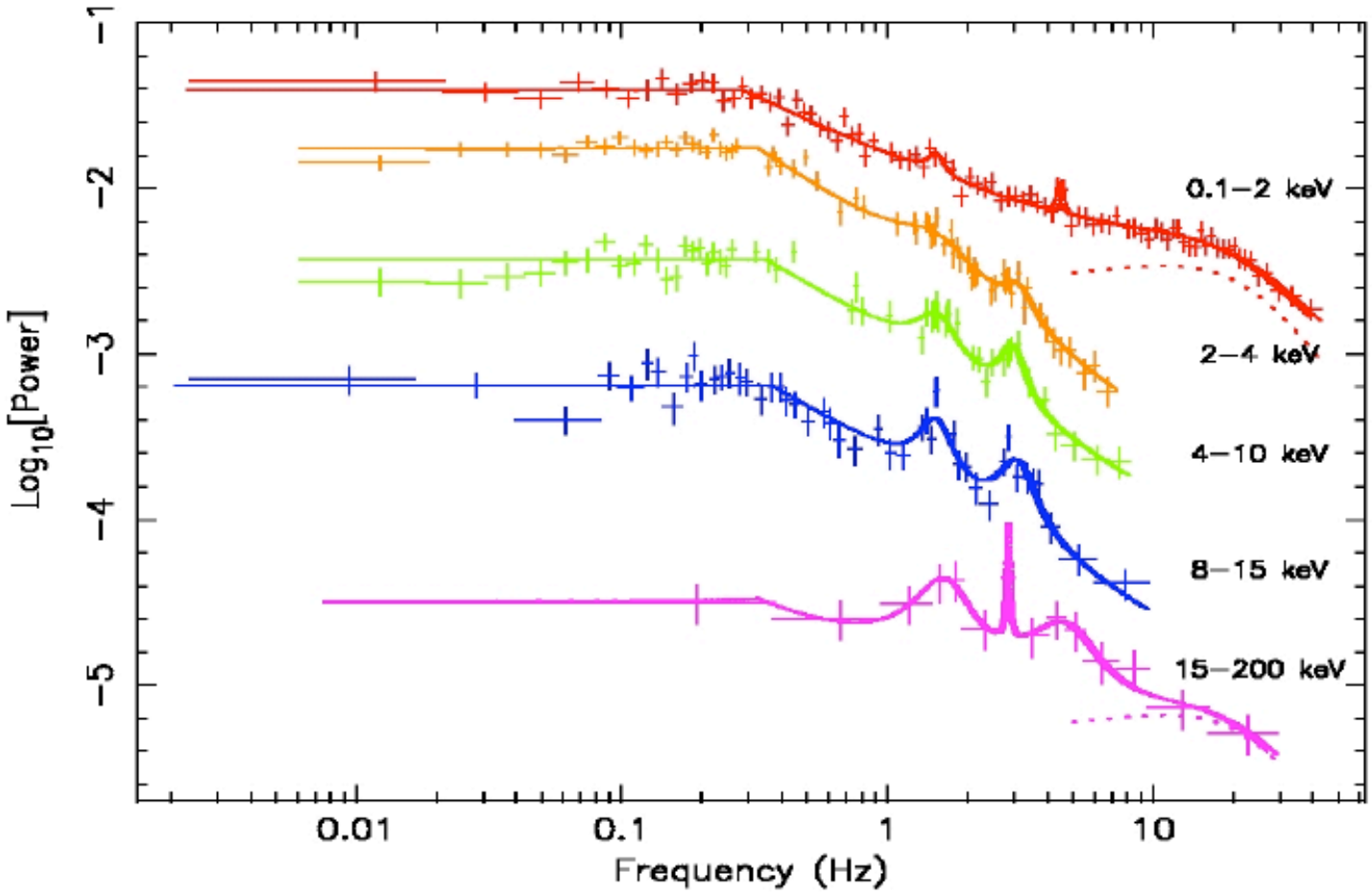

Montanari, T & Frontera 2006

BH mass determination:Cyg X-1

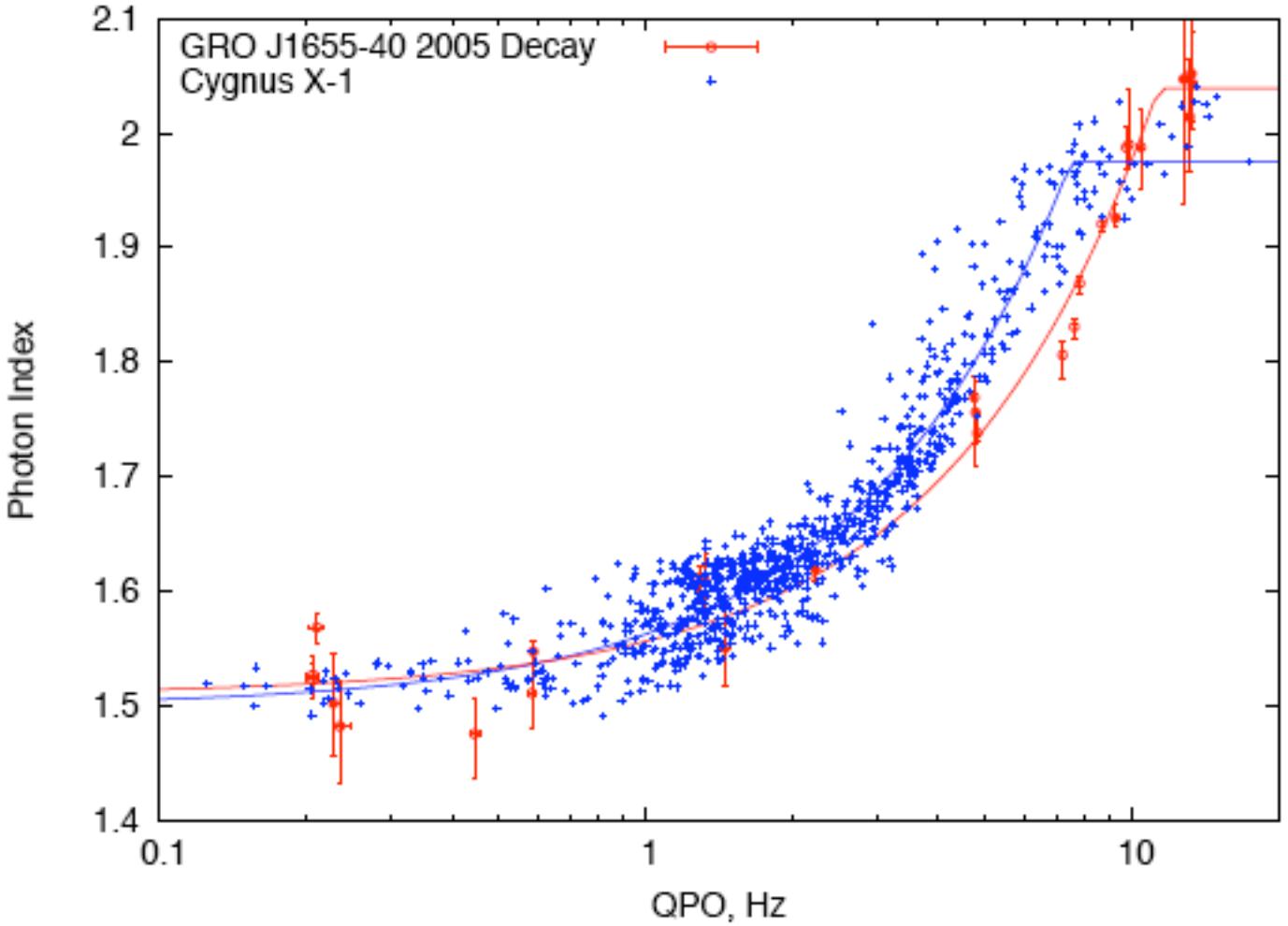

Fig. 2.— Determination of BH mass in Cyg X-1. Correlations for Cyg X-1 comprises RXTE-mission-long data from ST06 (blue color). Data for GRO 1655-40 is for the 2005 outburst decay. The sources show similar saturation levels for both ends of correlation. Index-QPO correlation scaling gives for the BH mass in Cyg X-1 $M_{CygX-1} = 8.5 \pm 1.2\, M_{\odot}$.

BH Candidate: GX 339-4

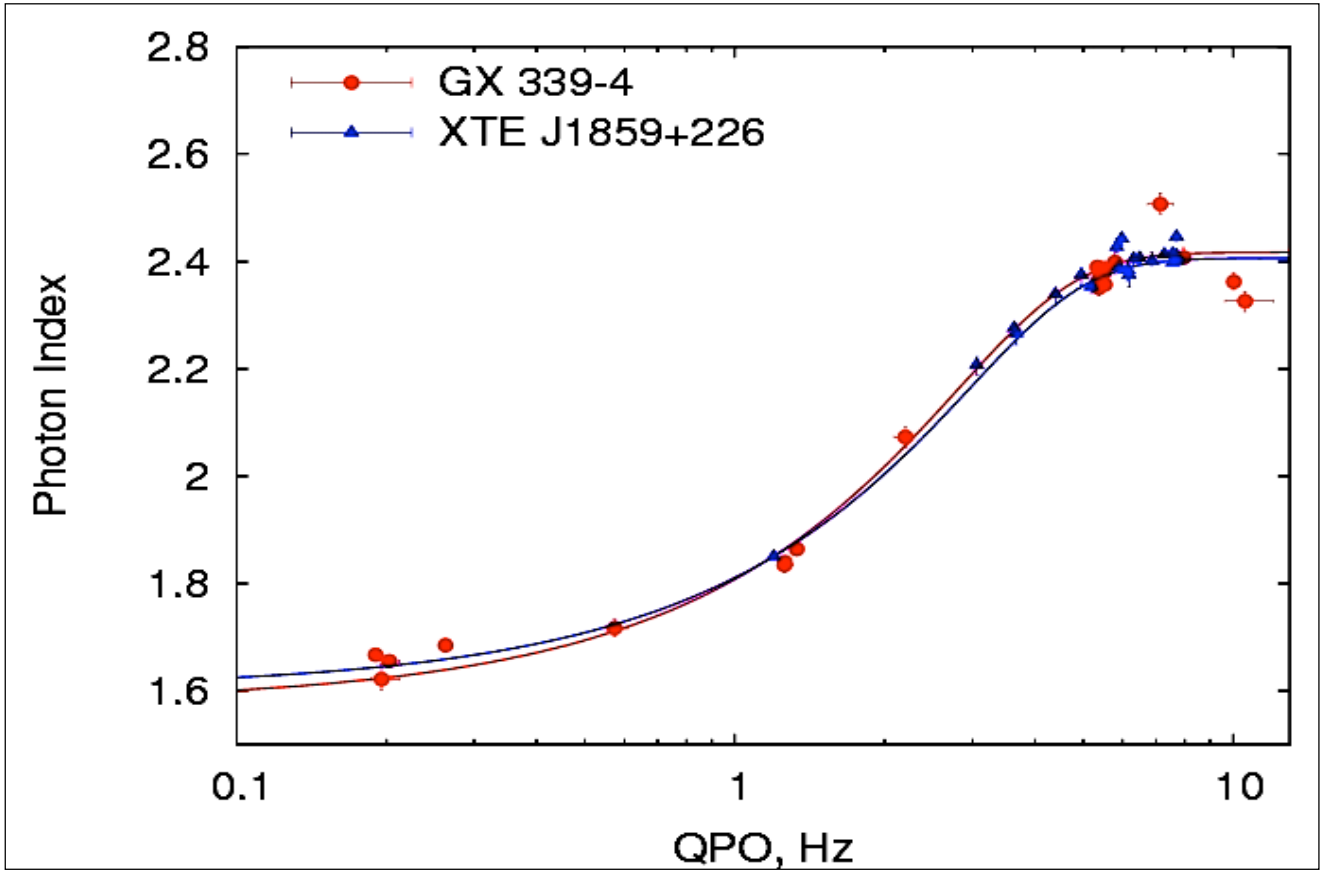

$M_{GX\ 339\text{-}4} \approx M_{XTE\ J1859+226} \sim (9.7 \pm 0.8)\ M_{SUN}$

QPO-Photon Index Correlations in BH sources

Cygnus X-1

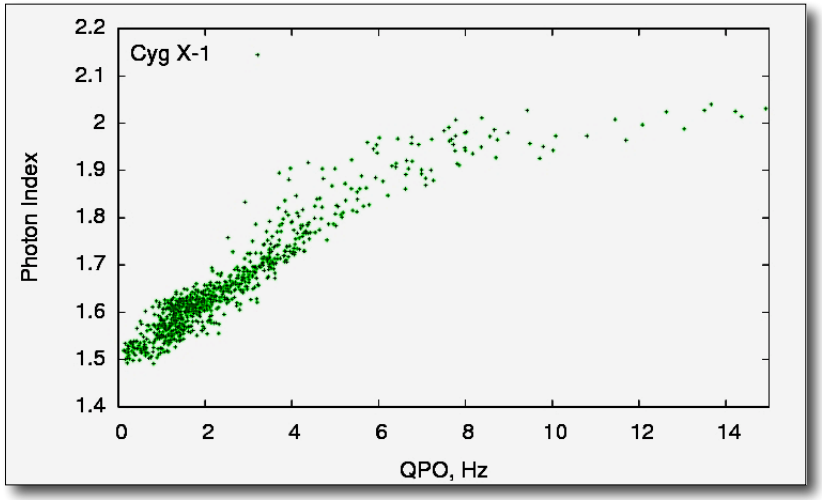

GRS 1915+105

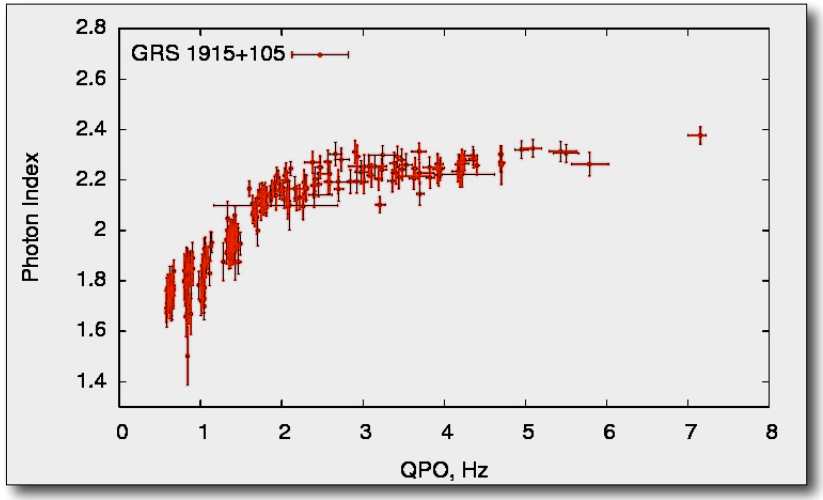

J1859+226 and 1550+564

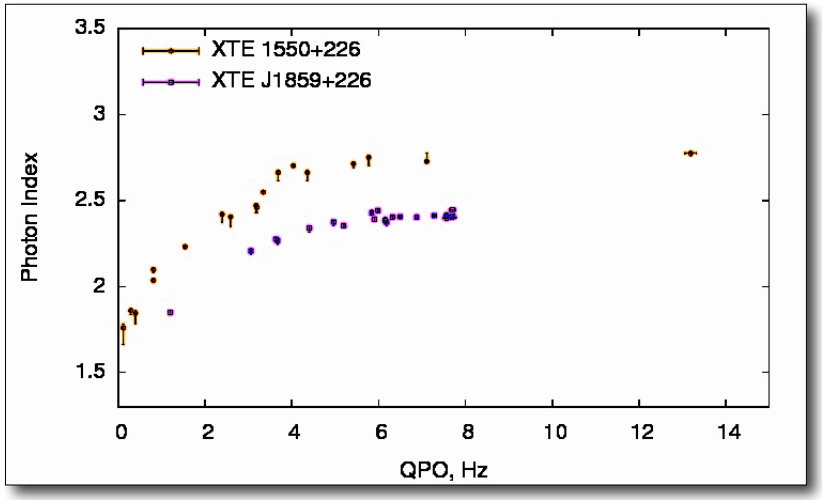

GRO J1655-40

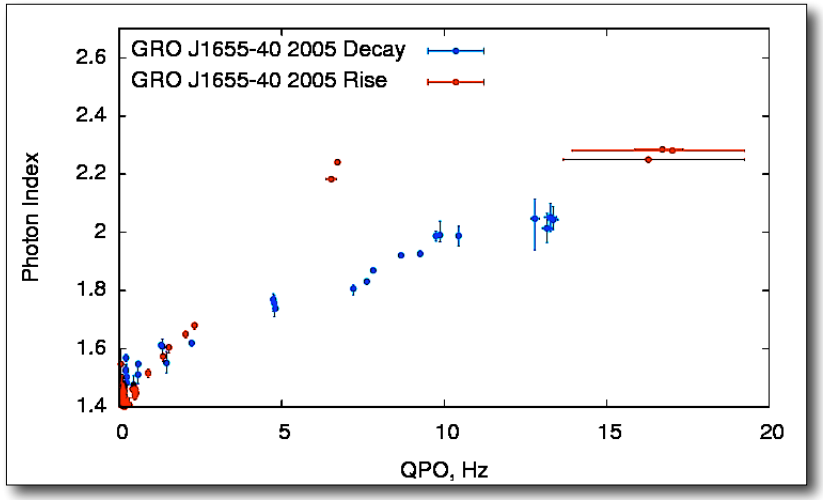

Index-Mdot saturation. GRS 1915+105

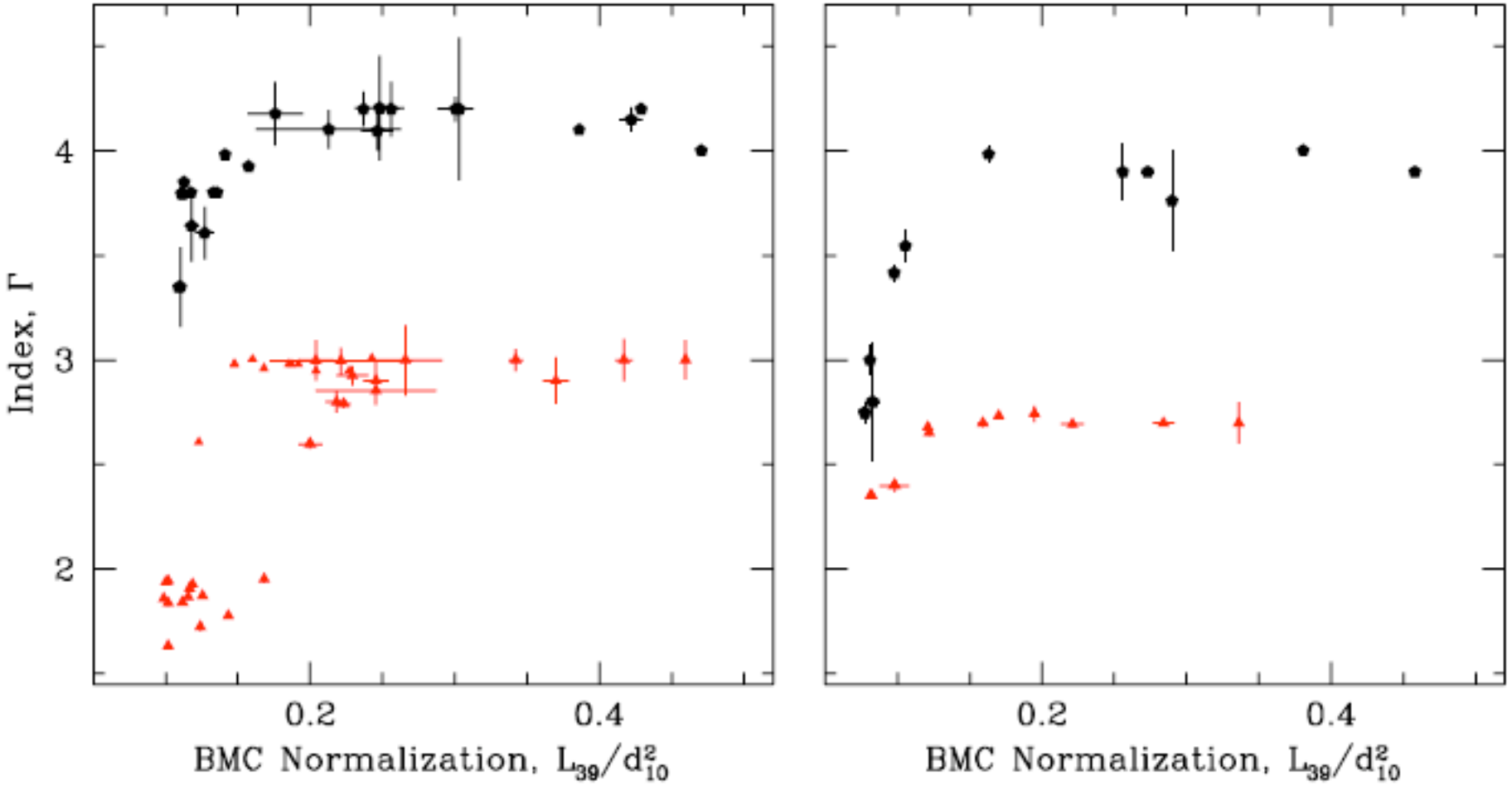

Seifina & T (2009)